FINAL REPORT
VOLUME 1

METALLURGICAL EVALUATION OF CAST DUPLEX STAINLESS STEELS AND THEIR WELDMENTS

SUBMITTED TO
U. S. DEPARTMENT OF ENERGY
Award Number - DE-FC07-00 ID13975

OCTOBER 1, 2000 - SEPTEMBER 30, 2005

SONGQING WEN
CARL D. LUNDIN
GREG BATTEN

MATERIALS JOINING GROUP
MATERIALS SCIENCE AND ENGINEERING
THE UNIVERSITY OF TENNESSEE, KNOXVILLE

CARL D. LUNDIN
PROFESSOR OF METALLURGY

MATERIALS JOINING GROUP
MATERIALS SCIENCE AND ENGINEERING
THE UNIVERSITY OF TENNESSEE
KNOXVILLE 37996-2200

TELEPHONE (865) 974-5310
FAX (865) 974-0880

lundin@utk.edu

This is Volume 1of 5 of the final report for
The Department of Energy
Grant # DE-FC07-00 ID13975 entitled
"Behavior of Duplex Stainless Steel Castings."

FOREWARD

The final report for the DOE Grant DE-FC07-00 IDI13975 consists of five volumes. The volumes provide in depth information on Cast Duplex and Cast Super Duplex Stainless Steels. Volume 1 is entitled "Metallurgical Evaluation of Cast Duplex Stainless Steels and their Weldments" involves comparison of selected grades of Duplex Stainless Steels and their welds with their wrought counterparts regarding corrosion performance, mechanical properties and weldability. Volume 2 entitled "The Development of Qualification Standards for Cast Duplex Stainless Steel" involves inter-laboratory testing and Volume 3 "The Development of Qualification Standards for Cast Super Duplex Stainless Steel" provides information on the testing of Super Duplex Stainless Steels to ASTM A923. Volume 4 is the "Guidance Document for the Evaluation of Super Duplex Stainless Steel" and involves the applicability of ASTM A923 to the Cast Super Duplex materials. Volume 5 is the data package for the incorporation of ASTM A890-5A material into the ASTM A923.

In volume 1 selected grades of Duplex Stainless Steel castings and their welds, in comparison with their wrought counterparts, were evaluated, regarding corrosion performance, mechanical properties and weldability. Multiple heats of cast duplex stainless steel were evaluated in the as-cast, solution annealed static cast and solution annealed centrifugal cast conditions, while their wrought counterparts were characterized in the solution annealed condition and in the form of as-rolled plate. Welding, including extensive assessment of autogenous welds and a preliminary study of composite welds, Shielded Metal Arc Weld (SMAW), was performed. The evaluations included Critical Pitting Temperature (CPT) testing, Intergranular Corrosion (IGC) testing, ASTM A923 (Methods A, B and C), Charpy impact testing, weldability testing (ASTM A494), ferrite measurement and microstructural evaluations.

Volume 2 deals with the Development of Qualification Standards for Cast Duplex Stainless Steel (A890-4A) which is equivalent to wrought 2205. This volume involves testing of cast Duplex Stainless Steel to several ASTM specifications, formulating and conducting industry round robin tests and studying the reproducibility of the results. ASTM E562 (Standard Test Method for Determining Volume Fraction by Systematic manual Point Count) and ASTM A923

(Standard Test Methods for Detecting Detrimental Intermetallic Phase in Wrought Duplex Austenitic/Ferritic Stainless Steels) were the specifications utilized in conducting this work. An ASTM E562 industry round robin, ASTM A923 applicability study, ASTM A923 industry round robin, and an ASTM A923 study of the effectiveness of existing foundry solution annealing procedures for producing cast Duplex Stainless Steel without intermetallic phases were implemented.

Volume 3 comprises of the Development of Qualification Standards for Cast Super Duplex Stainless Steel (A890-5A) which is equivalent to wrought 2507. The objective of this work was to determine the suitability of ASTM A923 "Standard Test methods for Detecting Detrimental Intermetallic Phase in Duplex Austenitic-Ferritic Stainless Steels" for 25 Cr Cast Super Duplex Stainless Steels (ASTM A890-5A). The various tests which were carried out were ASTM A923 Test Method A, B and C (Sodium Hydroxide Etch Test, Charpy Impact Test and Ferric Chloride Corrosion Test), ferrite measurement using Feritscope®, ASTM E562 Manual Point Count Method and X-Ray Diffraction, hardness measurement using Rockwell B and C and microstructural analysis using SEM and EDS.

Volume 4 is the guidance document for the evaluation of cast Super Duplex Stainless Steel which deals with the various evaluation methods which were defined and used for the work on volume 3 for the "Development of Qualification Standards for Cast Super Duplex Stainless Steel alloy A890-5A (2507 Wrought Equivalent)". The document explains in detail each test which was conducted. It also includes some of the results which were acquired during this work.

Volume 5 is the Data Package for the evaluation of Super Duplex Stainless Steel Castings prepared at the end of work comprised in volumes 3 and 4. The document deals with the various evaluation methods used in the work documented in volume 3 and 4. This document covers materials regarding evaluation of the A890-5A material in terms of inclusion in ASTM A923. The various tests which were conducted on the A890-5A material are included in this document.

ABSTRACT

Duplex stainless steels (DSS) are being specified for chloride containing environments due to their enhanced pitting and stress corrosion cracking resistance. They exhibit improved corrosion performance over the austenitic stainless steels. Duplex stainless steels also offer improved strength properties and are available in various wrought and cast forms.

Selected grades of duplex stainless steel castings and their welds, in comparison with their wrought counterparts, were evaluated, regarding corrosion performance and mechanical properties and weldability. Multiple heats of cast duplex stainless steel were evaluated in the as-cast, solution annealed (SA) static cast and SA centrifugal cast conditions, while their wrought counterparts were characterized in the SA condition and in the form of as-rolled plate. Welding, including extensive assessment of autogenous welds and a preliminary study of composite welds (shielded metal arc weld (SMAW)), was performed. The evaluations included critical pitting temperature (CPT) testing, intergranular corrosion (IGC) testing, ASTM A923 (Methods A, B and C), Charpy impact testing, weldability testing (ASTM A494), ferrite measurement and microstructural evaluations.

In the study, the corrosion performances of DSS castings were characterized and assessed, including the wrought counterparts for comparison. The evaluation filled the pore of lack of data for cast duplex stainless steels compared to wrought materials. A database of the pitting corrosion and IGC behavior of cast and wrought materials was generated for a greater depth of understanding for the behavior of cast duplex stainless steel. In addition, improved evaluation methods for DSS castings were developed according to ASTM A923, A262, G48 and A494.

The study revealed that when properly heat treated according to the specification, (1) DSS castings have equal or better pitting and intergranular corrosion resistance than their wrought counterparts; (2) Welding reduces the pitting and intergranular corrosion resistance for both the wrought and cast duplex alloys; (3) Castings generally have better toughness than their wrought counterparts in the temperature range of –80°C to +20°C; (4) All shield metal arc (SMA) test welds in DSS castings, with recommended or over matching filler metal, indicate that welding is not a significant factor when considering DSS applications.

TABLE OF CONTENTS

LIST OF FIGURES

LIST OF TABLES

I. Program Introduction

Duplex stainless steels, cast and wrought forms, have been in use since the 1930's. The first duplex stainless steel chemical tanks were built in the 1970 using alloy UR 50. Never-the-less, it is only until recently, that the duplex alloys became popular, due to the use of AOD refining technology combined with improved casting processes. This combination made it possible to effect rigid control over the chemical composition of the cast product so that the outstanding combination of corrosion resistance and toughness became an ease of control and, simultaneously, reduced the cost of the product.

Now, duplex stainless steels, which are now more and more considered to be industrial steels but no longer exotic alloys, have found widespread applications in the pulp and paper industry, chemical industry, transport/chemical tanks and pollution control equipment manufacture, offshore-gas and petroleum industry and a number of naval applications.

Although duplex stainless steels have enjoyed rapidly increasing popularity in recent years, the availability of these alloys in the cast form has fallen behind the availability of the wrought form. Duplex stainless steel castings are often used in pumps and valves in a variety of applications and are important components in the systems, where unexpected service failures can result in significant operational problems and expense. The performance is critical. Thus, of concern is variability and insufficient performance characteristics of duplex stainless steels in all forms, which can be related to significant in-service problems. And it is also of necessity to have

available, suitable methods and procedures for defining performance characteristics prior to service of duplex stainless steel cast materials.

II. Project Goals

This program involves two major areas of endeavor, interrelated and leading to a more fundamental understanding of the corrosion and fabrication behavior of duplex stainless steel castings and their welds in comparison with the wrought materials.

Therefore, foundries and component suppliers can reduce lead times and provide better duplex stainless steel castings for critical service in marine and industrial environments as a result of information developed in this study.

The following goals have been defined for this project:

- Evaluation for cast duplex stainless steel materials and their welds, in comparison with the wrought counterparts, regarding microstructure, corrosion resistance, weldability and mechanical properties

- Development of a database for the assessment of corrosion performance of cast duplex stainless steels and the welds

- Development of standardized test methods for corrosion and weldability evaluations and criterion for assessment with regard to potential service performance

III. Literature Review

1. Introduction

Duplex Stainless Steel (DSS) is defined as the group of stainless steels " that contains a two-phase structure (ferrite-austenite) and is more often a descriptor of an alloy where both phases are present in significant quantities [1]." DSSs offer improved corrosion and mechanical properties over austenitic stainless steels, so that they are regarded to have higher potential in extending life of process components.

DSSs have been around since the early 1900. Fairly amount of evaluation work has been conducted on DSS ever since. Publications of the research work can be found dated from 1930s. Six international conferences have been held on DSS since 1982. However, it was not until the 1970s that came in the most rapid alloy development and appliance. Furthermore, most of the study of DSS was on wrought materials, which made the understanding of cast DSS to fall behind. In addition, as welding is used to upgrade castings before final solution heat treatment and is employed in fabrication of cast-to-cast, wrought-to-cast and wrought-to-wrought components. The welding processes employed and utilizing of filler metal for the welding can lead to degradation of parent materials' properties, especially corrosion performance in varies regions of the weldment.

2. Materials

2.1. The Duplex Family - Development History, Chemistry, Applications

Duplex Stainless Steels were first produced by Avesta Jernverk in the year 1929 with an alloy called 453E (25%Cr-5%Ni). Another record of the earliest production of duplex stainless steel products dates back to 1933 through an alloying error at J. Holtzer Company, France. An 18%Cr-9%Ni-2.5%Mo austenitic stainless steel grade was made to a 20%Cr-8%Ni-2.5%Mo composition containing a high volume of ferrite in an austenitic matrix. This two-phase material was then studied and it was found that when it was properly solution heat treated, the alloy was not sensitive to Intergranular Corrosion (IGC) in various corrosive environments; a significant advantage compared to fully austenitic stainless steel [1, 2].

After the first discovery, several duplex alloys were patterned. But it was not until the 1950s, when the nickel shortage come up during Korean War that spurred new duplex alloy development [3]. However, due to the limitation on understanding of physical metallurgy and refining technique, the development of duplex alloys suffered from many problems such as corrosion, ductility and welding. The real rapid development occurred in 1970s with improved chemistry analysis capability and the introduction of Argon-Oxygen-Decarburization (AOD) refining process. The control of alloy chemistry and the removal of oxygen and sulfur were significantly improved.

In the early 1970s, the 22%Cr commercial grade duplex was developed in Germany and Sweden. It was claimed that this grade of duplex was not sensitive to IGC upon welding due to balanced chemistry.

In The 1980s, higher alloyed DSS grades came in favor, and developed into super DSS. They are made to withstand more aggressive environments, but also bearing higher risk of precipitation due to the higher alloying element content. In the making of super DSS, Cr and Ni forming elements are balanced and more nitrogen is added. The super DSSs are usually characterized by having a pitting resistance equivalent number (PREN*) greater than 40. The minimum PREN for the heat is often part of the purchase specification [5].

- PREN is the pitting resistance equivalent number defined as: PREN = Cr + 3.3 Mo + 16 N [4]

Duplex stainless steels are usually classified into four categories [5, 9]:

a. Lean Alloy

The low cost molybdenum free DSS of the type 23Cr-4Ni-0.1N, provide alternatives to AISI 304 and 316. However, the market for these steels has declined.

b. Standard 22%Cr

DSS of the type 22Cr-5Ni-3Mo-0.17N: these steels, which include SAF Alloy 2205 (cast: ASTM A890-4A), are the most popular and the least expensive in the duplex family. In addition, these alloys have a PREN ranging from 30 to 36, and corrosion resistance that lies between AISI 316 and 6 Mo superaustenitic stainless steels.

c. High Alloy

DSSs of the 25 Cr varieties have varying contents of Mo and N and also containing Cu or W as alloy elements. Wrought Ferralium 255 and cast ASTM A890-1B fit this category. This grade has a PREN ranging from 32 to 40.

d. Super Duplex

Super DSS of the type 25 Cr-7Ni-3.5Mo-0.27N has PREN values greater than 40. SAF Alloy 2507 (cast: ASTM A890-5A) and Zeron 100 (cast: ASTM A890-6A) fit this category [2, 3, 5-7].

Table 3-1 presents some of the typical duplex stainless steels in ASTM and other standard systems.

2.2. Metallurgy of DSS

During solidification, duplex first solidifies as ferrite. As temperature decreases, austenite develops. For cast duplex, a structure of austenite islands in a ferrite matrix can be observed. For wrought alloys, the microstructure has a morphology of laths of austenite in a ferrite matrix. Figure 3-1 shows the typical microstructure of DSS in wrought (a) and cast (b) form.

Table 3-1. Some Duplex Materials and Their Standard Designations

ASTM	UNS (Cast)	UNS (Wrought)	ACI	Trademark
A890-4A	J92205	S31803	CD-3MN	SAF Alloy 2205®
A890-5A	J93404	S32750	CE-3MN	SAF Alloy 2507®
A890-6A	J93380	S32760	CD-3MWCuN	Zeron 100®
A890-1B	___	S32550	CD-4MCuN	Ferralium 255®

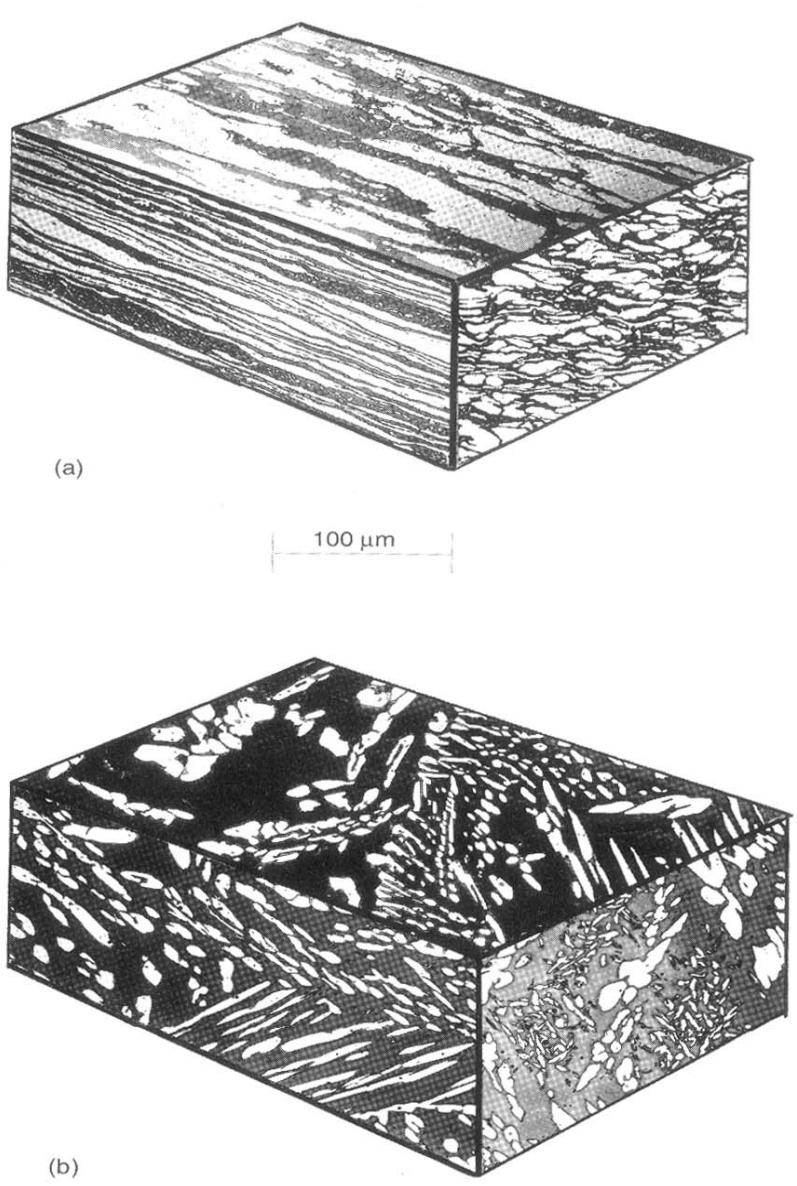

Figure 3-1. Typical microstructure of DSS in wrought (a) and cast (b) form

Generally, the ratio of ferrite to austenite in DSS depends mainly upon the chemical composition. The presence of ferrite with austenite provides better intergranular corrosion (IGC) resistance and stress corrosion cracking (SCC) resistance compared to fully austenitic stainless steels [2, 4]. Figure 3-2 shows the comparison of SCC of susceptibility for various stainless steels. In addition, ferrite is also beneficial in welding for it improves hot-cracking resistance.

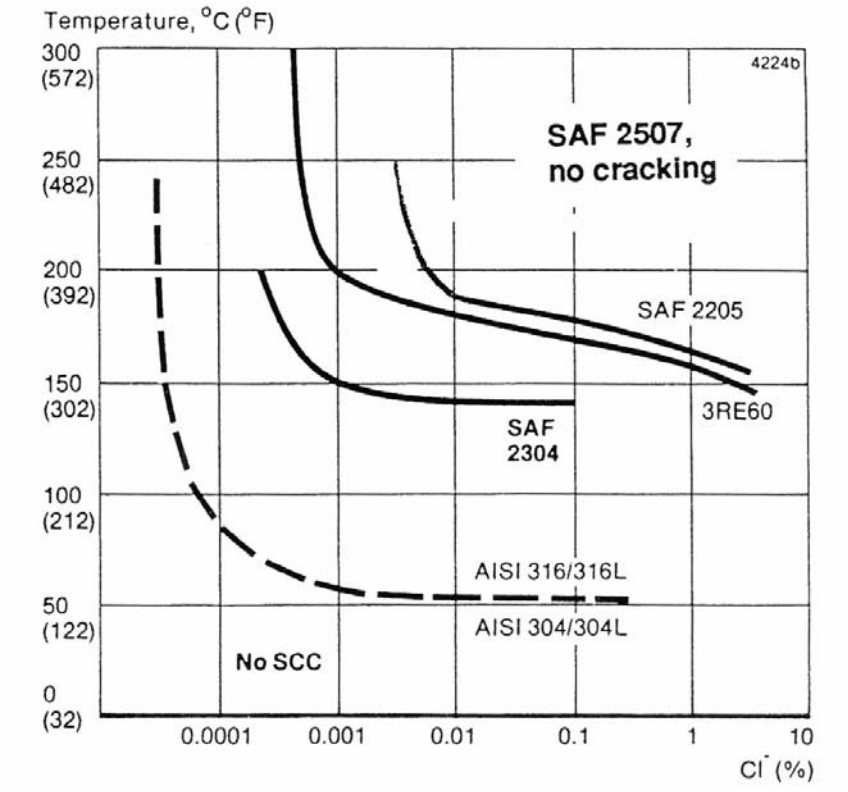

Figure 3-2. Iso-Corrosion Diagram Showing Stress Corrosion Cracking Susceptibility for Various Stainless Steels [2]

In spite of the positive affects, the presence of ferrite in austenite may also cause complex metallurgical reactions that include formation of a variety of secondary phases, all of which have adverse effects on corrosion resistance or mechanical properties, particularly impact toughness. Figure 3-3 shows the possible precipitates in DSS and it is evident that most of these precipitates concern ferrite or ferrite-promoting element such as Cr, Mo and W. These metallurgical reactions can take place over a wide temperature range from 300°C (572°F) to 1000°C (1832°F).

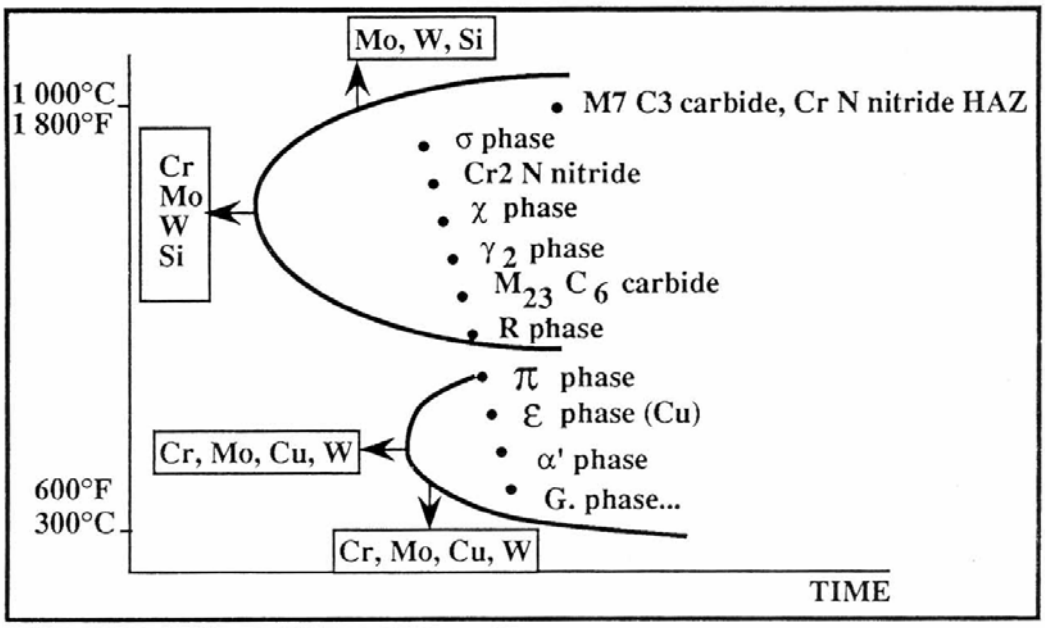

Figure 3-3. Possible Precipitates in Duplex Stainless Steels [2]

2.2.1. Secondary Phases

a) Sigma Phase

The most commonly formed and observed detrimental phase in duplex stainless steels is sigma (σ) phase [2-3, 8-12, 13-19, 22, 24, 90]. Typical chemical composition of sigma phase is Fe-30Cr-4Ni and 4-7 Mo [2], but sometimes as high as 10 Mo [8], depending on the original Mo composition of the alloy. Sigma phase has harmful effects on the mechanical properties, ductility and toughness, and it is detrimental to corrosion resistance of stainless alloys due to its chemical composition. It is evident from the typical composition for sigma phase that the higher Cr and Mo content (compared to the matrix) indicates that the matrix surrounding the sigma phase is depleted in Cr and Mo, which, in general, is detrimental to corrosion resistance.

Sigma precipitates in duplex stainless steels over a wider temperature range and in a shorter time [2, 8-9]. The presence of ferrite enhances the precipitation of sigma phase in many ways [2]. First of all, the composition of sigma is close to that of ferrite. Secondly, the diffusion rate of sigma-forming elements such as Cr, Mo and W in ferrite is 100 times faster in ferrite than that in austenite. Finally, ferrite/austenite interfaces are favorable sites for sigma phase nucleation.

It was also found that sigma phase nucleates preferentially at various locations in duplex stainless steels [2, 9-15]. It can be at ferrite/ferrite/austenite triple points or grow along ferrite/ferrite boundaries [12]. It is further suggested that nucleation is heterogeneous in nature and does not strongly depend on the crystallographic orientation relationships between the phases [12]. In addition, the reason why sigma phase

preferentially grows into ferrite is that ferrite phase is thermodynamically metastable at temperatures where sigma phase precipitates. Thus, formation of sigma is simply the transformation of the ferrite phase from a metastable state to an equilibrium state. Moreover, Atamert and King [12] suggested that the absence of any intragranular precipitation of sigma-phase is indeed a proof of heterogeneous nucleation and that the rate-controlling step is nucleation. According to the isothermal transformation studies of Redjaimia et al. [13] and Wang et al. [14] on 23Cr-5Ni-3Mo and Zeron 100, it was found that sigma phase also nucleates on $M_{23}C_6$ carbides or co-precipitates with secondary austenite. Contrary to what Atamert and King [12] suggested, both groups of authors [13, 14] indicated that the nucleation and growth of sigma is related to the crystallographic orientation relationships.

Identification of sigma phase by chemical composition is not recommended [8, 14]. It has been pointed out that chemical composition of sigma phase may vary when formed in different temperature ranges. Thorvaldsson et al. [16] compared composition of sigma phases in different alloy systems and dramatic differences were observed. In addition, other phases such as chi (χ) phase have similar compositions to sigma phase.

Depending on the chemical composition of the base material, sigma phase can form over a wide range of temperature from 600 °C (1112 °F) to 1000 °C (1832 °F) [11, 14, 15, 17-20]. Super duplex stainless steels tend to have the widest range [11, 14, 15, 18]. It was also found that sigma phase is a more stable phase compared to chi phase and R phase. In fact these two phases dissolve and convert into sigma phase after long time aging.

Solution annealing with fast cooling can remove sigma phase in the as-cast or as-rolled materials. It is also interesting to find that solution annealing at higher temperatures decreases the tendency to form sigma phase [11, 14-15, 17, 18]. The reason behind this phenomenon is that a high solution annealing temperature tends to increase the volume fraction of ferrite, which consequently is diluted with respect to ferrite-forming elements.

The morphology of sigma phase is different when it precipitates at the ferrite/austenite or at ferrite/ferrite interface or co-precipitates with secondary austenite [10,14]. Figure 3-4 shows two micrographs that illustrate different sigma-phase morphologies [12]. Identification of precipitates can be combined with crystallographic criteria. Chi phase, for example, is a type of precipitate that has a composition close to sigma phase but has a completely different crystalline structure [15, 19, 20]. Table 3-2 shows the lattice type, lattice parameters, and space group for sigma and chi and other types of precipitates.

b) Chi Phase

Chi (χ) phase is commonly found in duplex stainless steels but is usually present in much smaller quantities than sigma phase [8, 11, 17, 18, 21-23], however, it is just as harmful as sigma phase to the properties. In fact, because chi phase not only has a similar Cr content, compared to sigma phase, but also a significantly higher Mo content (~20%), chi phase is more detrimental to pitting corrosion resistance than sigma phase.

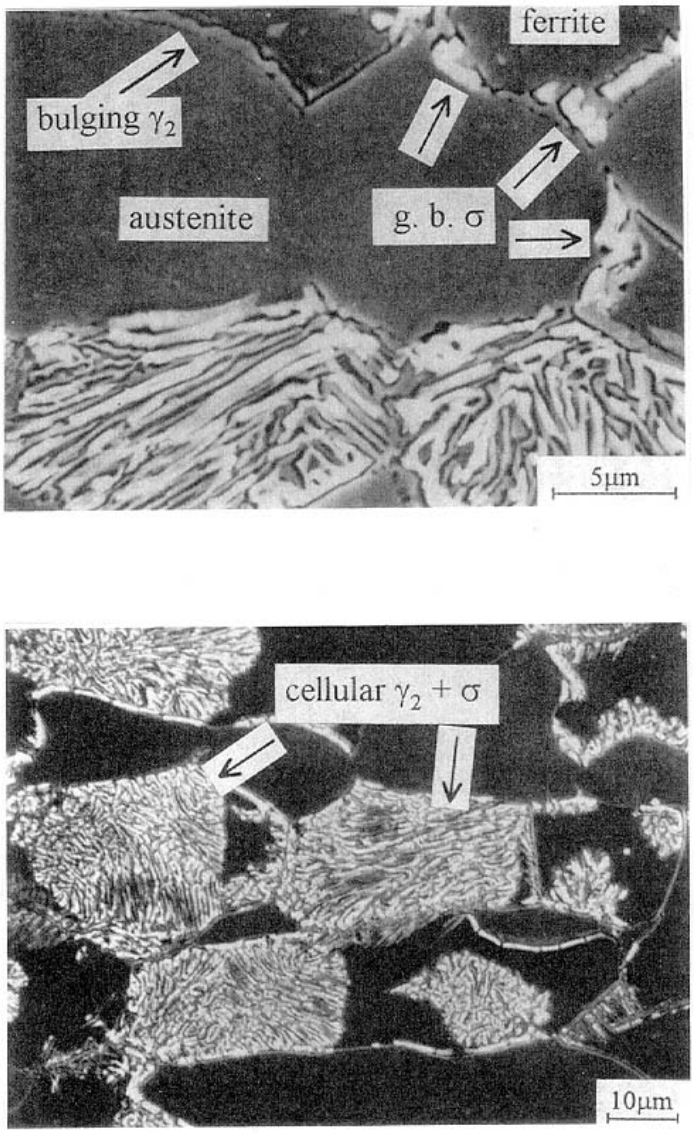

Figure 3-4.Micrographs Showing Different Morphologies of σ Phase [19]

Table 3-2. Crystallographic Date for Various Phases [19]

Type of Precipitate	Lattice Type	Space Group	Lattice Parameter (Å)
δ	BCC	Im3m	a=2.86-2.88
γ/ (γ_2)	FCC	Fm3m	a=3.58-3.62
σ	tetragonal	$P4_2/mnm$	a=8.79, c=4.54
χ	cubic	I43m	a=8.92
R	rhombohedral	R3	a=10.90, c=19.34
π-nitride	cubic	$P4_132$	a=6.47
Cr_2N	hexagonal	P31m	a=4.80, c=4.47
$M_{23}C_6$	cubic	Fm3m	a=10.56-10.65
M_7C_3	hexagonal	Pnma	a=4.52, b=6.99 c=12.11

Chi phase and sigma phase are not distinguishable using optical light microscopy. However, the two phases can be distinguished by TEM crystallographically.

Identifications can also be made easier by using backscattering (BS) SEM due to the difference in chemical composition (i.e., Mo) between the two precipitates.

Chi phase causes a much brighter contrast on BS SEM image than sigma phase. Figure 3-5 shows a micrograph illustrating this effect. For tungsten-containing super duplex stainless steels, the tungsten content in chi phase is also substantially higher than that in sigma phase [21].

Chi phase precipitates in the range of 700 to 900 °C (1292 to 1652 °F) and it precipitates faster at 800 to 850 °C (1472 to 1562 °F). However, upon long-term aging, chi phase will convert into sigma phase.

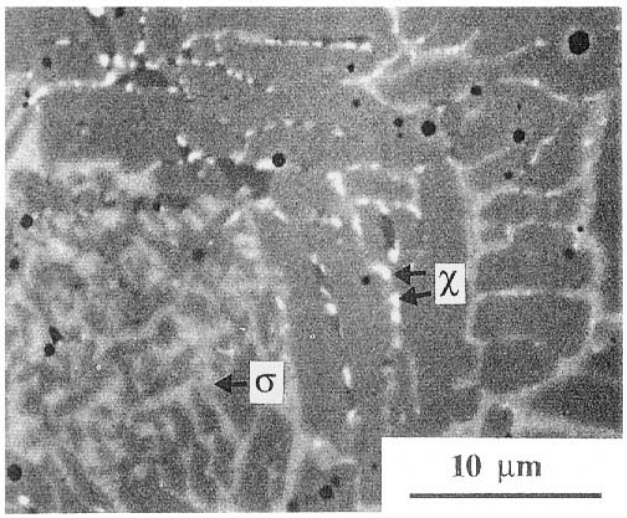

Figure 3-5. Micrograph Showing Different Contrast for Chi Phase and Sigma Phase Due to Difference in Chemical Composition. [16]

c) R Phase

R phase precipitates at 550 to 800 °C (1022 to 1472 °F) both intergranularly and intragranularly with an approximate composition of 30Fe-25Cr-35Mo-6Ni-4Si. R phase is extremely deleterious to pitting corrosion resistance and, like other intermetallic precipitates, detrimental to the toughness of the material.

R phase forms the fastest at the temperature range from 550 to 650 °C (1022°F to 1202 °F). At higher temperatures, the formation of R is rare and R phase particles are converted into sigma-phase after a relatively short aging time.

d) π Phase

π phase, which is often recognized as a nitride, has a proposed ideal chemical formula $Fe_7Mo_{13}N_4$. However, it was found that π phase contains approximately 28% Fe, 35% Cr, 3% Ni and 34% Mo. The approximate formation temperature for π phase is 600 °C (1112 °F). Similar to other intermetallic precipitates discussed above, π phase is also detrimental to toughness and pitting corrosion resistance [15, 18].

e) Secondary Austenite

Secondary austenite [10, 11, 14, 15, 18, 21, 24-28] is also a transformation product of ferrite with FCC crystal structure. The reason that this phase is termed secondary austenite is opposed to primary austenite. The significant difference that exists between the two types of austenite is the chemical composition.

In general, secondary austenite can precipitate in d ferrite by a eutectoid reaction (700~900°C/1290~1650°F), as Widmannstätten precipitates (650~700°C/1200~1290°F) and via a martensitic shear process (650°C/1202°F) [18, 24, 25].

Secondary austenite is usually identified at austenite/ferrite phase boundaries or at the interior of ferrite grains [25]. Whichever location is predominant is determined by the existence of suitable nuclei. Figure 3-6 show different types of morphologies of secondary austenite. It was noted that the morphologies are also related to chemical composition [10, 11, 21, 25]. Secondary austenites have different morphologies and composition than primary austenite. Thus, identification of secondary austenite does not present significant difficulties.

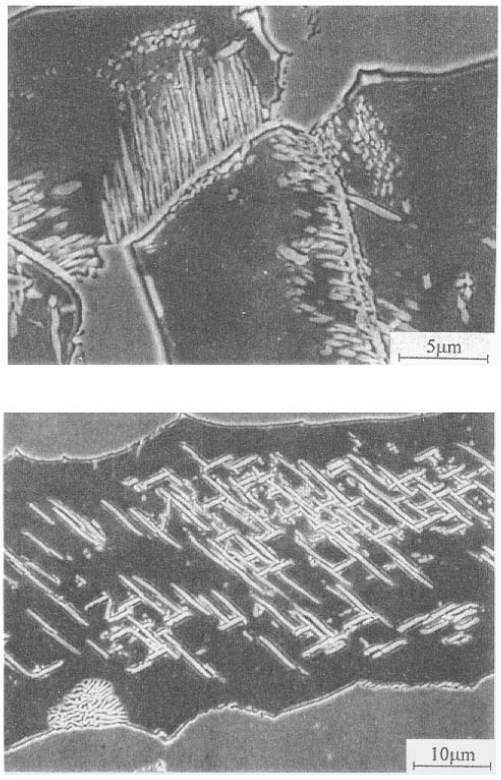

Figure 3-6. Different Secondary Austenite Morphologies [19]

f) Cr_2N

The formation of Cr_2N is likely to occur during rapid cooling from a high solution temperature because supersaturation of nitrogen in ferrite will occur as a consequence. The precipitation of Cr_2N is observed in the temperature range 700-900 °C (1292-1652 °F) and is mainly seen in high ferrite content regions [9, 11, 18, 29-32]. Nitrogen content affects the formation of Cr_2N. For a given cooling rate there is an intermediate nitrogen content that will result in the largest amount of Cr_2N [29].

Cr_2N was found to be elongated particles often precipitate intragranularly and globular particles intergranularly precipitate either at ferrite/ferrite grain boundaries or ferrite/austenite phase boundaries [9, 30].

g) Carbides

Carbides precipitate particular during processing in the temperature range of 800°F - 1500°F, predominantly at ferrite/austenite boundaries and result in reduction in intergranular corrosion resistance. They are not as significant in super duplex stainless steels than in traditional duplex stainless steels due to the lower carbon content.

h) α-Prime

α-Prime is a chromium-rich precipitate. Its precipitation is very much temperature dependent during the temperature range of 650°F-950°F and with increasing ferrite and Mo content. At 885°F, α-Prime forms in about ten hours. At 570°F, material

will loose toughness in 25 years. This limits the DSS to a maximum operation temperature of 550°F [3].

i) Copper Rich Precipitation of Less Common Phases

Copper rich precipitates have been observed in copper rich duplex stainless steels [18, 28, 33, 34]. The Cu-rich phases are very fine and are often preferentially attacked by electrolytic thinning thus leaving holes at grain boundaries [28, 34]. The effect of Cu precipitates with respect to toughness or corrosion resistance is not well known. However, research showed that copper precipitates can refine the microstructure, particularly austenite [33].

2.2.2. Microstructural Investigation Techniques

The evaluation of duplex stainless steel microstructures requires proper etching techniques for optical light microscopy (OLM) and scanning electron microscopy (SEM). Various etchants and electro-chemical etching techniques have been developed to help reveal duplex stainless steel microstructures [21, 23, 34, 35].

Some of the most often mentioned etchants/etching methods for DSSs and their effects are as follows:

1) Electrolytically etching in 10 % KOH solution at 5V. The etchant colored the ferrite yellow, sigma phase reddish brown, and the carbide black. Austenitic phase remained unattacked on etching [28].

2) Nilson et al. [21] developed a two-step electrolytic etching technique to obtain contrast from intermetallic phase. First use dilute nitric acid (HNO3) to make phase boundaries

visible, followed by saturated potassium hydroxide (KOH) to enhance the contrast of the precipitates. The authors also utilized a dye etchant called Beraha etchant to produce as-welded microstructures with secondary austenite in high contrast. The etchant consists of 2.2 g $(NH_4)HF_2$, 0.2 g $K_2S_2O_5$, 18 ml HCl, 100 ml distilled H_2O. Etching for a time in the range 10 to 20 seconds colors ferrite blue while austenite remains virtually uncolored.

3) Cheng et al. [35] applied a solution made of 50 g $K_3Fe(CN)_6$, 30 g KOH and 100 ml distilled water. Heating is required for this solution.

4) Sriram and Tromans [34] used Kallings reagent (1.5 g $CuCl_2$, 33 ml HCl, 33 ml alcohol and 33 ml distilled water) that etches ferrite dark and austenite light.

5) Electrolytic etching with 10% Oxalic acid or 40% NaOH solution is also commonly applied methods for etching duplex stainless steels.

6) Glyceregia, a mixture of HNO_3, HCl and glycerol, is another alternative for etching duplex stainless steels.

OLM is not sufficiently sensitive to identify secondary precipitates. Even SEM/EDX may not be sufficient to identify different precipitates and same precipitates formed at different temperature. Thus, to precisely identify secondary particles, transmission electron microscopy (TEM) is necessary. A typical sample thinning solution consists of 20% perchloric acid, 10% glycerol, and 70% ethyl alcohol. Thinning is usually done at 0 °C (32 °F) and 25-45 V using a “twin jet” polishing unit [9, 32].

2.2.3. Effect of Alloying Elements

Alloying elements contribute to the formation of ferrite/austenite microstructure. Each one of them has peculiar effects on the development of the structure and properties. Further, previous discussion of secondary phases indicates that precipitation of secondary particles involve Cr, Mo, W, Cu, N and other alloying elements. Thus, it is important to understand the role that each element plays in this complex metallurgical system.

Cr: It is well known that chromium is the essential element that makes steels stainless. Cr contents over 22% show marked increase in pitting corrosion resistance and crevice corrosion resistance. However, because Cr is also a strong sigma and ferrite former, it is usually held below 27% in order to retain ductility, toughness and corrosion resistance. It is noted that in heavy section castings, Cr is generally held to the low side of the range to reduce cracking in the as-cast condition [36].

Mo: Mo, like chromium, it is also a strong ferrite former, and has similar effects as Cr does on properties. Also, in case of heavy sections, Mo shall be held at the low side of the specified range for the reason of increased cracking susceptibility. However, research shows that if chloride stress corrosion cracking is a potential problem, Mo content should be held to a minimum of 3.5%.

Ni: Ni is an austenite promoting element. Its greatest effect is to balance the microstructure to provide the proper ferrite/austenite ratio. It also affects the corrosion and mechanical properties as well as the formation of secondary particles because Ni

stabilizes austenite [22, 36-39]. But excessive Ni results in an increase in the austenite content, promoting a greater concentration of ferrite stabilizer elements (Cr, Mo) in the remaining ferrite. This highly alloyed ferrite is more susceptible to the precipitation of sigma phase. Moreover, according to Varol et al. [22], Ni effectively increases the temperatures range over which sigma phase forms.

N: N is a particularly useful alloying element in DSS

1) It improves localized corrosion resistance and raises the critical pitting temperature and is 16 times more effective than chromium in this respect (see PREN equation);

2) It is a strong austenite former. In fact, nitrogen is about 20 times more effective than Ni as an austenite stabilizer on a weight percent basis [22], therefore, savings with regard to nickel often can be made;

3) It increases yield strength by solid solution strengthening, and unlike carbon, does not promote sensitization.

However, like other elements, the introduction of nitrogen also introduces metallurgical complexity into the duplex stainless steels. The solubility of nitrogen in liquid steel is the first concern. The importance of this is to prevent the occurrence of nitrogen degassing on casting solidification [40]. The nitrogen solubility in steels is highly composition dependent [22, 26, 40]. It was found that increasing the Cr, Mo and Mn content results in an increase in the equilibrium nitrogen solubility of the steel, while increasing the Si, Cu and content results in a decrease Ni [22, 26, 27, 37, 40]. Duplex stainless steels have been made with up to 0.87% N in a pressurized electroslag process [9].

SCRATA [36] recommends, from a foundry point of view, that nitrogen should not exceed about 0.14%, which is near the lower end of ASTM A890 specified range 0.10-0.30. Anson et al. [40], however, have shown that it is possible to safely increase the level of nitrogen in a duplex stainless alloy, at least for the 22Cr-5Ni-4Mo types. In addition, it has been reported that castings can have nitrogen levels as high as 0.28% without gas porosity defects [3].

The effect of nitrogen in stabilizing austenite is shown in Figure 3-7 [26]. The figure clearly shows that the addition of nitrogen is associated with an increase in the A_0 temperature, leading not only to an increase in austenite content at peak temperatures, but also transformation starts at higher temperatures during casting or welding cooling cycles [22]. Figure 3-8 also illustrates the effect of nitrogen on ferrite/austenite content [3].

W and Cu: W and Cu are two minor elements that are added to improving corrosion resistance. However, the addition of these two elements also complicates the already heterogeneous metallurgical system in DSS.

The addition of W causes more rapid kinetics with regard to intermetallic phase formation and a higher dissolution temperature for intermetallic phases compared with W-free DSS [21]. Hertzman et al. [41, 42] showed that super DSS welded with W-rich or W-Cu-rich filler metal are prone to precipitation of Chi-phase and secondary austenite. In addition, W acting like Cr and Mo, promotes sigma phase formation [12] and., it was indicated that the amount of Cr_2N tended to be increased by W additions.

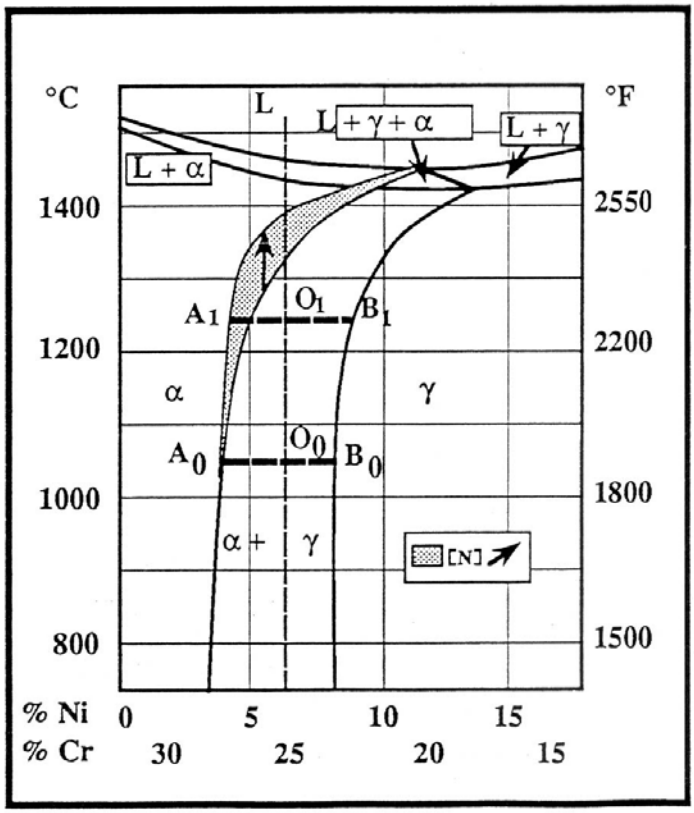

Figure 3-7. Schematic Effect of Nitrogen Additions on the Pseudo Binary Cr-Ni-68 Fe Phase Diagram [34]

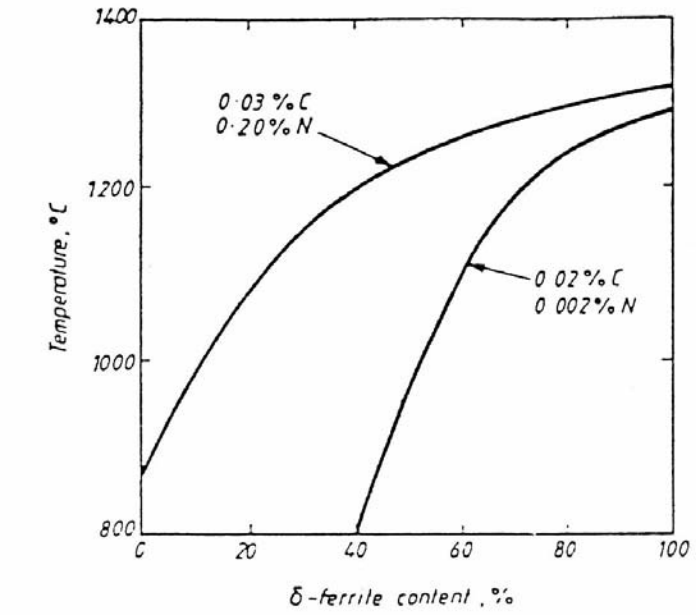

Figure 3-8. Effects of Peak Temperature and Nitrogen Content on the Ferrite Content [2]

Both Ogawa et al. [42] and Nilsson et al. [21] indicated that tungsten is generally beneficial when below 2%. Noted that CD-3MWCuN (cast Zeron 100), the only tungsten bearing ASTM standardized casting, contains only 0.5 to 1% tungsten, which is well below the maximum 2% limit that Ogawa et al. and Nilsson et al. suggest.

Cu promotes austenite formation if in a significant amount, such as 2% [43]. In applications like sulphuric acid or pollution equipment, Cu is really needed to impart the corrosion resistance [44]. Figure 3-9 shows the effect of Cu on corrosion rate in sulphuric acid environment [45].

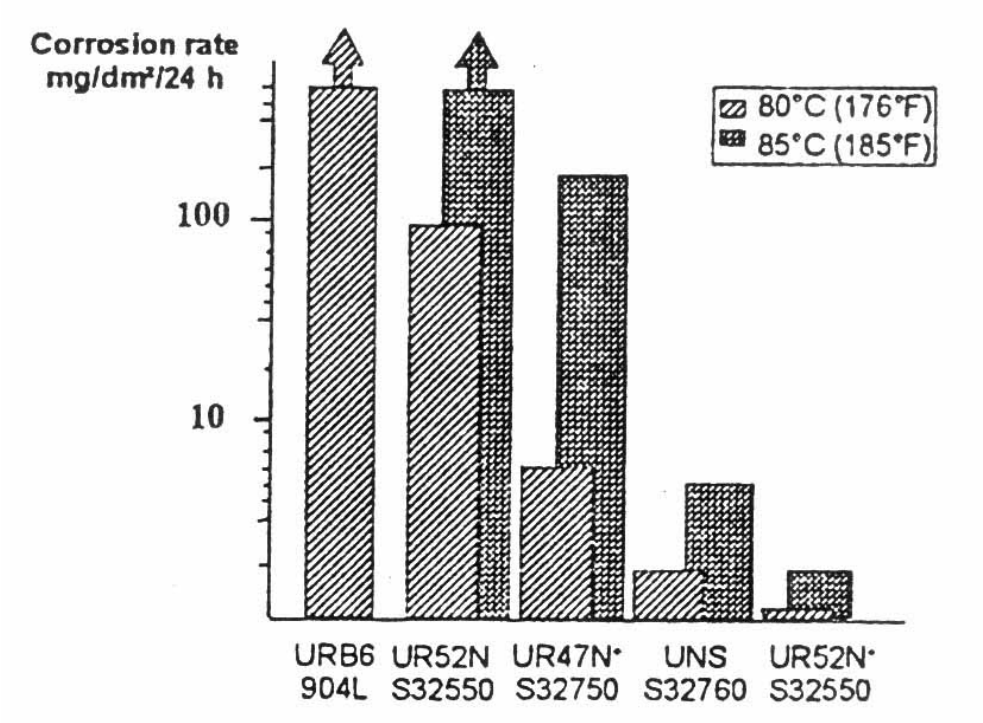

Figure 3-9. Corrosion Rate in 10% H_2SO_4 + 500 ppm Cl-Aerated, at 80°Cand 85°C [45]

Mn: Mn is not used to add intentionally. Though steels with maximum 0.1% Mn is found to have good corrosion resistance, it is also stated that Mn tends to combine with sulfur to form inclusions which weaken the passive film. The inclusions also promote galvanic cells and form hydrogen sulfide gas in acid solutions [3]. However, DSSs with up to 12% Mn addition have been developed in recent years [46-48]. Research showed that Mn-bearing DSS with about 0.2% N provide an economic grades capable of competing with traditional grades of stainless steels [46].

Si: Si is added to cast alloys to increase fluidity of the liquid metal. However, high silicon levels should be avoided as silicon is a strong sigma former [3, 36, 49]. Taylor [3] indicates that "silicon in combination with molybdenum can be particularly dangerous". SCRATA recommends that a 0.5-0.6% Si content is the best choice for duplex stainless castings.

2.2.4. Effect of Solution Heat Treating

Duplex stainless steels form harmful intermetallic phases during a slow cool. Slow cooling in the mold or due to a heavy section size can lead to the formation of embrittling intermetallic phases and result in undesirable mechanical properties and poor corrosion resistance. It is essentially important for treating heavy section casting with proper solution annealing to restore the properties of cast duplex stainless steels. Solution annealing is just as important to wrought materials as it is to cast materials.

As previously discussed, Ni increases the stability of sigma phase and Cr and Mo, both promote the formation of the sigma phase and other intermetallic phases. This

influence of elements on the stability of secondary phases also has a bearing on selecting solution annealing temperatures for duplex stainless alloys. Table 3-3 cites the exact heat treatment requirements given by ASTM A890-94a for some of the cast DSS alloys in A890.

2.2.4.1. Effect of Heat Treatment Temperature

Figure 3-10 is the modified ternary section of the Fe-Cr-Ni phase diagram. From the diagram, it is obvious that high solution annealing temperature results in an increase in ferrite content [10, 26, 27, 50-52]. Figure 3-8 [3] and Figure 3-11 [3] also illustrates this effect. In addition to higher ferrite content, higher solution annealing temperatures also have the following effects:

1) Lowers the partitioning coefficients [26]. As a result, the material is less sensitive to intermetallic phase transformations but more sensitive to secondary austenite and Cr_2N formation [26, 27].

2) Decreases chromium content and increases nickel content in the ferrite, as shown in Figure 3-11. Lai et al. [10] further demonstrated that this affect consequently slows the formation of sigma phase dramatically, which is consistent with Charles [26] and Kuroda and Matsuda [27].

3) Changes the ferrite and austenite morphologies. It was observed by Radenkovic et al. [50] that the morphology of the austenite changes from a relatively discontinuous network to continuous grain boundary morphology as the solution annealing temperature increases. In addition, the initially irregular shape boundaries

Table 3-3. Heat Treatment Requirements by ASTM A890-94a

Grade	Heat Treatment
4A	Heat to 1120 °C (2050 °F) for sufficient time to heat casting uniformly to temperature and water quench, or the casting may be furnace cooled to 1010 °C (1850 °F) minimum, hold for 15 minutes minimum and then water quench. A rapid cool by other means may be employed in lieu of water quench.
5A	Heat to 1120 °C (2050 °F) minimum, hold for sufficient time to heat casting to temperature, furnace cool to 1045 °C (1910 °F) minimum, quench in water or rapid cool by other means.
6A	Heat to 1100 °C (2010 °F) minimum, hold for sufficient time to heat casting uniformly to temperature, quench in water or cool rapidly by other means.
1B	Heat to 1040 °C (1900 °F) minimum, hold for sufficient time to heat casting uniformly to temperature, quench in water or rapid cool by other means.

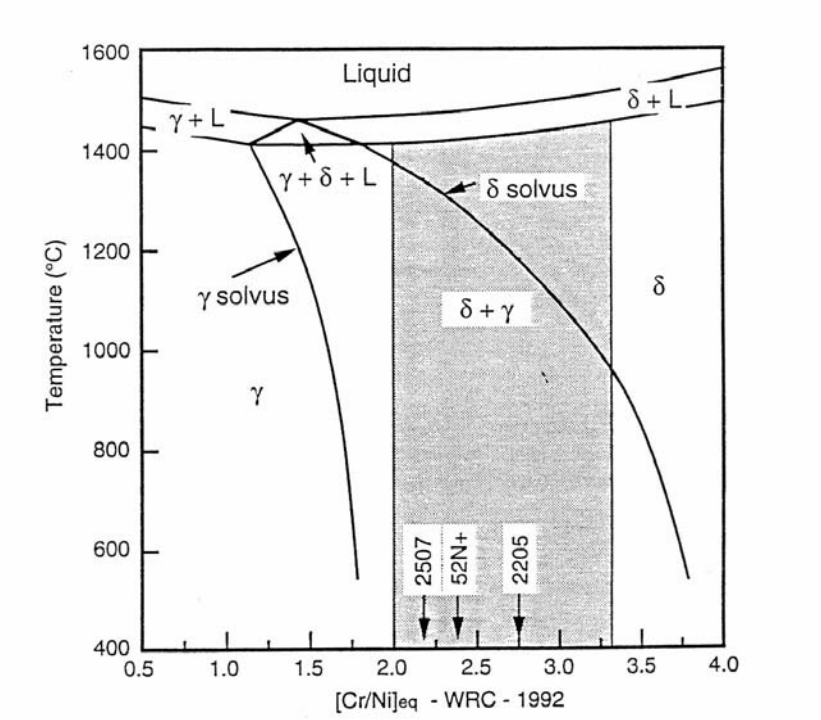

Figure 3-10. Modified Ternary Section of Fe-Cr-Ni Phase Diagram Plotted Using the WRC-1992 Equivalent Relationships

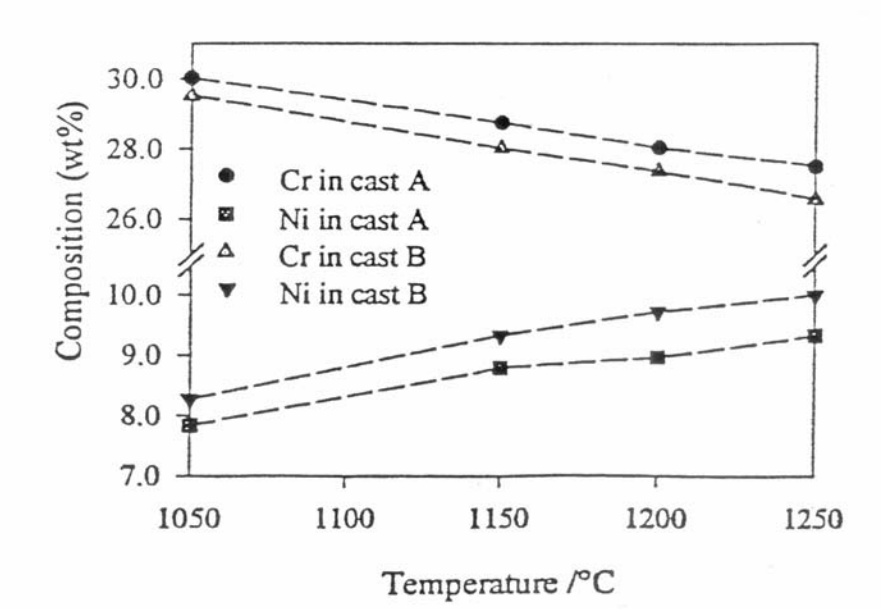

Figure 3-11. Effect of Annealing Temperature on Ferrite and Austenite Content

become smoother with an increase of the solution annealing temperature. Kuroda and Mastsuda [27] also noted that grain size increases with increasing peak temperature.

In summary, increasing the solution annealing temperature increases the ferrite content and thus lowers the impact toughness, ductility and corrosion resistance, which indicates the high solution annealing temperature may not be beneficial. However, depending on the alloy composition, particularly the nickel and nitrogen content, solution annealing temperature may have to be raised to ensure a complete dissolution of sigma phase and obtain a certain ferrite level. Therefore, solution annealing temperature should be chosen on the basis of specific heat chemistry rather than selecting a temperature based on the ASTM required minimum in Table 3-3.

2.2.4.2. Effect of other Heat Treatment Variables

Figure 3-12 [10] shows the effect of heat treatment time on the ferrite content. It is evident that the effect is also affected by the peak temperature, i.e., the higher the solution annealing temperature, the stronger the effect of time on the ferrite content. Note that grain growth is also faster at higher temperatures, which makes heat treatment at excessive temperatures undesirable.

Kotecki [51] examined the step annealing/cooling procedures using SAF 2205 and Ferralium 255 weld metals. No particular advantages or disadvantages were observed.

3. Corrosion Behavior of DSS

It is known that duplex stainless steels have excellent stress corrosion cracking (SCC) resistance due to the presence of combined ferrite and austenite microstructure. This is shown in the previous part. Thus, SCC of duplex stainless steels will not be discussed in this review.

The review on corrosion is focused on pitting corrosion and intergranular corrosion of duplex stainless steels, as these two corrosion mechanisms will be the primary subjects to be investigated in this program.

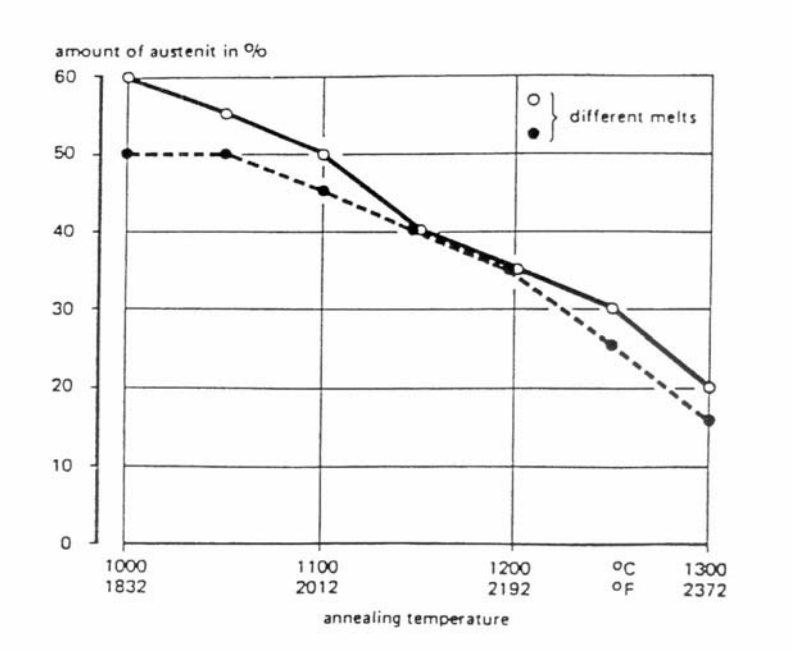

Figure 3-12. Effect of Solution Annealing Temperatures on the Chemical Composition of the Ferrite and Austenite Phases

3.1. Pitting Corrosion

The alloying elements governing the pitting resistance of stainless steels in chloride environments are essentially chromium, molybdenum and nitrogen. Attempts have been made to establish a mathematical formula describing the relationship between the amount of these elements and the pitting corrosion potential. The most commonly used expression is the so-called pitting resistance equivalent number (PREN), which has been introduced in the previous section of this review. However, many researchers [18, 34, 38-39, 53-55] have pointed out that PREN calculated from the bulk alloy composition may be misleading in duplex alloys because they contain austenite and ferrite, which have different compositions. Austenite is enriched with N whereas ferrite is richer in Cr and Mo. It has been found that, in general, austenite has a lower PREN than ferrite in the base material, whereas austenite has higher PREN than ferrite in the weld metal. However, Bernhardsson [54] showed theoretical calculation results that, by adjusting the ferrite/austenite balance via adjusting Ni and the heat treatment temperature, it is possible to achieve an equal PREN for both ferrite and austenite (Figure 3-13). With the introduction of tungsten as an active alloying element, the following expression has been proposed:

$$PREW^{*} = Cr + 3.3\,Mo + 1.15\,W + 16\,N \qquad \text{Equation 2.}^{*}$$

* Source: Gunn, R. N., “Duplex Stainless Steels-Microstructure, Properties and Applications,” Abington Publishing, Cambridge, England, 1997, p 6.[1]. Noted that the CPT for SAF 2507 can be as high as 80 °C (176 °F). However, it must be realized that these results are obtained for

optimum conditions; that is, the material is well heat treated, the composition is well balanced and surface is well prepared. Realistically, materials in service may not achieve the CPT obtained in laboratory experiments.

To achieve the best pitting corrosion resistance, the physical metallurgy and welding metallurgy of duplex stainless steels must be understood since the pitting resistance performance is a reflection of the microstructural integrity. The following areas that need to be addressed are:

1) Balance ferrite and austenite: too much ferrite can cause the formation of Cr2N or other intermetallic phases and too much austenite will not only reduce the nitrogen concentration in austenite but also will result in greater segregation of Cr and Mo in the austenite [56].

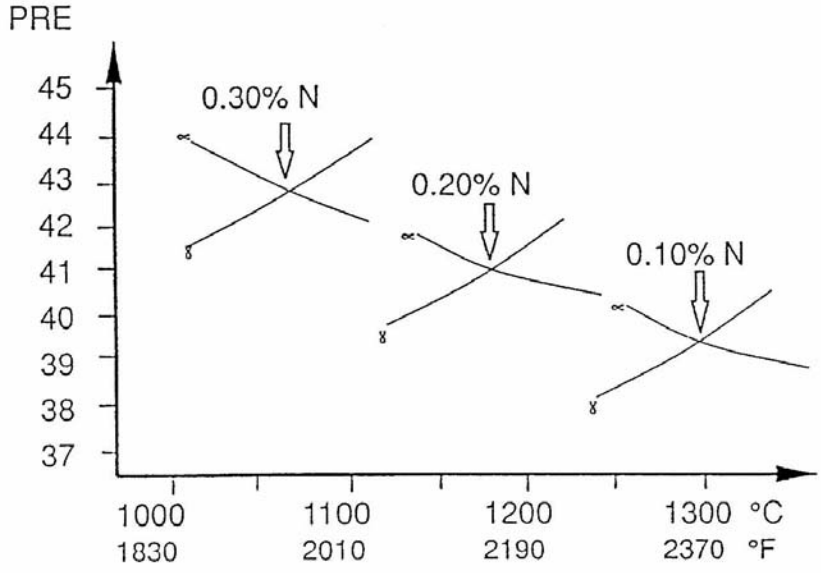

Figure 3-13. Theoretical Calculations Based on Alloys with 25% Cr and 4% Mo. Ni was varied to keep Constant Ferrite Content

2) Control Ni content: Ni only should be used for controlling phase balance. High Ni will result in too much austenite and not enough Ni will promote the formation of too much ferrite. Higher Ni content also stabilizes sigma phase.

3) Select proper heat treatment temperature: unlike the solution heat treatment of fully austenitic stainless steels, solution annealing temperature has a significant effect on the balance of ferrite/austenite in duplex materials. For a given nitrogen content, the higher the solution annealing temperature, the higher the ferrite content will become.

4) Select proper welding procedures: this includes selection of welding parameters, joint geometry, heat input, filler metal and shielding/backing gases as needed. Excessive dilution and extremely fast or slow cooling rates should all be avoided.

3.2. Intergranular Corrosion

As mentioned in the Introduction, one advantage duplex stainless steels have over austenitic stainless steels is enhanced intergranular corrosion resistance. Studies [20, 24, 28, 57-59] have shown that if duplex stainless steels are properly solution annealed, i.e., free of intermetallic compounds and chromium carbides, then duplex stainless steels are immune to intergranular corrosion. The corrosion rates measured/calculated are generated by general corrosion, which is influenced by alloy composition, particularly Mo. It was found that a high Mo content in oxidizing environments would result in higher general corrosion rates [53].

Phase balance also plays an also an important role in improving intergranular corrosion resistance. Gooch [56] indicated that high ferrite weld HAZ's are sensitive to intergranular corrosion. However, if an adequate amount of austenite is formed, duplex

stainless steels are resistant to intergranular attack. Thus, microstructure control is again of paramount importance.

4. Welding of DSS

4.1. Welding Metallurgy

As welding is an important method in castings upgrading and fabrication, to weld DSS, it is important to understand how duplex stainless steels transform at different cooling rates, the effect of peak temperature in the HAZ and filler metal dilution.

4.1.1. Segregation of Alloying Elements

Farrar [49] pointed out that it is the local microsegregation of chromium and molybdenum but not the bulk concentration that controls the transformation of delta-ferrite and formation of intermetallic phases. Diffusion of Cr and Mo during ferrite to austenite transformation strongly influences the formation of intermetallic phases.

Atamert and King [60] found that Cr partitioning was not significantly influenced by temperature. Molybdenum, however, was found to partition preferentially to ferrite as temperature decreases. A strong partitioning of nickel to austenite was observed to decrease gradually with increasing temperature. Nitrogen was found to have the most profound effect on phase balance, increasing the amount of austenite and reducing the amount of ferrite. The volume fraction of austenite is highly sensitive to small nitrogen additions, which suggests that the phase balance in the weld metal can be controlled successfully by nitrogen.

Ogawa and Koseki [38] conducted similar investigations. These authors found that among Cr, Mo and Ni, the microsegregation of Ni and Mo is more pronounced than that of Cr, and Ni is more pronounced than Mo. However, the reason was not clear. It was also found that partitioning of Cr, Mo and Ni during ferrite solidification is not as great as in austenite solidification. Furthermore, it is indicated that the partitioning of Cr, Mo and Ni between the ferrite and the austenite was not significant in welds. However an increase in Ni and/or nitrogen promoted partitioning by raising the austenite transformation temperature. Again, indicate nitrogen has a dominant effect on the formation of weld metal austenite.

4.1.2. Heat Affected Zone (HAZ)

The HAZ experiences a range of thermal histories with peak temperatures from ambient to the solidus, adjacent to the weld. With fairly rapid heating and cooling, and in multipass welds, repeated exposure to elevated temperatures, the total thermal cycle at any one point in the HAZ is often complicated. Thus, acquiring an understanding of metallurgical consequences in terms of ferrite/austenite balance, precipitation of secondary phases, grain growth and the width of the HAZ, all of which consequently affect mechanical properties and corrosion resistance of the steel, is of vital importance.

The importance of controlling the ferrite-austenite balance in the weld HAZ is because too high a ferrite content will significantly deteriorate intergranular corrosion resistance [56], and decrease impact toughness [32, 61-72].

For a given plate thickness, the higher the heat input, the slower the cooling rate. Meanwhile, for a given heat input, the thicker the plate, the faster the cooling rate. Thus,

it is important to realize that the welding heat input cannot be considered alone. However, for the sake of the following discussion, the plate thickness and joint configuration is assumed to be the same.

For duplex stainless steels, it has been found that ferrite content is a function of heat input/cooling rate. The lower the heat input, the higher the ferrite content and the lower the impact toughness [32, 61-72]. A simple explanation for the phenomenon is that the higher cooling rates suppress the diffusion-controlled processes in austenite reformation, hence, the original phase ratio of ferrite to austenite is shifted toward higher ferrite content [32] (Figure 3-14). The transformation rate is the fastest at approximately 850 °C (1562 °F) in Fe-C-Cr-Ni alloys. The nose is shifted upwards and also towards the left on the TTT axes with increasing levels of austenite stabilizing elements such as nickel and nitrogen. For super duplex stainless steels, the nose of the C-curve is at about 1050 °C (1922 °F) and the transformation to g starts within a few seconds at this temperature.

High cooling rates do reduce the tendency of sigma and chi precipitation. But Lippold et al. [69] and Kirineva and Hannerz [70] showed the presence of chromium-rich nitrides (Cr_2N) is observed over a wide range of cooling rates and the effect is particularly evident for microstructures with a high proportion of ferrite (usually the result of a fast cooling rate). Increased ferrite content and increased nitrogen levels cause a risk of chromium nitride formation in ferrite; due to the lower solubility of nitrogen in ferrite.

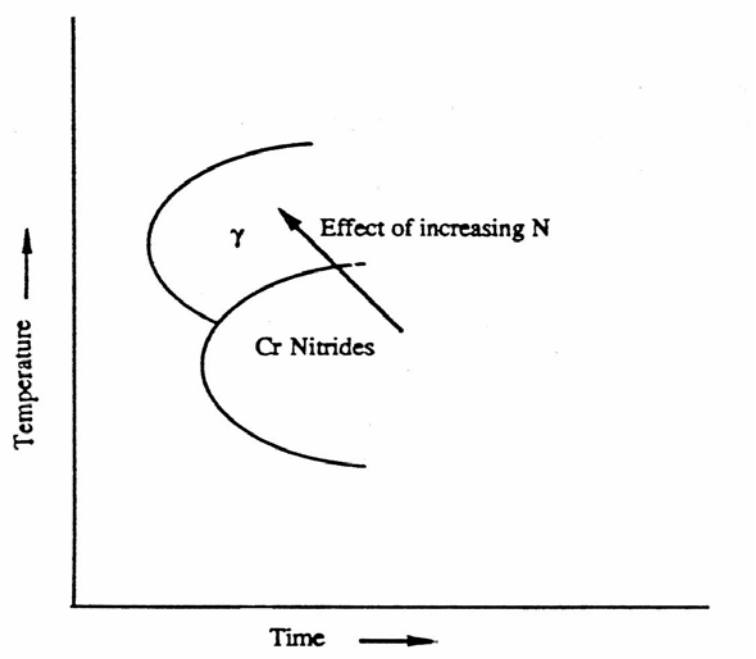

Figure 3-14. Schematic TTT Diagram showing the C-Curve Kinetics and the Effect of Increasing Nitrogen on the Austenite and Cr_2N [32]

Excessively high heat input may reduce the ferrite content but the risk of intermetallic precipitation significantly increases. In addition, high heat input usually results in the material being at peak temperatures for longer times and thus substantial grain growth may occur (at least for wrought alloys), which consequently, lowers the impact toughness [32, 69, 70, 73, 74].

As mentioned previously, alloying elements, particular nickel and nitrogen, can raise the temperature range in which ferrite transforms to austenite upon cooling. Thus, studies that compare sensitivity with respect to cooling rate for different grades of duplex stainless steels have been conducted.

Research indicated that ferrite level in the HAZ of 2205 alloy is higher than 2507. This is believed due to the greater temperature range between the solidus and ferrite solvus temperature of 2507 [69, 71, 67]. Figure 3-10 and 3-15 [70] illustrates the results.

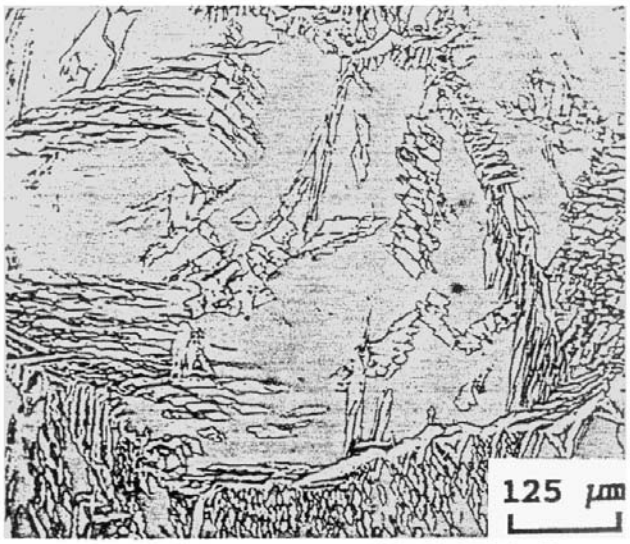

Microstructure of SAF 2205 after Gleeble simulation $\Delta t_{12/8}$ = 93.0 s

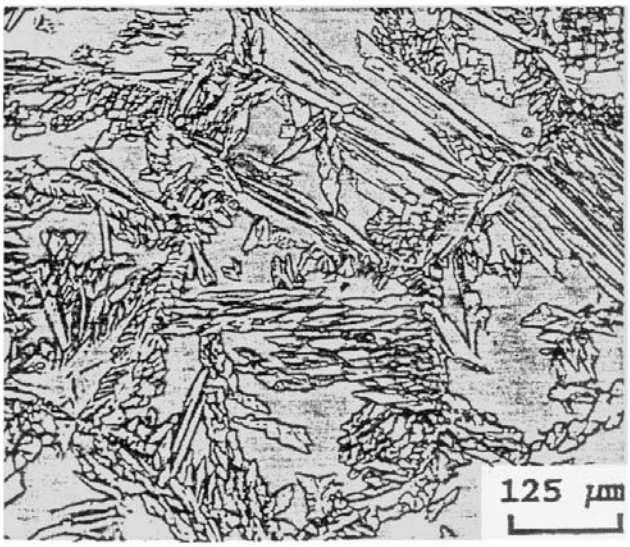

Microstructure of SAF 2507 after Gleeble simulation $\Delta t_{12/8}$ = 93.5 s

Figure 3-15. Micrographs Showing Microstructures of SAF 2205 and 2507 after Gleeble simulation at Dt = 93.0 s

Lippold et al. [75] compared the effect of cooling rate on Alloy SAF 2205 and Ferralium 255, which has higher chromium content but similar nickel and nitrogen content. The results show that for cooling rates ranging from 2C°(3.6F°)/min. to 50C°(90F°)/min., the ferrite content in the HAZ is nearly identical for both alloys, which again demonstrates that nickel and nitrogen are dominant elements in controlling ferrite content.

Hoffmeister and Lothongkum [71] investigated the effect of nitrogen by varying the nitrogen content in super duplex stainless steels and found that increasing the nitrogen content not only raised the A4 temperature but also accelerated the ferrite to austenite transformation, which is consistent with the previous discussion. In addition, the authors indicated that a medium nitrogen content, such as ~0.10%, can be detrimental due to precipitation of Cr_2N when the cooling rate is high.

Nickel and nitrogen also stabilize austenite and delay austenite transformation to ferrite to higher temperatures upon heating. This particular aspect was of interest in a study of the effect of peak temperature and time at peak temperature for different grades of duplex stainless steels.

The welding thermal cycle peak temperature most often studied by researchers is 1350 °C (2462 °F), at which ferritization occurs even for super duplex stainless steels. In general, for a given cooling rate, the higher the peak temperature the higher the ferrite content. However, heating rate and base metal structure also affect the final ferrite and austenite balance [32, 69]. Fast heating rates retard the dissolution of the austenite and thus may prevent a high ferrite content in the HAZ [32, 69]. In addition, for wrought materials the interphase spacing may also affect the ferrite and austenite content in the HAZ [32].

High peak temperatures also may cause grain growth problems in wrought materials; lower impact toughness [32, 69, 70, 73, 74]. However, peak temperature is not the only factor that influences grain growth in the HAZ. Ferrite grain growth highly depends on the heat input and cooling rate. Furthermore, grain growth is controlled by dissolution of austenite. Atamert and King [32] indicated that when the spacing between austenite particles is large, grain growth is extensive. Interestingly enough, according to Ferreira and Hertzman [74], the ferrite grain size had a strong influence on the austenite reformation rate. That is, the larger the ferrite grain size, the lower the austenite content, which is another reason why higher peak temperature lowered the austenite content in the HAZ.

Draugelates et al. [65, 66] investigated the effect of peak temperature and cooling time on the HAZ structure in cast duplex stainless steels. No significant differences were found compared to the above discussion. However, the authors did not discuss the grain growth issue for cast duplex stainless steels, which already exhibit a larger grain size than wrought materials. Unfortunately, this subject was not discussed elsewhere either.

All the above discussion concerning the HAZ was limited to single pass welding. It is important to understand the effect of reheating on the HAZ structure since multipass welding is a requirement in industrial practice.

In multipass weld deposits, the HAZ from the first cycle can be reheated by subsequent passes, to a degree dependent on the position of the HAZ relative to the heat source. Figure 3-16, from Atamert and King [32] schematically shows six regions that experience different thermal cycles. It is evident that not all HAZ's (regions 1 and 2) are affected by the second cycle. However, regions that are affected by the second thermal

cycle may experience significant microstructural change. In multipass welds, the underlying weld metal is also reheated by the deposition of each subsequent pass. Atamert et al. [76] characterized four regions, shown in Figure 3-17, in their analysis. It was found that region 2, in general, has a significantly lower austenite volume, which is not desirable due to reduced toughness and corrosion resistance. However, the authors found that a low austenite content in region 2 is not the case in low heat input welds and suggested that time available for transformation to d ferrite is restricted by the rapid heating and cooling rates associated with low heat input. The authors also performed computer modeling, which indicated that the low austenite region 2 can be eliminated; at least for GTA welding.

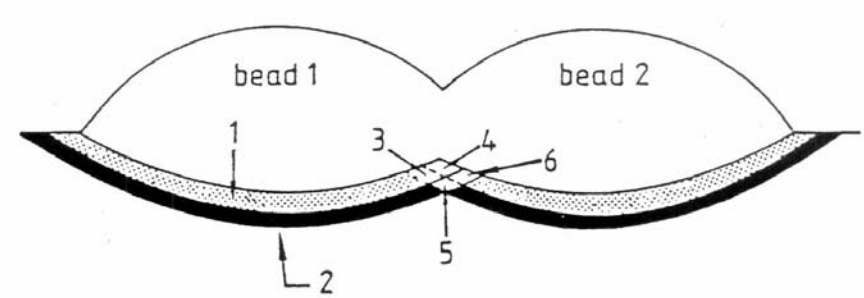

Region	First cycle	Second cycle
1	$T_{peak} > T_\delta$	...
2	$T_f < T_{peak} < T_\delta$	...
3	$T_{peak} > T_\delta$	$T_f < T_{peak} < T_\delta$
4	$T_{peak} > T_\delta$	$T_{peak} > T_\delta$
5	$T_f < T_{peak} < T_\delta$	$T_f < T_{peak} < T_\delta$
6	$T_f < T_{peak} < T_\delta$	$T_{peak} > T_\delta$

Figure 3-16. Schematic Showing HAZs Experience Different Thermal Cycles [32]

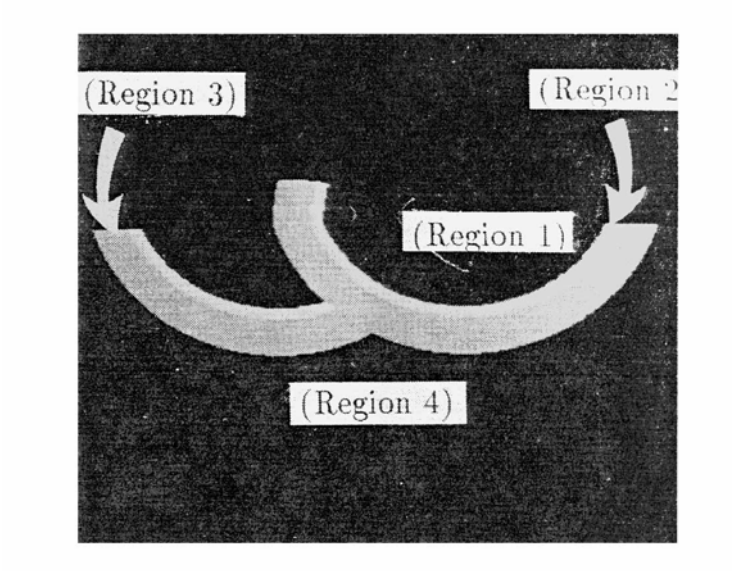

Region 1	Peak Temp. > Ts
Region 2	Ts > Peak Temp. > Td
Region 3	Td > Peak Temp. > Tf
Region 4	Tf > Peak Temp.

Where Ts = solidus temperature

Td = ferritization temperature

Tf = a temperature high enough to allow precipitation of austenite

Figure 3-17. Schematic Diagram Illustrating the Relative Positions of the Different Thermal Cycles in a Two Pass Weld Deposit [70]

A maximum interpass temperature of 150 °C (302 °F) is usually recommended for multipass welding of duplex stainless steels [77, 78]. Higher interpass temperature results in a slower cooling rate, which for austenitic stainless steels may cause

sensitization and for duplex stainless steel may cause precipitation of various undesirable secondary phases. Since no systematic research has been conducted on this subject, contradictory speculation exists on which type of duplex stainless steel can tolerate higher interpass temperature without forming intermetallics.

4.1.3. Weld Fusion Zone (FZ)

Since a weld metal is similar to a casting, it will exhibit segregation of alloying elements. However, the primary solidification phase with duplex steels is normally ferrite, and this causes minimum segregation of chromium and molybdenum during solidification. Moreover, diffusion rates are high at temperatures just below the melting point, and homogenization of alloy elements in the ferrite can take place [56].

The situation regarding partitioning of elements between ferrite and austenite upon solid state transformation during a welding cycle is complex. Depending on the heat input, the composition and corrosion resistance of the ferrite and austenite phases can vary. At low heat input, the ferrite-austenite transformation is controlled by nitrogen, and thus there may be little difference between the substitutional element contents of the two phases on cooling to room temperature, although nitrogen will be enriched in the austenite. At high heat input, there is sufficient time for diffusion of Cr, Mo and Ni to occur, and thus there may be significant differences in final alloy content between two phases [56, 79].

Welding without the addition of filler material or excessive dilution with base metal should be avoided unless postweld solution annealing is to be performed [31]. Duplex stainless steels are often welded with overmatching filler metals, which usually

contain at least a 2% higher nickel content than the base metal. However, if the filler composition is biased to austenite by adding nickel, an adverse weldment performance may result due to the following reasons [79]:

1) Increasing the nickel content promote austenite formation and dilution of nitrogen content in the austenite and thus lower the corrosion resistance of the austenite and therefore the weld metal.

2) High Ni promotes austenite formation but also promotes a greater concentration of ferrite stabilizing elements (Cr, Mo) in the remaining ferrite. This results in more susceptible to the precipitation of sigma phase at temperatures in the range from 650-950 °C (1202-1742 °F). Consequently, higher postweld solution heat treatment temperatures (1100 to 1150 °C/2010 to 2100 °F) must be utilized to dissolve all sigma phase. [22].

3) If the dilution from the parent steel is low, ferrite levels can be too low to even satisfy the weld metal strength requirements.

4.2. Weldability

For this discussion, weldability means the relative ease of producing a defect-free weld with adequate mechanical properties and corrosion resistance. The principal defects of interest are hot cracks (fusion zone or heat affected zone hot cracking) and cold cracks (hydrogen assisted cracking). Welding considerations and proper welding procedures, to not only avoid defects, but also to achieve the desirable level of performance is important.

4.2.1. Fusion Zone Solidification Cracking

Weld solidification cracking requires the presence of a crack-susceptible microstructure, which forms at the final stage of solidification due to the presence of low melting, impurity enriched liquid films. If duplex stainless steels solidify in a primary austenite solidification mode, which occurs when Cr_{eq}/Ni_{eq} ratio (see the WRC-1992 diagram Figure 3-18) is below 1.5, severe partitioning of impurities such as S and P will occur. These impurities then tend to form liquid films, which effectively wet austenite/austenite grain boundaries, thus promoting weld fusion zone solidification cracking [22, 75]. If the weld metal chemistry shows a Cr_{eq}/Ni_{eq} ratio above 2.0, the solidification mode is highly ferritic and a cracking tendency also exists. A duplex (ferrite + austenite) solidification mode occurs when Cr_{eq}/Ni_{eq} ratio is between 1.5 and 2.0 and this mode offers the optimum resistance to hot cracking.

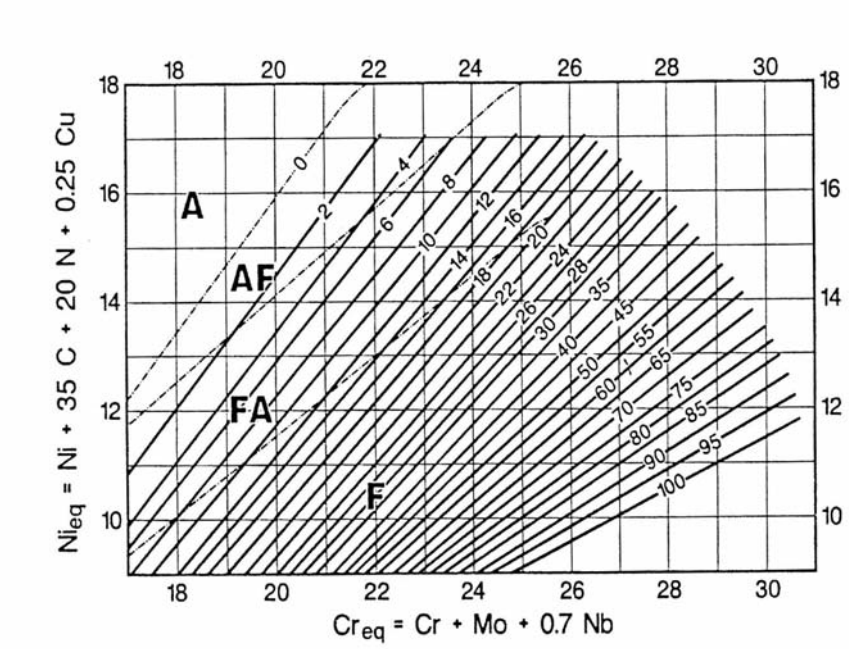

Figure 3-18. The WRC-1992 Diagram [43]

Not many research results regarding fusion zone solidification cracking have been published for duplex stainless steels. The main reason is that fabrication experience with a number of commercial duplex stainless steels had suggested the weld solidification cracking is not a significant problem [80]. It has been suggested that duplex stainless alloys solidify as ferrite as the primary phase and thus are less susceptible to cracking than those that solidify solely to austenite. The difference in cracking susceptibility as a function of primary solidification product is generally ascribed to the greater affinity of the ferrite phase for the impurity elements such as sulfur and phosphorus and the reduced tendency for liquid films to wet ferrite/ferrite boundaries[81].

4.2.2. Heat Affected Zone Liquation Cracking

The susceptibility of the duplex stainless steel to liquation-related HAZ cracking is negligible according to Lippold et al. [82]. The authors attributed the resistance to HAZ liquation cracking to the fact that the duplex stainless steels typically contain low impurity levels and that ferritic microstructures are generally resistant to grain boundary liquation due to the high diffusivity of alloying and impurity elements at elevated temperature.

4.2.3. Hydrogen Associated Cold Cracking

The presence of ferrite in duplex stainless steels increases the duplex stainless steel susceptibility to cold cracking. Cold cracking, also known as hydrogen cracking, is determined by three factors: susceptible microstructure, hydrogen and stress.

The susceptible microstructure refers to microstructures that have high strength, low toughness and high diffusivity for hydrogen. Highly ferritic structures are considered susceptible. Hydrogen can be introduced into the weld metal from many sources, most commonly from moisture absorbed by the electrode or from the atmosphere due to poor shielding during the welding process. Hydrogen-bearing shielding gases are employed during welding since they improve weld pool fluidity, prevent surface oxidation and provide higher productivity. However, the effect of hydrogen on cracking tendency must be considered.

Research results [83-89] have consistently shown that hydrogen cracking susceptibility of duplex stainless steels increases with increasing ferrite content. Thus, assuming H_2 is unavoidable, ferrite content has to be controlled to solve the hydrogen cracking problems.

Another method to eliminate hydrogen cracking is to solution heat treat the weldment immediately after welding [84]. However, previous discussions have shown that preheating or postweld heat treatment may not be suitable or possible depending on the chemistry and section size of the material. Therefore, if it is at all possible, H_2 should be eliminated from the welding process.

4.2.4. Corrosion Behavior of Duplex Stainless Steel Welds

Duplex stainless welds, if properly fabricated, have fairly good corrosion resistance compared to the parent materials. However, corrosion behavior of DSS welds shall be considered when welding is employed for fabrication, since welding produces thermal cycle(s) on materials may result in secondary phase upon cooling with improper

processes. The presence of these phases definitely, to some extend, lead to degradation of the corrosion resistance of the weldment. According to Karlsson [90], pitting and crevice corrosion is decreased by presence of intermetallic phases; general corrosion and intergranular corrosion is not affected significantly unless the presence of intermetallic phases reach a certain level; stress corrosion cracking is significantly decreases by the presence of these phases. P. Woollin did quantitative research on superduplex welds with intermetallic in Sour Media show that the strain to failure of all-weld superduplex decreases with the increasing of the amount of local intermetallic phase, also it suggested that the size of intermatallic particles is more important than volume fraction [91].

4.3. Welding Considerations

4.3.1. Filler Metal

Filler metal selection is critical to maintaining the mechanical and corrosion properties of the weld and HAZ. In the fusion zone of GTAW, the microstructure can be significantly high in ferrite, resulting in poor toughness and corrosion resistance. Autogenous welds should not be applied unless the part will receive a postweld solution treatment.

The use of matching filler metal generally does not improve the situation, due to the dilution effect, which results in high ferrite levels in the weld. Like autogenous welds, welds with matching filler metal should receive a postweld solution treatment [3, 92].

Filler metals that have a modified chemistry compared to base metal are generally accepted. The filler metal chemistry is modified to provide comparable mechanical

properties and better corrosion resistance and to allow for the loss of particular elements in the arc [3]. To accomplish the above goals, filler metals are higher in nickel and contain nitrogen.

As discussed previously, weld metal toughness is affected by not only the ferrite content but also the oxygen content. Covered electrodes with high silicon content such as rutile electrodes also give a high oxygen content in the weld metal. Basic covered electrodes give lower silicon and oxygen contents [92]. Flux core arc welding is usually known for its difficulty in control of the oxygen content in the weld. Atamert et al. [93] claimed that flux-cored wires with low oxygen concentration and optimum nitrogen solubility display excellent corrosion resistance and the required mechanical properties have been developed (composition was not available). Pak and Rigdal [94], on the other hand, used readily available consumable wires OK Tubrod 14.27 and OK Tubrod 14.37 and found that these wires can produce weld metals that fulfill the common requirements for duplex stainless steel welding.

Ni-base filler metals are often used for better corrosion resistance, especially for root passes where the dilution is the highest. However, Holmberg [92] stated that the combination of Ni-base fillers in the root and duplex fillers in the intermediate passes and cap passes may result in brittle microstructures. Ödegärd and Fager [95] found that welding super duplex stainless steel using high Ni filler metal produced Cr_2N in the reheated regions and resulted in lower toughness. Although the development of welding filler electrodes/wires for duplex and super duplex stainless steels has been rapid, the standardization of welding consumables is limited [96]. Below are the national and international standards or working documents for covered electrode [96]:

1) AWS A 5.4-92

2) AWS A 5.9-93

3) CEN (TC121 PREN)

4) IIW (Subcommittee IIE. Doc. II-E-118-91)

4.3.2. Heat Input

Heat input is a very important factor for welding of DSS because this energy input controls the overall cooling for adequate austenite formation in the welds. Too low a heat input will result in excessive ferrite thus reducing toughness, corrosion resistance and increasing materials susceptibility to hydrogen embrittlement. On the other side, too high a heat input would result in a slow cooling rate; which may cause formation of secondary phases like sigma, thus reduce toughness and corrosion resistance. A practical limit for DSS is provided by the cooling time between 1200 and 800°C, $\Delta t_{?2/8}$, as it covers the temperature range over which austenite formation occurs. Preferred cooling time for shall be approximately 4 to 15 sec, which correspond a cooling rate of 20-50 °C/s[1]. Correspondence to the proper cooling rate, heat input range can be maintained for each grade of DSS, for example 22%Cr grades, 0.5-2.5kj/mm is recommended for 10-15mm thickness [97, 98].

4.3.3. Shielding/Backing Gas

The role of welding gases in the fabrication of duplex stainless steel has been of interest, especially for gas tungsten arc welding [99-103].

Nitrogen is known to have a beneficial effect on duplex stainless steels and the above work has quantified the effect of nitrogen additions to both the shielding and backing gases using manual GTAW. It was shown that nitrogen additions to both the shielding gases and backing gases significantly improves the pitting corrosion resistance compared to normal pure argon shielding and backing gases. Figure 3-19 [100] illustrates the effect of various shielding gas composition on critical pitting temperature (CPT). While backing gases are encouraged to be 100% N_2, the nitrogen content in shielding gas has to be limited to below 5% due to weldability problems. Besides adding nitrogen to argon, helium and hydrogen can also be added to achieve more penetration. However, if hydrogen is used in the shielding gas, ferrite content must be properly

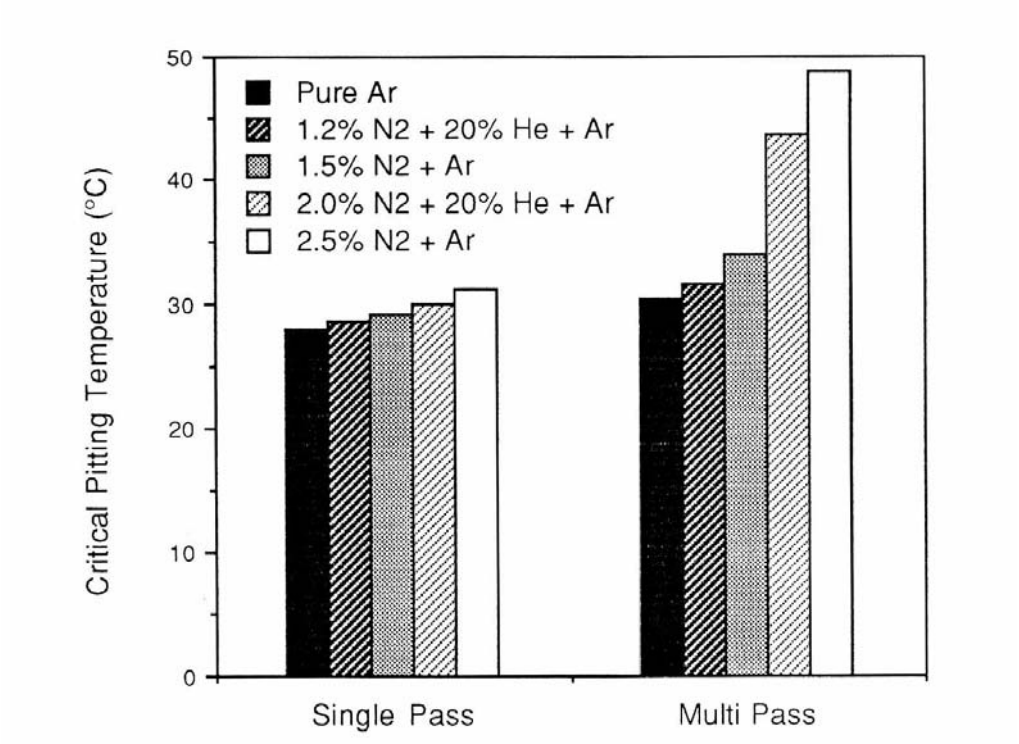

Figure 3-19. Effect of Shielding Gas Compositions on Pitting Corrosion Resistance of Duplex Stainless Steels

controlled to prevent hydrogen cracking. Also, noted that H_2 enhances nitrogen loss in the weld pool [86].

GMAW is another process that requires attention to the shielding and backing gases [104, 105]. However, oxygen additions may result in lower weld metal toughness for duplex stainless steels. In addition, carbon pick-up in the weld metal due to CO_2 addition in the shielding gas may occur. A quaternary gas mixture containing Ar, 5% He, 2% CO_2 and 2% N_2, which is called Arcal 129 and commercially available, has shown good results and has not shown carbon pickup [139].

4.3.4. Preheat and Multi-Pass

In case of multi-pass welding, usually, preheat is not necessary for DSSs. Preheat and interpass temperature should be always lower than 150°C (300°F) for the purpose of adjust heat input to control ferrite austenite or secondary phases, however, the maximum interpass temperature depend on the grade and arc energy employed [1, 106]. It is recommended by Sandvic that interpass temperature for SAF 2304and SAF 2205 shall be maximum 480F, and SAF 2507; 300°F[97].

4.4.Welding Processes

Depending on the process and economy-related conditions, many welding processes can be applied to duplex stainless steels [96, 107-114]:

a. SMAW Shielded Metal Arc Welding (stick electrode welding)

b. GTAW Gas Tungsten Arc Welding

c. GMAW Gas Metal Arc Welding

d. FCAW Flux Cored Arc Welding

e. SAW Submerged Arc Welding

f. PAW Plasma Arc Welding

All these process has its unique characteristics for welding of DSS. Others welding processes are considered immature processes for duplex stainless steels [113]. The reason is that these processes are characterized by rapid cooling rates, which generally lead to excessively high ferrite content in the weld and HAZ. On the other hand, electroslag welding (ESW) is also not suitable for welding duplex stainless steels because of its high heat input and extremely slow cooling rate.

SMAW and GTAW are the two processes most frequently used. Thus the attention of the review is focused on these two processes, discussion of other arc welding processes will be brief.

4.4.1. SMAW

SMAW has the advantage of being a very versatile method that can be used for all position welding. In addition, for repair welding of castings and other structures, SMAW is usually selected [107].

Either rutile or basic covered electrodes can be used for welding duplex stainless steels. While welders prefer rutile coated welding consumables for good slag detachability (beneficial for root pass welding) and smooth weld bead appearance, welds made with rutile coated electrodes generally have low impact toughness due to high silicon and oxygen content [107-110]. Basic electrodes, on the other hand, result in a

poor appearance and difficult slag detachability but exhibit good impact values at low temperatures. It was shown that basic welding consumables have a lower oxygen and silicon content in the deposited weld metal.

Moisture control is important not only to prevent hydrogen cracking, but also porosity [107, 109, 111, 115]. One method is to re-dry electrodes for about two hours at 250 to 350 °C (480 - 660 °F) before welding. Another alternative is to use extra-moisture-resistant (EMR) electrodes, which have a guaranteed low coating moisture content.

In SMAW, the weld pool is protected by gases and slag from the electrode covering. To maximize this protection, Holmberg [111] recommended that an arc as short as possible should be maintained. A long arc can produce weld porosity, excessive oxides, excessive heat input and reduced mechanical properties.

The control of heat input, as discussed previously, affects the ferrite content of the weld metal and heat affected zone. Too low a heat input will result in a fast cooling rate and consequently brittle weld metal due to high ferrite and Cr_2N precipitates. On the other hand, too high heat input will result in precipitation of intermetallic phases such as sigma due to a slow cooling rate. Thus, heat input for welding duplex stainless steels must fall within a certain range. Holmberg [111] recommended 0.2-1.5 KJ/mm (5-38 KJ/in.) heat input for welding SAF 2507; for 22Cr duplex stainless steels, 0.5-2.5 KJ/mm (12.7-63.5 KJ/in.) heat input has been considered suitable for a fairly broad thickness range. The metal should be deposited in a straight bead with the width of weave not exceeding twice the electrode diameter to ensure a proper heat input. For detailed

information regarding selecting welding parameters, readers are encouraged to consult the material producers.

4.4.2. GTAW

Although the GTAW process is slow when compared to other processes, it is ideal for making high-quality root passes in pipe welding. The process prevents residual slag, spatter, and oxidation of the inside root pass, with proper backing. Moreover, greater control and repeatability can be achieved by using an automated GTAW process.

As the result of absence of slag and oxidation, another advantage of GTAW is that the process also provides the best impact toughness for the weld metal comparing to other processes, as illustrated by Figure 3-20 [108]. However, this advantage cannot be realized if excessive dilution occurs or shielding and backing gas are not correct.

To avoid dilution, which is the most severe in the root pass, filler metal must be added. Varieties of filler metals are available for GTAW duplex stainless steel. GTAW without filler metal (autogenous) is not recommended unless PWHT is planned [107, 109, 111]. Another “dilution” which usually occurs with GTAW duplex stainless steels is the loss of nitrogen during the process. Nitrogen is well known to have a strong effect on promoting austenite formation and loss of nitrogen tends to result in high ferrite content in the weld. Thus, an inert gas shielding may not be adequate for GTAW duplex stainless steels. Common practice is to add 5 % N_2 into Ar (more than 5% N_2 will cause a non-stable arc). In addition, when welding the root pass, 100% N_2 as backing gas, is recommended. More discussions of shielding and backing gas effects will be presented.

Heat input range for GTAW process is similar to SMAW, i.e., 0.5-2.5 KJ/mm (12.7-63.5 KJ/in.).

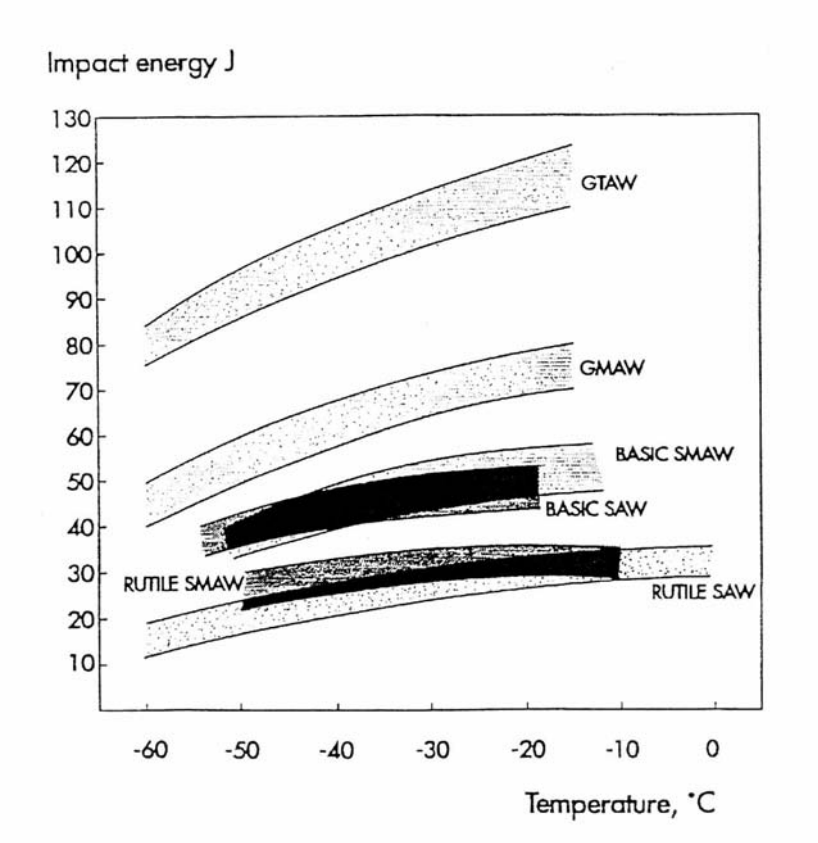

Figure 3-20. Effect of Welding Process on Impact Toughness [108]

5. Toughness

Charpy impact test is a supplementary requirement for duplex stainless steel castings specified in ASTM A890-99. The supplementary requirement S9 included in ASTM A781M-00 states that:

"Charpy impact test properties shall be determined on each heat from a set of three Charpy V-notch specimens made from a test coupon in accordance with Test Methods and Definitions A 370, and tested at a test temperature agreed upon between the manufacturer and purchasers. Test specimens shall be prepared as Type A and tested in accordance with Test Methods and Definitions A370."

Druce et al. [116] studied the effects of notch geometry on the impact toughness using cast duplex stainless steel and concluded that the best notch geometry is the V-notch specified by ASTM.

No guidelines regarding the extraction of Charpy impact test specimens have been issued by ASTM. Gossett [117] indicated that the orientation of the sample is very important. Unfortunately, no definitive suggestions were given.

It has been mentioned several times that a high ferrite content and the presence of intermetallic compounds deteriorates impact toughness. The factors that control the formation of ferrite and intermetallic phases have been discussed in detail.

Another well-known factor that affects the toughness of a material is the oxygen/oxide content and other inclusions content. While there is not an extensive data base illustrating the effect of oxygen on impact toughness of cast duplex stainless steels, sufficient data have shown that duplex weld metal toughness may vary significantly when

deposited by different welding processes and that the coating of the electrode, namely, rutile vs. basic is critical.

Overall, duplex stainless steels have excellent impact toughness. However, weld metal toughness is generally lower than base metal. Many variables, such as alloy content, solution annealing temperature, cooling rate, weld heat input, HAZ peak temperature will affect the toughness. ASTM standards do not specify any minimum impact toughness for duplex stainless steel castings.

6. Ferrite Prediction and Measurement

An appropriate ferrite content is essential in duplex stainless steels to achieve an excellent combination of strength, toughness and corrosion resistance. Moreover, an appropriate level of ferrite also significantly reduces susceptibility to hot cracking and microfissuring. Therefore, it is essential to be able to predict ferrite content in duplex stainless steel castings and welds so that chemical composition can be adjusted to achieve the desired ferrite content.

6.1. Diagrams

The earliest work on this complex and important issue was accomplished by Schaeffler [118] in 1949 on weld metals. Schaeffler's work was modified by Delong [119], whose work was again modified several times by a host of researchers, led by Kotecki [43, 120, 121], who also has accomplished significant work on ferrite measurement.

The basic idea of ferrite content prediction has not changed since 1949. A diagram contains phase fields and iso-ferrite lines that permit prediction of the weld structure from composition. Figure 3-21 is the Schoefer diagram, Figure 3-18; the 1992 WRC Diagram. The procedure involves calculating a "chromium equivalent" (Cr_{eq}) and a "nickel equivalent" (Ni_{eq}) for each base metal and for the proposed filler metal, plotting each equivalent on the diagram, drawing tie lines between the plotted points, proportioning according to expected dilution, to obtain an estimate of the weld metals ferrite content.

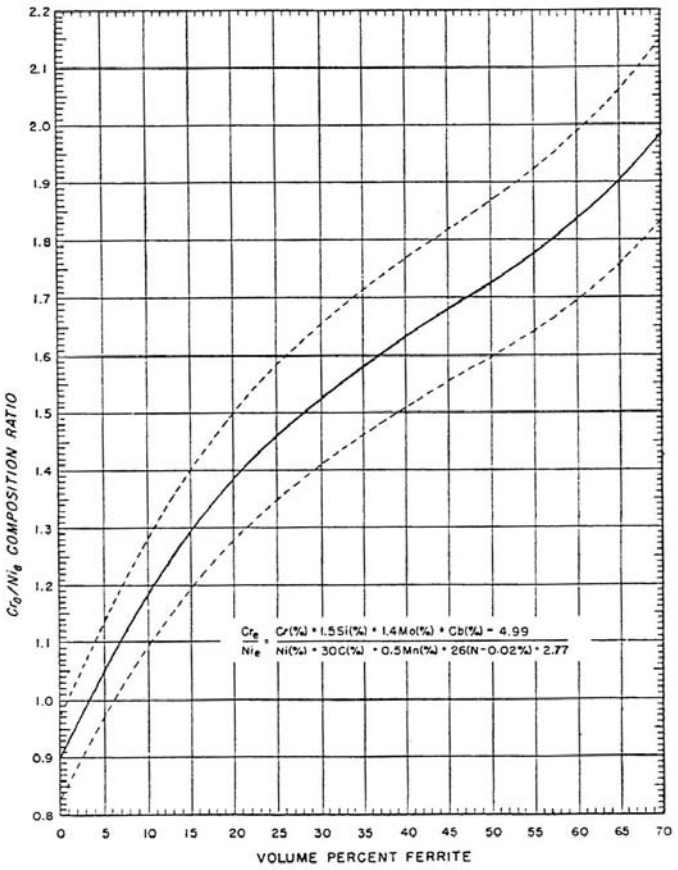

Figure 3-21. The Schoefer diagram (From ASTM A 800-91)

Schoefer Diagram was adopted by ASTM and used in specification A-800-91. Calculation of the total Cr_{eq} and Ni_{eq} for the alloy composition by:

$$Cr_{eq} = Cr + 1.5\ Si + 1.4\ Mo + Nb - 4.99 \quad \text{Equation 3}$$

$$Ni_{eq} = Ni + 30\ C + 0.5\ Mn + 26(N - 0.02) + 2.77 \quad \text{Equation 4}$$

For the WRC-1992 Diagram [43], the Cr_{eq} and Ni_{eq} are calculated as:

$$Cr_{eq} = Cr + Mo + 0.7\ Nb \quad \text{Equation 5}$$

$$Ni_{eq} = Ni + 35\ C + 20\ N + 0.25\ Cu \quad \text{Equation 6}$$

ASTM A800-91 states that the Schoefer diagram is applicable to alloys containing elements in the following ranges:

C	Mn	Si	Cr	Ni	Mo	Co	N
0.20 max	2.00 max	2.00 max	17.0 ~ 28.0	4.0 ~ 13.0	4.00 max	1.00 max	0.20 max

Thus, it is evident that for modern duplex stainless steels, especially super DSS can easily exceed the Schoefer diagram maximum limitations, which raises concerns about the accuracy of the estimation. However, at the present time, there are no alternate "quick" methods for estimating ferrite content in cast duplex stainless steels. At the same time, there is always a degree of variance in the chemical analysis of an alloy. Accuracy

of the prediction of ferrite in this manner will depend on the accuracy of chemical analysis.

In addition, as discussed previously, cooling rate is a dominant factor affecting the ferrite content. Thus, ferrite content at different locations in individual castings can vary considerably, depending on section size.

6.2. Ferrite Measurement

The discussions of ferrite content prediction have shown that significant errors may occur using various constitution diagrams. Thus, an accurate ferrite measurement is important to ensure that a desirable level of the ferrite/austenite balance is achieved in duplex stainless castings.

Various ferrite measurement techniques have been established and some have been standardized. In the following sections, the advantage and disadvantages of the most commonly applied methods will be discussed and compared.

6.2.1. Point Count

Point counting per ASTM E 562 has been the traditional method used to determine the ferrite content of duplex stainless steel castings and weld metal in terms of volume fraction or ferrite percentage. The method involves preparing a specimen using standard metallographic procedures, selecting a proper magnification, grid and finally, counting intersections of the grid with the ferrite phase. The point counting is a destructive method and requires a significant effort encompassing several days,

moreover, it may not be accurate due to individual bias, improper magnification and improper grid size employed.

6.2.2. Magne -Gage: Magnetic Adhesion Method

Various methods/instruments have been developed utilizing the ferromagnetic property of ferrite to determine the ferrite content in duplex stainless steel weld metals and castings. Among these methods, the Magne-Gage is one of the most widely applied methods.

Figure 3-22 [122] shows a standard Magne Gage. The advantage of the Magne Gage is the excellent reproducibility. The disadvantage of the Mange Gage is that it is rather a laboratory than field use instrument because it must be used on a relatively stable and level surface in order to obtain accurate readings [3]. In addition, the Magne Gage is not suited for measuring ferrite content in a narrow HAZ due to the size (sphere of influence) of the magnet.

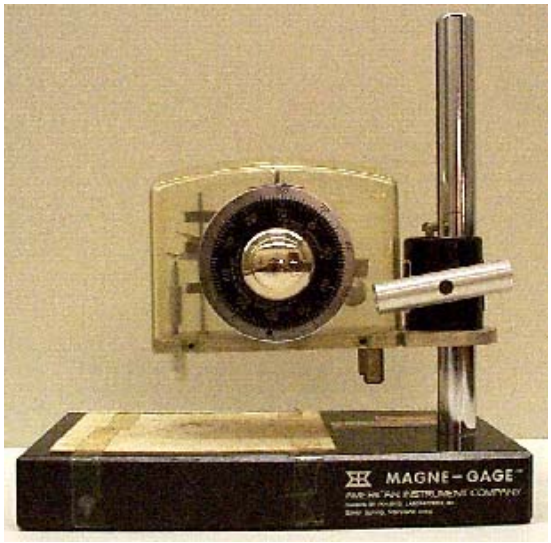

Figure 3-22. A Photograph of a Standard Magne-Gage [122]

6.2.3. Eddy Current Method: Magnetic Induction Method

Instrumentation using magnetic induction method for the eddy current technique may include a control and display unit, with control, measurement, display, and processing circuits as well as a hand-held eddy current probe that may be of pencil or angle shape [123].

The magnetic induction method relies on a low frequency alternating current through the field coil (see Figure 3-23-a), generating an alternating magnetic field that penetrates into the specimen. The interaction between field and specimen induces in the detection coil an alternating voltage, proportional to the ferrite content in the volume of measurement, which means this method determines the ferrite content in terms of volume percentage. The Feritscope® (Figure 3-23-b) is one of the commercially available instruments that utilizes the above principles and is widely applied with calibration procedures established and documented in ANSI AWS/A4.2-92 and ASTM A799-92.

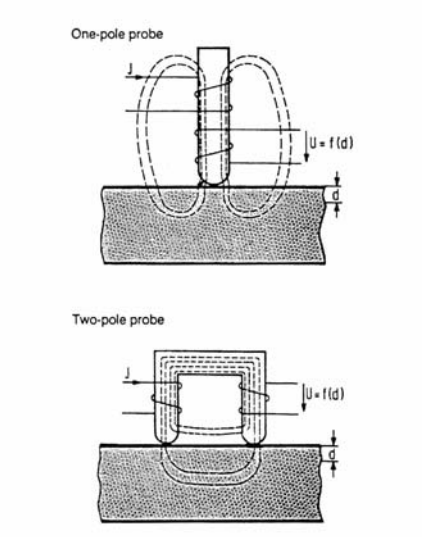

(a)

(b)

Figure 3-23. Ferrite Measurement with Single and Two-Pole Probes (a), and Feritscope® (b) [123]

The accuracy of the Feritscope® is affected by electromagnetic properties of the ferrite and morphology of the ferrite [123]. Many factors such as the distance between the probe pole and the surface of the specimen being measured and the curvature of the test specimen can also affect the accuracy of the Feritscope®.

6.3. Ferrite Number (FN) vs. Ferrite Percent (FP)

The three widely used ferrite determination methods, namely point counting and the Feritscope® and the Magne-Gage present ferrite content in either percentages or Ferrite Number system. Unfortunately, there is not a simple relationship between Ferrite Number and ferrite percent mainly because the relationship depends upon the composition of the ferrite [124]. Brantsma and Nijhof [125] concluded that Ferrite Numbers were clearly preferable to “ferrite percents” for determination of ferrite in duplex stainless steel weld metals. However, Kotecki [124] indicated that it is not the case with cast alloys, for the ferrite in castings is much coarser and more regularly shaped than in the weld metal.

Numerous attempts to correlate FN and FP have been undertaken and some relationships are summarized in Reference 86. Taylor [3] also suggested a relationship as follows:

$$\% \text{ Ferrite} = 0.55(\text{EFN}) + 10.6 \qquad \text{Equation 7}$$

Note that the Extended Ferrite Number is used in the equation, thus, Ferrite Numbers in the range of 0-28 are not applicable for this equation.

7. Casting Related Issues

Niederau and Overbeck [126] pointed out differences between cast and wrought products:

1) The grain size in the casting is coarser than in a mechanically deformed wrought structure. The processing differences generally result in more pronounced microsegregation in a cast structure with attendant differences in corrosion behavior.

2) Casting section sizes are usually greater than wrought products. Therefore, it is more difficult to avoid second phases precipitation and reduce segregation during heat treatment or welding.

3) Nitrogen solubility in castings may be limited.

However, as discussed previously, nitrogen can be added to castings to 0.28% without causing any gas defects [3]. Thus, to make optimum duplex stainless steel castings, it is important to give significant attention to the details in the production process.

Casting Production

Melting of duplex cast alloys may be done either in the electric arc or the induction furnace [3, 36, 127, 128]. During the melting process, control of chemical composition and removal of tramp elements are the most important aspects. Argon-Oxygen-Decarburization (AOD) refining is highly recommended. Taylor [3] and SCRATA [36] have more recommendations regarding melting.

Deoxidization practices using titanium, zirconium or aluminum should be avoided [3, 36, 127, 128]because these alloys have a strong affinity for nitrogen. If deoxidizers are used, calcium-based compounds are recommended.

Duplex stainless steels have excellent castability in both static and centrifugal casting processes [3, 129]. It is desirable to keep the pouring temperature as low as possible to minimize the grain size. However, the final decision on pouring temperature depends on mold complexity and section size [36].

It is also recommended by Taylor [3] and Birks and Roberts [130] that all duplex stainless steel castings receive a solution treatment after shakeout and prior to riser removal. This procedure reduces the likelihood for cracking during subsequent processing. As far as solution heat treatment procedures are concerned, a proper solution annealing temperature should be determined based on the alloy composition and in accordance with the ASTM A890-94a minimum requirements.

ASTM A 890-99

ASTM A890-94a is the only standard for duplex stainless steel castings. However the standard, requires attention and optimization in the following areas:

1) Lack of ferrite/austenite balance requirement.
2) Lack of minimum Charpy impact toughness requirement.
3) Lack of minimum corrosion resistance requirement (the PREN > 40 requirement for Grades 5A and 6A is meaningless, because a material can have a satisfactory PREN, but not satisfactory corrosion performance).
4) Lack of upper solution annealing temperature limit.

5) Chemical composition range, particularly N, may be too wide.

8. Service Performance of DSS

Table 3-4 summarizes the overall view of the areas that DSSs are used [1]. New applications of DSSs in the industry and their service performance have been studied over the past [131-133]. Service performance data acquired over the years of DSS in the pulp and paper industry, chemical industry, transport, pollution control, oil and gas production, structural and architectural and other field showed that the application of duplex stainless steels alloys in industry is a “successful story.”

Table 3-4. Application of Different Duplex Stainless Steels by Industry Sector

Industry	Alloy lean 23% Cr	Standard 22% Cr	Alloy lean 25% Cr	Superduplex
Chemical	Piping; instrumentation tubing	Pumps; fans; centrifuges; sulphur melting coils; chemical tankers	Urea strippers; reactor agitators; heat exchangers	Salt evaporation tubing; pumps; amine equipment; sea water cooling systems
Petrochemical	Tubular reactors with a carbon steel shell	Desalination; desulphurisation; distillation	Pump casings; desulphurisation equipment	Tubes and pipes in chloride and HCl media
Pulp and paper	Digester preheater, evaporators; bleaching pulp storage tanks	Digesters in sulphate and sulphite plants; black and white liquor tanks; oxygen impregnators	Digesters; digester preheaters	Bleaching equipment
Power generation	Feed water heaters; reheaters	Injection pipe in geothermal wells		Heat exchangers and systems in geothermal wells and saline brines
Flue gas desulphurisers		Evaporation plant; centrifugal fans	Liners in evaporator towers	
Oil and gas	Coolers; piping systems; tensioning systems; instrumentation tubing	Flare booms; frame work; slotted oil liners; wirelines; down hole tubing; subsea flowlines	Diving bells; pumps	Heat exchangers and systems in geothermal wells and saline brines; sea water cooling systems; fire water piping; pumps; pressure vessels; valve blocks; down hole tubing; process piping and vessels

IV. Materials and Experimental Procedures

1. Materials

The materials evaluated in this program included ASTM A890-4A, 5A, 6A, 1B and 1B variant "CD7MCuN" (currently not in the ASTM A890 and ACI designation). The wrought counterparts of the four ASTM duplex grades are Alloy 2205®, Alloy 2507®, Zeron 100®,and Ferralium 255® . Cast materials were evaluated in the as-cast and solution annealed static cast and solution annealed centrifugal cast condition. In compared in with castings, the wrought counterparts were also evaluated. The wrought materials were all tested with as-received solution annealed wrought plate. Table 4-1 summarizes the test materials and their test conditions.

Table 4-1. Condition of Cast Materials

Material	Condition			Total Heats Tested
	As-cast	Solution Annealed		
		Static Cast	Centrifugal Cast	
ASTM A890-4A	1	4	1	4
ASTM A890-5A	1	3	1	3
ASTM A890-6A	1	3	---	3
ASTM A890-1B	1	4	---	4
CD7MCuN*	---	2	1	2

* "CD7CuN" is yet neither ACI designation nor in the ASTM specification.

ASTM A890-4A is the most commonly utilized commercial duplex stainless steels. It is also the most popular and least expensive alloy in the duplex family. This grade has a PREN ranging from 30 to 36, and corrosion resistance that lies between AISI 316 and the 6-Mo superaustenitic stainless steels. The wrought counterpart of ASTM A890-4A is Alloy 2205. Four ASTM A890-4A heats, provided by four foundries, were tested. The chemical composition, in contrast with ASTM specified composition, for these four heats is presented in Table 4-2-1. Heat 1 was tested in the as-cast and solution annealed static cast condition. Heat 2 and 3 were tested only in the SA static cast condition. Heat 4 was tested in the SA static cast and SA centrifugal cast condition.

Table 4-2-1. Chemical Composition of ASTM A890-4A

	ASTM	Heat 1	Heat 2	Heat 3	Heat 4
C	0.03 max	0.026	0.026	0.034	0.02
Mn	1.50 max	0.376	0.704	0.491	0.95
Si	1.00 max	0.808	0.548	0.722	0.56
Cr	21.0 – 23.5	22.1	20.99	22.28	22.3
Ni	4.5 – 6.5	6.00	5.59	6.21	5.5
S	0.04 max	0.010	0.009	0.009	0.007
P	0.020 max	0.030	0.022	0.016	0.016
Mo	2.5 – 3.5	2.91	3.07	2.97	3.0
Cu	1.00 max	0.178	0.356	0.055	0.075
N	0.10 - 0.30	0.2255	0.1615	0.1266	0.20
W	-	0.054	0.114	0.038	-

ASTM A890-5A and 6A are super duplex stainless steels of the type 25 Cr-7Ni-3.5Mo-0.27N. Alloy 2507® and Zeron 100® are the wrought counterparts of the ASTM A890-5A and 6A, respectively. Three ASTM A890-5A heats, from three different foundries, were tested. The chemical composition is presented in Table 4-2-2. Heat 1 was tested in the as-cast and SA static cast condition. Heat 2 was tested only in the SA static cast condition. Heat 3 was tested in the SA static cast and SA centrifugal cast condition.

Three ASTM A890-6A heats, from three foundries, were tested. The chemical composition of the three heats is presented in Table 4-2-3. All three 6A heats were tested in the static cast form. Heat 1 was tested in both the as-cast and SA condition and Heats 2 and 3 were only evaluated in the SA condition.

Table 4-2-2. Chemical Composition of ASTM A890-5A

	ASTM	Heat 1	Heat 2	Heat 3
C	0.03 max	0.04	0.026	0.02
Mn	1.50 max	0.779	0.507	0.78
Si	1.00 max	0.683	0.336	0.64
Cr	24.0 – 26.0	25.65	24.65	24.0
Ni	6.0 – 8.0	7.82	7.44	7.6
S	0.04 max	0.011	0.002	0.008
P	0.04 max	0.027	0.024	0.011
Mo	4.0 – 5.0	4.72	4.53	4.5
Cu	-	0.500	0.517	-
N	0.10 - 0.30	0.1790	0.1910	0.18
W	-	0.065	0.033	-

Table 4-2-3. Chemical Composition of ASTM A890-6A

	ASTM	Heat 1	Heat 2	Heat 3
C	0.03 max	0.033	0.036	0.029
Mn	1.00 max	0.691	0.162	0.88
Si	1.00 max	0.895	0.822	0.73
Cr	24.0 – 26.0	27.00	25.64	24.9
Ni	6.5 – 8.5	8.36	7.54	8.37
S	0.030 max	0.007	0.008	0.0005
P	0.025 max	0.027	0.024	0.021
Mo	3.0 – 4.0	4.06	3.66	3.57
Cu	0.5 – 1.0	0.407	0.859	0.83
N	0.20 - 0.30	0.2513	0.2296	0.215
W	0.5 – 1.0	0.700	0.653	0.53

ASTM A890-1B, whose wrought counterpart is Ferralium 255®, and its variant, "CD7MCuN", belong to the 25% Cr variety. Four ASTM A890-1B heats were tested. Table 4-2-4 shows the chemical composition of these heats. Heat 1 was tested in the as-cast and SA static cast condition. The other three heats were only tested in the SA static cast condition. Two "CD7MCuN" heats were tested. Their chemical compositions are presented in Table 4-2-5. One "CD7MCuN" heat was tested in the SA static cast condition. The other was tested in the SA static cast and SA centrifugal cast condition.

Table 4-2-4. Chemical Composition of ASTM A890-1B

	ASTM	Heat 1	Heat 2	Heat 3	Heat 4
C	0.04 max	0.042	0.032	0.029	0.028
Mn	1.0 max	0.663	0.626	0.387	0.485
Si	1.0 max	0.842	0.999	0.692	0.899
Cr	24.5 – 26.5	23.79	25.41	25.50	24.61
Ni	4.7 – 6.0	5.13	5.42	5.62	5.07
S	0.04 max	0.009	0.010	0.010	0.001
P	0.04 max	0.017	0.039	0.024	0.034
Mo	1.7 - 2.3	2.50	2.14	1.93	2.04
Cu	2.7 - 3.3	2.81	3.02	3.09	3.09
N	0.10 - 0.25	0.1741	0.1313	0.1614	0.1474
W	-	0.036	0.081	0.022	0.020

Table 4-2-5. Chemical Composition of “CD7McuN”

	Heat 1	Heat 2
C	0.038	0.03
Mn	0.995	0.94
Si	0.979	0.68
Cr	24.96	24.8
Ni	5.54	5.5
S	0.008	0.005
P	0.018	0.023
Mo	2.92	2.9
Cu	1.79	1.94
N	0.1284	0.2
W	0.012	-

2. Test Methods

2.1. Critical Pitting Temperature (CPT) Test

2.1.1 Specimen Preparation

1) Extract 1" X 1" X 1/8" test coupons from the casting (see Figure 4-1 for typical extraction example)
2) Affix the coupon on a specimen holder using double stick tape. Grind the coupon on 120-grit abrasive paper and then on 600-grit abrasive paper, to obtain a uniform 600-grit surface finish on all surfaces (including the edges). Sharp edges should be rounded.
3) Rinse thoroughly and dry.
4) Weigh specimen to the nearest 0.001g.

Note: Autogenously welded specimens are prepared using an automatic GTA welder. Specimens are welded in a copper fixture to maintain suitable cooling rates and to prevent distortion. The welding parameters (100A, 12V, 10in (25.4cm) / min. travel speed) were chosen to provide a suitably sized weld on the coupon specified above. Argon shielding gas is used. It is to be noted that welding must be conducted before grinding to a 600 grit surface finish.

2.1.2 Test Solution Preparation

Test solution for CPT is 6% ferric chloride + 1% HCl. To make a 1000mL of test solution, dissolve 100g of reagent grade ferric chloride ($FeCl_3 \cdot 6H_2O$) in 900mL of distilled water, stir until completely dissolved. Pour the solution into a clean glass flask.

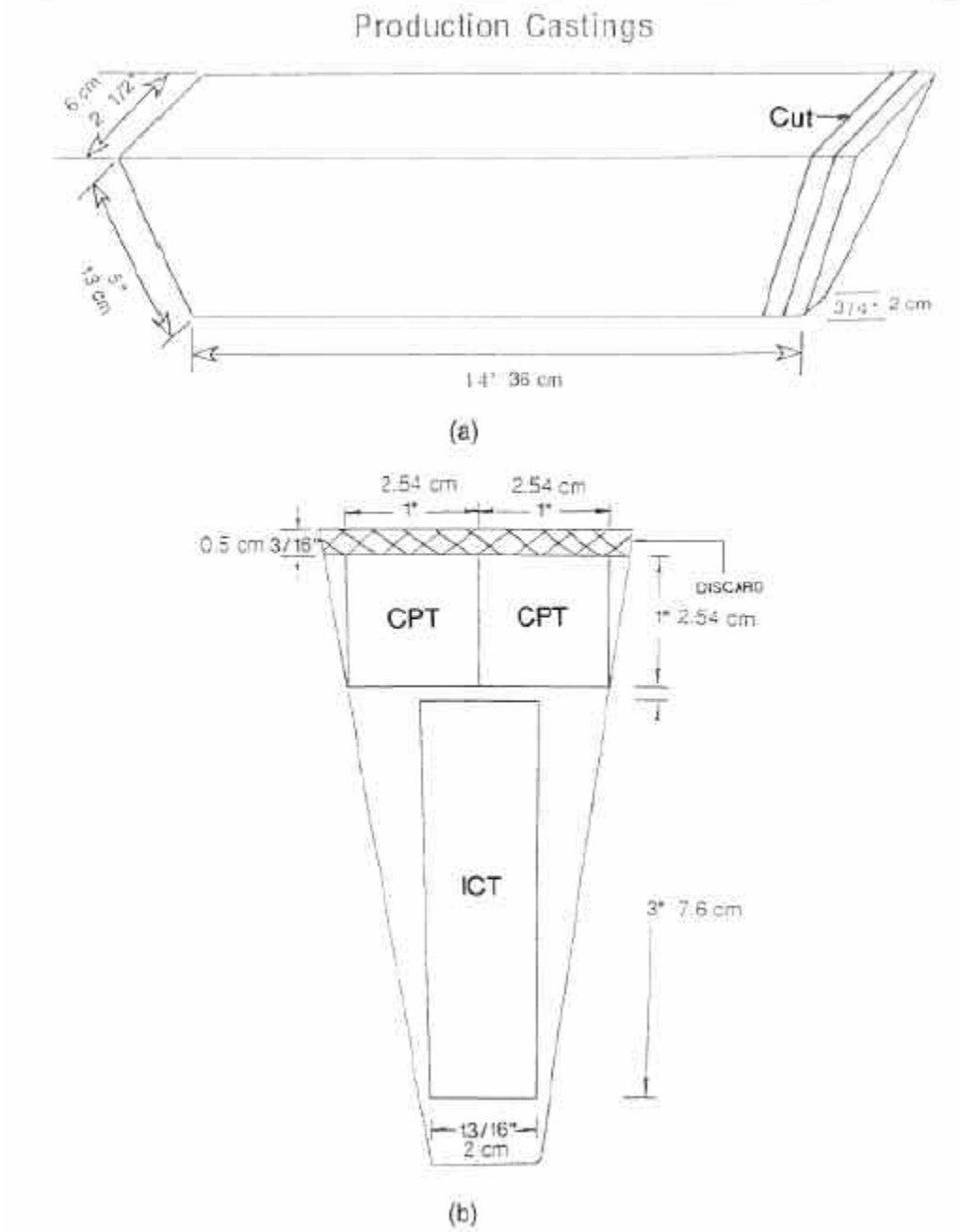

Figure 4-1. Corrosion Test Specimen Machinery Sketch (a). Production Casting (b). Schematic Drawing Showing the Extraction of Corrosion Test Specimens

Note: For ASTM G48-97, the standard test solution for CPT testing is 6% $FeCl_3$ + 1% HCl. To make this standard solution, 24mL of reagent grade concentrated (36.5-38.0%) hydrochloric acid (HCl) is added to 1000mL 6% $FeCl_3$ solution to obtain a solution that contains 6% $FeCl_3$ and 1% HCl by weight. The purpose of using this acidified solution is to obtain a pH-controlled environment over the test temperature range and to minimize precipitation in the solution.

2.1.3 Test Apparatus

A typical CPT test apparatus is shown in Figure 4-2. The water bath enables the test temperature to be controlled to an accuracy of 0.1C°.

Figure 4-2. CPT Test Apparatus

2.1.4 Procedure

1) Transfer the flask that contains test solution to the bath and allow the system to come to equilibrium at the temperature of interest.

2) Place the specimen in a glass holder and immerse in the test solution, after the solution has reached the desired temperature. No more than one specimen should be placed in a test container. The total test period is 24 hours.

   Note: According to ASTM G48-97, the starting temperature may be estimated by the following equation:

   $$CPT\ (°C) = (2.5 \times \%\ Cr) + (7.6 \times \%\ Mo) + (31.9 \times \%N) - 41.0$$

   Testing shall begin at the nearest increment of 5°C estimated by the above equation. The minimum temperature of test is 0°C and the maximum temperature of test is 85°C. Testing may be done at a higher temperature (85°C was the highest temperature of testing in an ASTM CPT round-robin).

3) At the end of the test period, remove the specimen, rinse with water, and scrub with a nylon brush under running water and place in methanol with ultrasonic agitation to remove corrosion products and dry.

2.1.5 Examination and Evaluation

1) Check surfaces of the specimen under a low-power binocular microscope at 20x magnification. The pitting criterion is that, if the primary surfaces of the specimen exhibit two or more pits at 20X magnification, the sample is considered pitted (higher magnification may be employed for more definitive observation if there is any uncertainty in suspected pitting at 20X). Edge pits are disregarded.

2) If pitting attack is defined, lower the bath temperature 5°C and, using a new specimen and fresh solution, repeat testing.

3) If no pitting attack is defined, raise the bath temperature 10°C using a new specimen and fresh solution, repeat testing.

4) The critical pitting temperature (CPT) is defined as the lowest temperature at which pitting occurs.

2.1.6 Repeat Testing

Duplicate testing shall be conducted at the CPT and 5°C below the CPT to verify pitting behavior.

2.2 Intergranular Corrosion Testing

2.2.1 Preparation of Test Specimen

1) Extract 3 1/8" X 3/4" X 1/8" coupons. (See Figure 4-1 for typical example)

2) All surfaces of the test specimen shall be ground, to a uniform surface finish of 120-grit. Sharp specimen edges should be rounded.

3) Determine the dimensions of the test specimen exposed surfaces and weigh the specimen to the nearest 0.001g.

4) Autogenously welded samples are prepared using an automatic GTA welder. Specimens are welded in a copper fixture to control cooling rate and prevent distortion. The welding parameters (100A, 12V, 10in (25.4cm) / min. travel speed) are chosen to provide a suitable size weld on the coupon defined above.

Argon shielding is used. The weld face must be re-ground to a uniform 120 grit finish before ICT.

2.2.2 Test Apparatus

A typical ICT apparatus is shown in Figure 4-3. A heater and the Erlenmeyer flask together with the finger condenser and water cooling circulation system, are typical.

2.2.3 Test Solution Preparation

1) The standard test solution for ICT is the Ferric Sulfate-Sulfuric Acid Test Solution (ASTM A262 B)

   "**Caution:** Protect the eyes and use rubber gloves for handling acid. Mix solution under a hood."

2) Pour 600ml distilled water into an Erlenmeyer flask.

   Note: Make sure all glassware is clean. "During the testing, there is some deposition of iron oxides on the upper part of the Erlenmeyer flask. This can be readily removed, after a test is completed, by boiling a solution of 10% hydrochloric acid in the flask."

3) Measure 354.0mL of reagent grade sulfuric acid (concentration range from 95.0 to 98.0 % by weight), and add the acid slowly to the Erlenmeyer flask containing distilled water avoiding excessive heating.

4) Weigh 37.50g of reagent grade ferric sulfate (contains 75% $Fe_2(SO_4)_3$) and add to the sulfuric acid solution.

Figure 4-3. ICT Apparatus

5) Place boiling chips in the flask.

6) Cover flask with condenser and circulate cooling water.

7) Boil solution until ferric sulfate is completely dissolved.

2.2.4 Procedure

1) Place specimen in a glass cradle and immerse in boiling Ferric Sulfate-Sulfuric Acid solution.

2) Mark liquid level on flask to provide a check on vapor loss (which would result in increased concentration). If there is an appreciable change in the level, the test must be repeated with a fresh solution and a re-ground specimen.

3) Continue immersion testing of the specimen for a total of 120 hours, remove specimen, rinse in water and use ultrasonic agitation to remove the corrosion products, and dry.

4) Weigh the tested specimen to the nearest 0.001g, and determine the weight loss of the specimen.

2.2.5 Calculation of Intergranular Corrosion Rate

The effect of the acid solution on the material shall be measured by determining the loss of weight of the specimen. The corrosion rate can be reported as mils of penetration per year, Calculated as follows:

Mil per year (mpy) = (K x W) / (A x t x d)

where:

K = 3450000
W = weight loss, g
A = area, cm2
t = time of exposure, 120 hr
d = density, 8.0g / cm3

2.2.6 Bend Testing of the ICT Specimen

1) A typical bend test fixture is shown in Figure 4-4. The fixture is constructed so as to provide a 2t radius of bend, where “t” is the specimen thickness.

2) The specimen shall be forced into the die by applying load on the plunger until the specimen touches the bottom of the die.

Note: A test specimen with an autogenous weld, shall be placed with the weld surface in tension.

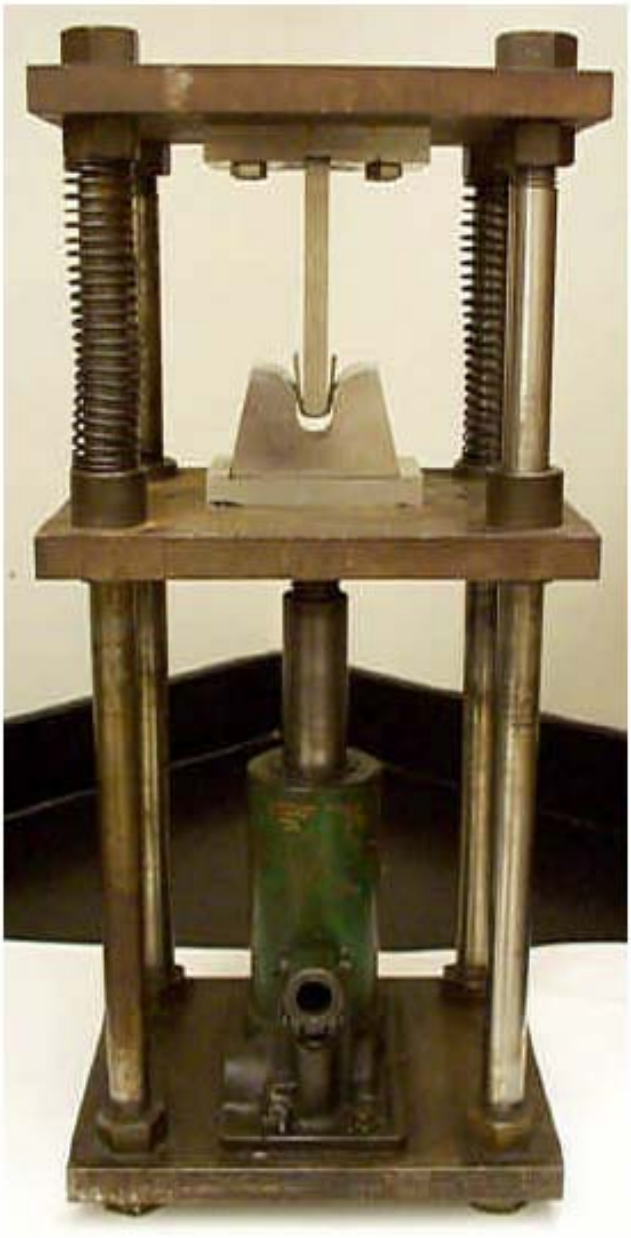

Figure 4-4. Bend Test Fixture

3) Observe the bent surface under a low-power microscope at 5X to 20X magnification. The appearance of fissures, cracks or separations along grain boundaries indicates the presence of intergranular attack.

4) When an evaluation is questionable, metallographic examination of the outer radius from a cross section of the bend specimen at a magnification of 100X to 250X may be used to determine the presence or absence of intergranular attack.

2.3 NORSOK Pitting Corrosion Test

The NORSOK test is an industry testing practice specification (Rev. 1, 1994). It utilizes a test method based on the ASTM G48-A, “Ferric Chloride Pitting Test”, which is basically an immersion test as the CPT test. The differences between the two tests are:

1) NORSOK requires samples be pickled utilizing a 20% HNO3 + 5% HF solution at 60°C for 5 minutes prior to testing.

2) Test temperature shall be 50°C.

The acceptance criteria are that there is no pitting at 20X magnification and the weight loss shall be less than 4.0 g/m2.

2.4. Charpy Impact test

Charpy Impact tests were conducted in accordance with ASTM A370, “Standard Methods and Definitions for Mechanical Testing of Steel Products”, and ASTM E23, “Standard Method for Notched Bar Impact Testing of Metallic Materials”.

The Charpy V-notched specimens, used in this evaluation, were machined according to the specification in ASTM E23. Figure 4-5 shows the standard dimension of Charpy test sample use in this study.

For the wrought materials, all of the Charpy specimens were extracted from 1/4 t location in the plates with a longitudinal (LT) orientation. The plate thickness is in the range of 7/8" to 1". Identification marks were placed on the ends.

For the cast materials, all of the Charpy bars were extracted from the wedge-shaped cast blocks with long axis of the Charpy bar parallel to one side of the wedge. Letter A, B or C is marked on the ends to indicate the geometry of sample extraction from the wedge castings. As depicted in Figure 4-6, notch is machined on the samples.

The Charpy impact test machine is a pendulum type of rigid construction and it is capable to provide sufficient impact to break the specimen in one blow (most of the time). The machine is consisted of a pendulum and a based that contains two specimen anvil blocks to locate the sample. Figure 4-7 shows picture of a typical Charpy machine with sample situated in the anvil.

Charpy impact testing follows the procedure of ASTM E23:

1) Set the energy indicator of the Charpy machine at the maximum reading.
2) Use self-centering tong to take the Charpy bar from its cooling/heating medium if test temperature is not ambient temperature, to place the Charpy bar in the proper position on the specimen anvils.

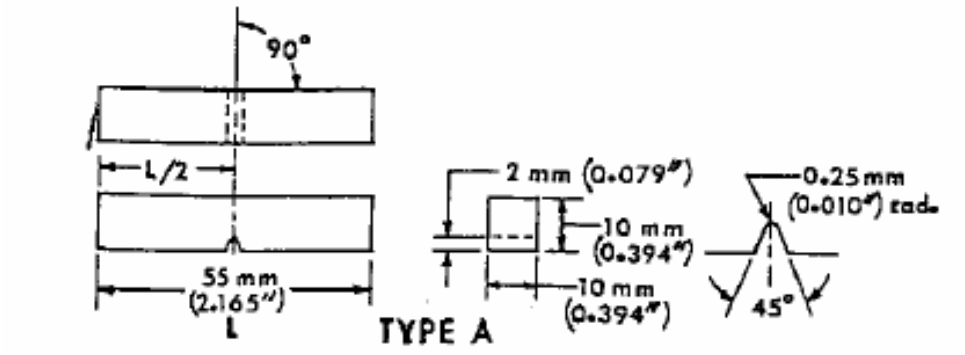

Figure 4-5 Standard Dimension of Charpy Test Specimen (Type A) Used in this Study.

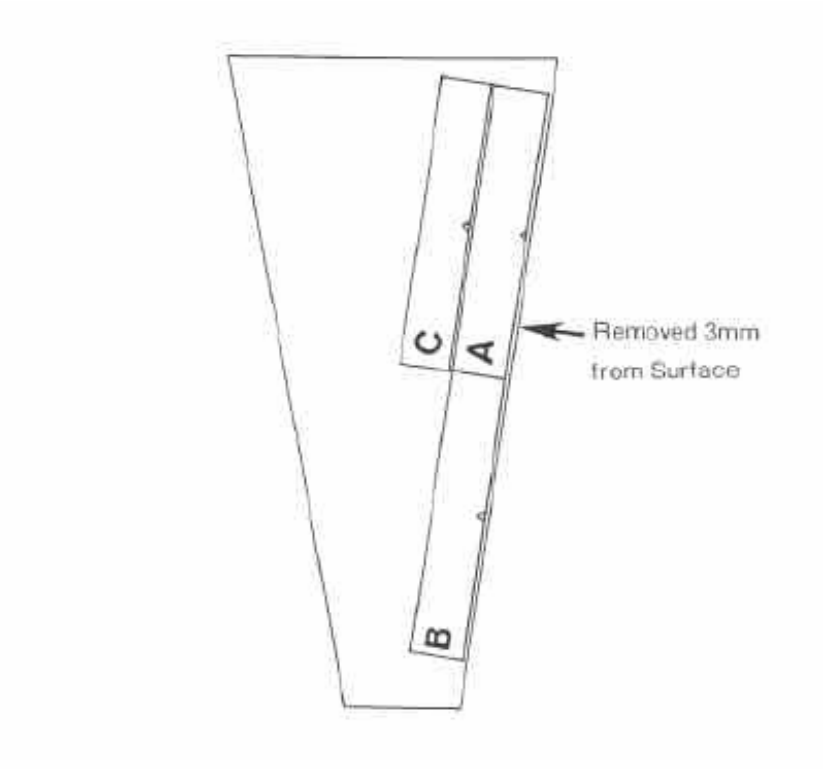

Figure 4-6. Charpy Impact Test Specimen (V-notched) Extraction Sketch

Figure 4-7 Charpy Test Apparatus Setup

3) Release the pendulum smoothly. Read the value of indicator on the scale.

Note: It shall not take more than 5 seconds if cooling/heating is applied.

4) Gather the broken specimen and dip the pieces into acetone.

5) If any specimen fails to break, no repeat test shall be given, record the fact.

6) If specimen jams in the machine, disregard the result and check the test machine.

Information that shall obtain from the test including: Energy absorbed, lateral expansion, fracture appearance, all of which shall be measured as a function of test temperature.

2.5. Weldability Bend Test (ASTM A494)

Weldability evaluation is to be conducted in accordance with ASTM A494 and ASTM A488. The 6” X 3 1/4” X 1” “bath tub” blocks, defined in ASTM A494, will be extracted from the SA castings. EDM wire cutting is employed to machine the “bath tub” in the blocks. The weldability sample, defined in ASTM A494, is shown in Figure 4-8 Shielded Metal Arc Welding (SMAW) is used to weld and fill the “bath tub” grooves in the castings. No PWHT shall be given according to ASTM A494; that is, all samples will need to be added in be bent in the as-welded condition. Extensive efforts are made to remove interpass slag although slag inclusions were present in some bend samples. The welded blocks are sliced into two 3/8” thick bend samples from the cross section of each ”bath tub”. Bend test using the same fixture as the 2t bend test followed IGC test (shown in Figure 4-4). The surfaces of the bend test region, i.e., the cross section of the weld, are to be carefully examined. All observable weld discontinuities are to be marked for evaluation with respect to bend criteria. The bent samples are to be examined according to ASTM A494 weldability bend test acceptance criteria, which states that:

1. Cracks, as tears in the casting in the fusion zone or heat-affected zone of the macro-specimen shall be cause for rejection. Cracks originating at the weld bead undercuts, at weld slag inclusions, or at casting defects shall not be cause for rejection.
2. Cracks or other open defects exceeding 1/8-in (3.2mm) measured in any direction on the convex surface of the bent specimens shall be cause for rejection, except that cracks occurring on the corners while testing and cracks origination at weld bead undercuts shall not be considered.

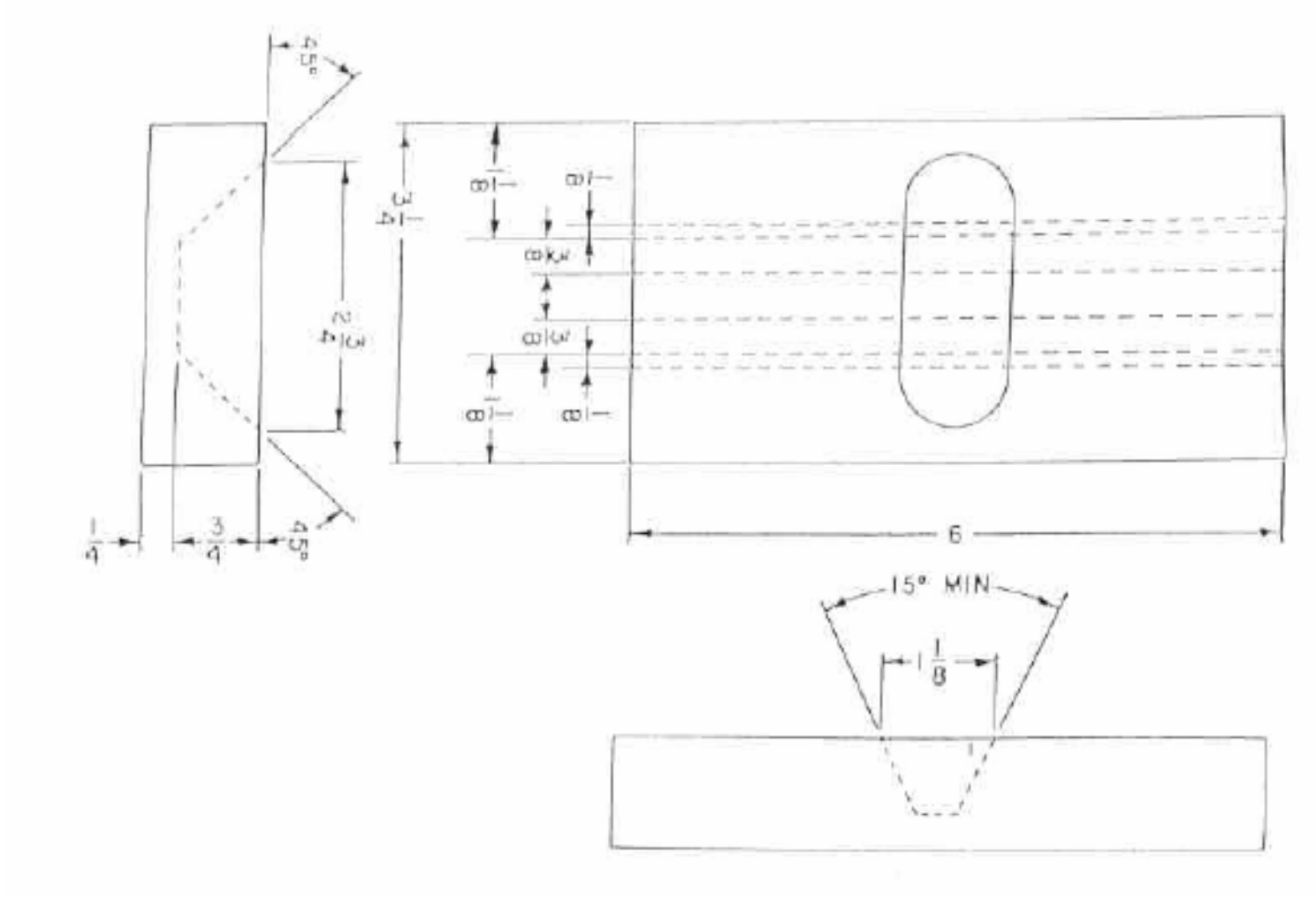

Figure 4-8. Weldability Sample (ASTM A494)

2.6. Solution Annealing Heat Treatments

A series of heat treatment schedule, based on the specification and metallurgy of the alloys, will be applied to as-cast 4A and 6A materials. This heat treatment schedule is presented in Table 4-3. In the schedule, three heat treatment temperatures were selected (2000°F, 2050°F & 2100°F) followed by different cooling methods (air cool and water quench). Two thermal arrest procedures were applied with the 2050°F heat treatment temperature. One thermal arrest method required castings be cooled to 1850°F (1010°C) minimum for a duration of 15 minutes prior to quenching. The other was conducted at 1950°F (1065°C) for a duration of one hour prior to the final quench. Totally, there were ten different heat treatment conditions for each alloy, making a total of twenty tested lots. All the above heat treatment practices are completed at a sponsor foundry.

CPT testing, ICT, NORSOK evaluations, ASTM A923 Method C and ferrite measurements are to be conducted on all of the heat treated 4A and 6A materials.

2.7. ASTM A923 Method A, B, C

ASTM A923, “Standard Test Method for Detecting Detrimental Intermetallic Phase in Wrought Duplex Austenitic/Ferritic Stainless Steels”, is a new standard that has been developed for use with wrought duplex stainless steels. The purpose of these test methods is to allow detection of the presence of intermetallic phases in mill products of duplex stainless steels to the extent that toughness or corrosion resistance is significantly affected. It is designed to address wrought Alloy 2205, but employed for testing of casting and wrought DSS alloys in this projects.

Table 4-3. Duplex Stainless Steel Casting Heat Treatment Study Schedule

HT Schedule No.	Heat Treatment Temperature (°F, °C)	Treatment Time	Arrest Method	Quench Method
1	2000°F (1090°C)	4 Hours	N/A	Water Quench
2	2000°F (1090°C)	4 Hours	N/A	Air Cool
3	2050°F (1120°C)	4 Hours	N/A	Water Quench
4	2050°F (1120°C)	4 Hours	N/A	Air Cool
5	2050°F (1120°C)	4 Hours	See Note 1	Water Quench
6	2050°F (1120°C)	4 Hours	See Note 1	Air Cool
7	2050°F (1120°C)	4 Hours	See Note 2	Water Quench
8	2050°F (1120°C)	4 Hours	See Note 2	Air Cool
9	2100°F (1150°C)	4 Hours	N/A	Water Quench
10	2100°F (1150°C)	4 Hours	N/A	Air Cool

Note 1: Thermal Arrest (Per ASTM A890-4A) requires that the castings be cooled to 1850°F (1010°C) minimum for a duration of 15 minutes (minimum) prior to quenching. Total arrest time will be 1 hour.

Note 2: Thermal Arrest will be conducted at 1950°F (1065°C) for a duration of 1 hour prior to quenching.

Method A: Sodium Hydroxide Etch Test for Classification of Etched Structures of Duplex Stainless Steels

ASTM A923 Method A, Sodium Hydroxide etch test for classification of etch structures of duplex stainless steels, may be used to screen specimens intended for testing in Method B and Method C. Test Method A is to be used for the acceptance of material but not for rejection. If the sample reveals an acceptable etch structure using test Method A, it does not need to be subjected to test Methods B and C.

The materials are to be polished and etched with 40% sodium hydroxide, 1 to 3 V dc for 5 to 60s. When etching is performed with a platinum cathode for 5 to 60s, any intermetallic phase is revealed by yellow, then brown, staining, followed by staining of the ferrite. Following etching, samples are to be rinsed thoroughly in hot water and in acetone or alcohol, followed by air drying. The etched surface shall be examined microscopically at 500X. Signs of precipitation or waviness along the phase boundaries are not acceptable. ASTM A923 Test Method A classifies etch structures into four categories as presented in Figures 4-9.

• Unaffected Structure (Figure 4-9-1) - The ferrite has been etched without revelation of intermetallic phase. The interphase boundaries are smooth.

• Possibly Affected Structure (Figure 4-9-2) - The ferrite has been etched with isolated indications of possible intermetallic phase. The interphase boundaries may show a fine waviness.

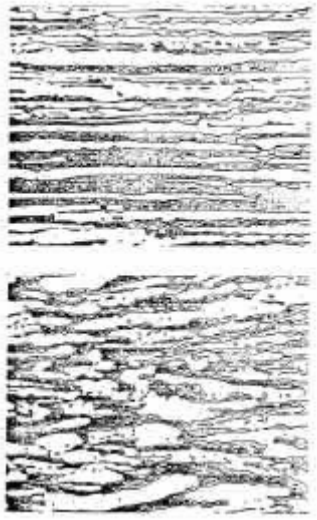

Figure 4-9-1. Unaffected Structure

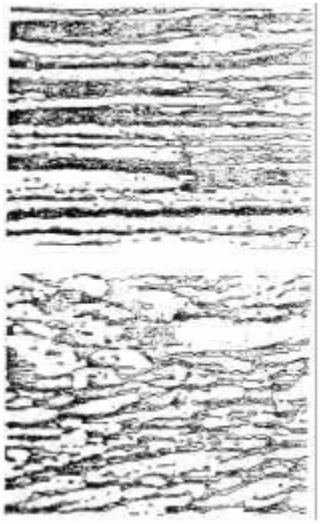

Figure 4-9-2. Possibly Affected Structure

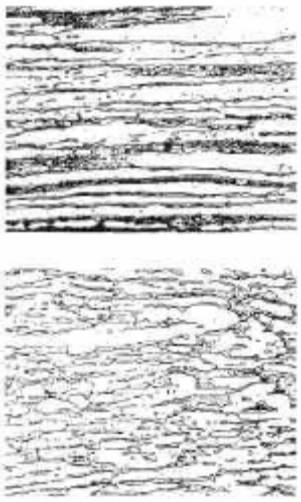

Figure 4-9-3. Affected Structure

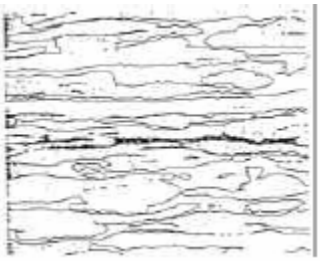

Figure 4-9-4. Centerline Structure

Note: Magnification is 500X.

Photomicrographs are all from

ASTM A923.

• Affected Structure (Figure 4-9-3) - The indications of an intermetallic phase are readily revealed before or simultaneously with the staining of the ferrite during etching.

• Centerline Structure (Figure 4-9-4) - An intermetallic phase is observed as a continuous or semi-continuous phase in the mid-thickness region of the product, with or without the affected structure out side of the mid-thickness region, indicative of segregation.

Method B: Charpy Impact Test for Classification of Structures of Duplex Stainless Steels

Test Method B is a Charpy impact test. It detects reductions in toughness resulting from processing irregularities. Variations in toughness may be attributable to an intermetallic phase or to other causes not necessarily detectable by Test Method A. This test method follows the procedure for conducting Charpy V-notch impact tests as a method of detecting the precipitation of detrimental intermetallic phases in DSS. Sample preparation and test procedures are to be performed in accordance with ASTM A370 and E23 (see section 2.2.5, Charpy Impact Test, for detail). Unless otherwise specified, the Charpy Impact test is performed at –40°F (-40°C). The acceptance criterion for wrought base metal is 40 ft-lbs. (54.2J) at –40°F (-40°C).

Method C: Ferric Chloride Corrosion Test for Classification of Structures of Duplex Stainless Steels

Test Method C, is similar to ASTM G48-A, “Ferric Chloride Pitting Test”. However, there are differences between the two test methods. This method defines the test temperature for base metal samples as 25°C, and for welds; 22°C. Sample

preparation and test solution preparation for this test method follow the same procedures for the CPT test (see section 2.1). The corrosion rate is calculated in accordance with the weight loss and total surface area, using the formula below:

Corrosion rate (mdd*) = weight loss (mg) / [specimen area (dm2) x time (days)]

* mdd; mg/ dm2/day

The acceptance criterion is that the corrosion rate shall not exceed 10mdd.

The method detects a loss of corrosion resistance associated with a local depletion of chromium and molybdenum as a result of the precipitation of chromium-rich and possibly molybdenum-rich phases, but not limited to intermetallic phases. An affected structure should be associated with significant weight loss in the corrosion test.

2.8. Ferrite Measurement

As discussed in the literature, phase balance is an essential factor in duplex stainless steels. Ferrite determination is used to assist the evaluations. Measurement is to be conducted utilizing a Fisher Model MP–3C Feritscope® (shown in Figure 3-23b). It is an easy-to-use, practical field instrument. The Feritscope® makes measurements by placing a probe into contact with the surface to be measured and holding it in place until an audible tone is heard. There are four available applications, each is designed for use over a specifically calibrated FN range. Individual reading, using the Feritscope®, requires no more than three seconds and an operator can take readings in very rapid succession. On-board statistics are available.

2.9. OLM

Microstructural relationships can provide improved understanding of material behavior and assist in defining changes necessary to improve performance. An explanation of experimental variation can usually be found when microstructures are defined.

Samples for metallographic evaluation are to be extracted from the castings and wrought plates, mounted with epoxy. Metallographic samples then are ground to 600-grit. Polishing of the sample including coarse polishing and fine polishing. The finished sample shall have a surface finish of 0.05mm then etched with solute sensitive etchants. Electrolytic etching in 10% oxalic acid or 40% sodium hydroxide and Glycerigia (HNO_3, HCl, Glycerol) were selected for this study. Moreover, in order to identify sigma phase, a stain-etching technique employing a 10% sodium cyanide electrolyte (current density: 1A/in2, etching time: 5s) maybe used in addition to 10% oxalic acid etching.

2.10. SEM & EDS

Detailed microstructural evaluation were conducted using Scanning Electron Microscopy (SEM) and Energy Dispersive Spectroscopy (EDS) on metallographically prepared samples. Specific attention was placed on the identification of the shape, distribution, chemistry and microstructure of secondary phases present in the material.

V. Results and Discussion

1. Corrosion Behavior of Cast Duplex Stainless Steels

1.1. CPT

CPT corrosion tests, according to ASTM G48, utilized a test period of 24 hours in 6% ferric chloride plus 1% HCl. All materials, ASTM A890-4A, 5A, 6A, 1B and "CD7MCuN", in the as-cast, SA static and SA centrifugal cast condition, and the wrought counterparts, were CPT tested. The base castings of super duplex type ASTM A890-5A and 6A exhibit the highest solution annealed CPT, as compared to ASTM A890-4A, 1B and "CD7MCuN", indicating improved pitting resistance. Castings in the as-cast condition show the lowest CPT than SA castings and the wrought materials.

ASTM A890-4A

Four ASTM A890-4A heats and one heat of Alloy 2205 were CPT tested. Heat 1 was tested in four conditions; the as-cast, as-cast + autogenously welded, SA and SA + autogenously welded condition. Heats 2, 3 and 4 were tested in the SA and SA + autogenously welded condition. Centrifugal casting from Heat 4 was also tested in SA and SA + Autogenous welded condition. The CPT results are summarized in Table 5-1-1 for ASTM A890-4A and wrought Alloy 2205. The CPT of Heat 1 in the as-cast condition is 25°C. The CPT of autogenously welded as-cast Heat 1 decreased to 15°C. The CPT's of Heats 1 through 4 SA static cast materials, vary from 35°C to 50°C, and the CPT's in the SA + autogenously welded condition are in the range of from below 0°C to 30°C. It is to be noted that Heat 2, in the SA condition, exhibits the lowest SA base

Table 5-1-1. Duplex Stainless Steel CPT Test Results, ASTM A890-4A

(ASTM G48, 6 % $FeCl_3$, 24 hrs.)

Material	Heat No.	Condition	CPT (°C)
ASTM A 890-4A	Heat 1	As-cast	25
ASTM A 890-4A	Heat 1	As-cast Autogenous welded	15
ASTM A 890-4A	Heat 1	Solution annealed	40
ASTM A 890-4A	Heat 1	SA Autogenous welded	30
ASTM A 890-4A	Heat 2	Solution annealed	35
ASTM A 890-4A	Heat 2	SA Autogenous welded	≤ 0
ASTM A 890-4A	Heat 3	Solution annealed	50
ASTM A 890-4A	Heat 3	SA Autogenous welded	≤ 0
ASTM A 890-4A	Heat 4	Solution annealed	45
ASTM A 890-4A	Heat 4	SA Autogenous welded	20
ASTM A 890-4A	Heat 4 CC*	Solution annealed	50
ASTM A 890-4A	Heat 4 CC*	SA Autogenous welded	15
Alloy 2205	Alloy 2205	Wrought	40
Alloy 2205	Alloy 2205	Wrought Autogenous welded	25

* CC - centrifugal cast

casting CPT (35°C), while Heat 3 has the highest (50°C). This result indicates that the difference in the CPT, between heats of the same material, can be significant.

For Heat 4, the CPT of the SA centrifugal casting is 50°C. It is 5 C° higher than the CPT of the SA static casting (45°C). Thus, it appears that there is little difference in pitting resistance between these casting methods. The CPT of the SA + autogenously welded centrifugal casting is 15°C. In addition, the wrought counterpart alloy 2205 shows a lower CPT (40°C) than most of the 4A cast materials in the SA condition. The CPT of autogenously welded Alloy 2205 is 25°C. Thus, it is evident that autogenous welding has a significant negative effect on the CPT, regardless of the material condition. The CPT test results can be summarized as follows:

1. The pitting corrosion resistance is the worst in the as-cast condition (ASTM A890 requires a SA for all grades). After solution annealing, it is significantly improved. There is a variation in CPT between SA cast heats and casting procedures (SA static casting and SA centrifugal casting). However, regarding the 5°C increment, these maybe simply scatter of the data.
2. Wrought materials have similar pitting corrosion resistance as compared to castings in the SA condition.
3. Autogenous welding decreases the pitting corrosion resistance regardless of the cast material condition, also for wrought materials.

ASTM A890-5A

Three ASTM A890-5A heats and one heat of Alloy 2507 were tested for the determination of the CPT's. Heat 1 was tested in the as-cast, SA and SA + autogenously welded condition. Heats 2 & 3 were tested in the SA and SA + autogenously welded condition. Additionally, Heat 3 was also tested in the SA centrifugal cast condition. The CPT results are summarized in Table 5-1-2 for ASTM A890-5A and wrought Alloy 2507. The CPT of Heat 1 in the as-cast condition is < 0°C. The CPT's of Heats 1, 2 & 3, SA static cast materials rank from 50°C to 65°C, and the CPT of SA + autogenously welded materials from these three heats range from 40°C or 45°C. Heat 2, in the SA condition, has the lowest SA CPT (50°C), while Heat 1 and Heat 3 have the same CPT (65°C) in SA condition. A difference in the CPT, between heats of the same material is evident, as with ASTM A890-4A.

The CPT of Heat 3, SA centrifugal casting, is 50°C. This is 15 C° lower than the CPT of the SA static casting of the same material (65°C). No evidence was found to explain this difference in pitting resistance between the two different casting methods. The CPT of the SA + autogenously welded centrifugal casting was 30°C.

The wrought counterpart, Alloy 2507, showed a CPT of 80°C, higher than any of the 5A cast materials, in the SA condition. The CPT of autogenously welded Alloy 2507 is 45°C.

Table 5-1-2 Duplex Stainless Steel CPT Test Results, ASTM A890-5A

(ASTM G48, 6 % $FeCl_3$, 24 hrs.)

Material	Heat No.	Condition	CPT (°C)
ASTM A 890-5A	Heat 1	As-cast	≤ 0
ASTM A 890-5A	Heat 1	Solution annealed	65
ASTM A 890-5A	Heat 1	SA Autogenous welded	45
ASTM A 890-5A	Heat 2	Solution annealed	50
ASTM A 890-5A	Heat 2	SA Autogenous welded	40
ASTM A 890-5A	Heat 3	Solution annealed	65
ASTM A 890-5A	Heat 3	SA Autogenous welded	45
ASTM A 890-5A	Heat 3 CC*	Solution annealed	50
ASTM A 890-5A	Heat 3 CC*	SA Autogenous welded	30
Alloy 2507	Alloy2507	Wrought	80
Alloy 2507	Alloy2507	Wrought Autogenous welded	45

* CC - centrifugal cast

ASTM A890-6A

The CPT of three ASTM A890-6A heats and one heat of wrought Zeron 100, were determined in the SA and SA + autogenouslly welded condition. Results are shown in Table 5-1-3. The highest CPT of the three 6A SA static cast materials is 70°C, the lowest, is 55°C. SA + autogenously welded CPT's rank from 40°C to 55°C. The CPT of base metal of wrought counterpart Zeron 100 is 65°C. When autogenously welded, the CPT is reduced to 30°C.

Table 5-1-3 Duplex Stainless Steel CPT Test Results, ASTM A890-6A

(ASTM G48, 6 % $FeCl_3$, 24 hrs.)

Material	Heat No.	Condition	CPT (°C)
ASTM A 890-6A	Heat 1	Solution annealed	65
ASTM A 890-6A	Heat 1	SA Autogenous welded	55
ASTM A 890-6A	Heat 2	Solution annealed	70
ASTM A 890-6A	Heat 2	SA Autogenous welded	45
ASTM A 890-6A	Heat 3	Solution annealed	55
ASTM A 890-6A	Heat 3	SA Autogenous welded	40
Zeron 100	Zeron 100	Wrought	65
Zeron 100	Zeron 100	Wrought Autogenous welded	30

ASTM A890-1B

Four ASTM A890-1B heats and one heat of wrought Ferralium 255 were CPT tested. Heat 1 was tested in the as-cast, as-cast + autogenously welded, SA and SA + autogenously welded condition. Heats 2, 3 and 4 were tested in the SA and SA + autogenously welded condition. The CPT results are summarized in Table 5-1-4 for ASTM A890-1B and wrought alloy Ferralium 255. The CPT of Heat 1, in the as-cast condition, is 15°C. The CPT's of autogenously welded as-cast 1B remains the same (15°C). The CPT of the 1B, SA static cast materials, fall into the range of 30°C to 40°C. In the SA + autogenously welded condition, the CPT's of these materials range from 10°C to 25°C. Wrought counterpart Ferralium 255 has a CPT of 45°C, and 25°C for the

Table 5-1-4 Duplex Stainless Steel CPT Test Results, ASTM A890-1B

(ASTM G48, 6 % $FeCl_3$, 24 hrs.)

Material	Heat No.	Condition	CPT (°C)
ASTM A 890-1B	Heat 1	As-cast	15
ASTM A 890-1B	Heat 1	As-cast Autogenous welded	15
ASTM A 890-1B	Heat 1	Solution annealed	35
ASTM A 890-1B	Heat 1	SA Autogenous welded	25
ASTM A 890-1B	Heat 2	Solution annealed	40
ASTM A 890-1B	Heat 2	SA Autogenous welded	15
ASTM A 890-1B	Heat 3	Solution annealed	30
ASTM A 890-1B	Heat 3	SA Autogenous welded	15
ASTM A 890-1B	Heat 4	Solution annealed	35
ASTM A 890-1B	Heat 4	SA Autogenous welded	10
Ferralium 255	Ferr. 255	Wrought	45
Ferralium 255	Ferr. 255	Wrought Autogenous welded (Ar)	25
Ferralium 255	Ferr. 255	Wrought Autogenous welded (Ar + 5%N_2)	30

“CD7MCuN”

Two “CD7MCuN” heats were tested for the determination of CPT’s. Heat 1 was tested in the SA static cast condition. Heat 2 was tested in both the SA static cast and SA centrifugal cast condition. Autogenous welding was applied to both heats. Heat 1 SA static cast revealed a CPT of 45°C, and the CPT of the SA + autogenously welded coupon is 5°C. The CPT’s of Heat 2 in the SA static cast and SA centrifugal cast condition are 40°C and 50°C, respectively. The CPT’s of the SA + autogenously welded static cast and centrifugal cast are 15°C. The results are presented in Table 5-1-5.

Table 5-1-5 Duplex Stainless Steel CPT Test Results, CD7MCuN

(ASTM G48, 6 % $FeCl_3$, 24 hrs.)

Material	Heat No.	Condition	CPT (°C)
CD7MCuN	Heat 1	Solution Annealed	45
CD7MCuN	Heat 1	SA Autogenous Welded	5
CD7MCuN	Heat 2	Solution Annealed	40
CD7MCuN	Heat 2	SA Autogenous Welded	15
CD7MCuN-CC	Heat 2 CC*	Solution Annealed	50
CD7MCuN-CC	Heat 2 CC*	SA Autogenous Welded	15

* CC - centrifugal cast

1.2. IGC

The intergranular corrosion resistance evaluation was conducted according to ASTM A262 Practice B with an ancillary adopted “Bend Test”. Samples, in the form of a 3 1/8" X 3/4" X 1/8" coupon, were prepared to a uniform 120-grit surface finish. Intergranular corrosion tests (ICT) were conducted in a boiling Ferric Sulfate-Sulfuric Acid ($Fe(SO_4)_3$ - 50% H_2SO_4) solution for a 120-hour test period. After ICT testing, samples were 2t bend tested to assist in the revelation of the extent of intergranular corrosion.

ASTM A890-4A

Four ASTM A890-4A heats and one heat of Alloy 2205 were ICT tested. Heat 1 was tested in the as-cast, as-cast + autogenously welded, SA and SA + autogenously welded condition. Heats 2, 3 and 4 were tested in the SA and SA + autogenously welded static cast condition. Heats 1, 2 and 3 were tested only in the SA static cast condition and Heat 4 was tested in both the SA static and centrifugal cast conditions. The ICT results for ASTM A890-4A are presented in Table 5-2-1. The IGC rate of Heat 1 in the as-cast condition is the highest of the materials tested (62.23mpy). The as-cast Heat 1 ICT samples showed intergranular separations after bending. The Heat 1 autogenously welded as-cast samples, showed an average of 47.00mpy. The autogenously welded as-cast ICT samples also showed intergranular separations (in the base metal, not in the welded region) after bending. IGC rates and bend test behavior of SA Heats 1, 2, 3 & 4 are very similar, regardless of casting method (static or centrifugal). In general, autogenous welding increased the IGC rate of SA materials to a minor extent with the

Table 5-2-1. Intergranular Corrosion Test and Bend Test Results, ASTM A890-4A

(ASTM A262 Practice B, Ferric Sulfate-Sulfuric Acid, Boiling, 120 hrs.)

Material	Code	Condition	Corrosion Rate (mpy)	Bending Results (After ICT)
ASTM A890-4A	Heat 1	As-cast	61.26	Intergranular Separations
			63.29	
ASTM A890-4A	Heat 1	As-cast (A-W)	49.76	Intergranular Separations in the BM
			44.23	
ASTM A890-4A	Heat 1	Solution Annealed	12.93	No Separations
			12.43	
ASTM A890-4A	Heat 1	SA (A-W)	15.25	Interdendritic Separations in the WM & HAZ
			15.18	
ASTM A890-4A	Heat 2	Solution Annealed	10.84	No separations
			15.51	Minor separation
ASTM A890-4A	Heat 2	SA (A-W)	11.73	No separations
			17.59	Minor separation
ASTM A890A-4A	Heat 3	Solution Annealed	11.21	No separations
			11.08	
ASTM A890-4A	Heat 3	SA (A-W)	21.13	Interdendritic separations in the weld
			21.72	
ASTM A890-4A	Heat 4	Solution Annealed	10.81	No separations
			10.50	
ASTM A890-4A	Heat 4	SA (A-W)	10.90	Separations in the HAZ
			11.21	
ASTM A890A-4A	Heat 4 CC*	Solution Annealed	11.17	Minor separation
			10.86	No separations
ASTM A890-4A	Heat 4 CC*	SA (A-W)	11.18	Separations
			10.75	
Alloy 2205	Alloy 2205	Wrought	16.60	No Separations
			16.11	
Alloy 2205	Alloy 2205	Wrought (A-W)	20.72	Interdendritic Separations in the WM
			19.90	

* CC - centrifugal cast

corrosion taking place in the weld fusion zone. The ICT results also showed heat-to-heat behavioral differences. For example, Heat 3 SA static cast base metal show an average of 11.15mpy, with no grain boundary separations observed after bending. The average IGC rate for SA + autogeously welded is 21.43mpy, with interdendritic separations observed in the weld fusion zone. For Heat 4, the SA static cast base metal has an average of 10.65mpy, with no separations observed after bending. The average of its SA + autogeously welded is 11.05mpy, with separations observed in the HAZ. Wrought Alloy 2205 shows a higher IGC rate than the SA castings even when they are autogenously welded. No separations were observed on the SA casting base metal bent samples, but interdendritic separations appeared in the fusion zone of autogenous welds. The IGC test results are summarized as follows:

1. The as-cast condition shows the highest intergranular corrosion rate, and the most extensive separations (some intergranular fractures) upon bending.
2. Solution annealing reveals a significant decrease in the IGC rate compared to the as-cast materials.
3. The wrought counterpart alloys showed higher IGC rates but similar bending behavior when compared to the SA cast materials.
4. Welding decreases the IGC rates in the as-cast condition, but for the SA cast materials and wrought counterparts, welding increased the IGC rates to a minor extent.

ASTM A890-5A

Three ASTM A890-5A heats and one heat of Alloy 2507 were evaluated by ICT. Heat 1 was tested in the as-cast, as-cast + autogenously welded, SA and SA + autogenously welded condition. Heats 2 & 3 were tested in the SA static cast and SA + autogenously welded conditions. In addition, Heat 3 was tested in the SA centrifugal cast condition. Table 5-2-2 shows the ICT results for ASTM A890-5A materials. Compared to ASTM A890-4A materials, the same trends on ICT behavior were observed for the ASTM A890-5A materials. However, the IGC rates of ASTM A890-5A, solution annealed cast (Avg. 7.58mpy) and wrought materials (Avg. 8.29mpy), were lower than ASTM A890-4A materials in the corresponding conditions (Avg. 11.74mpy for SA static cast and centrifugal cast / Avg. 16.36mpy for wrought Alloy 2507). SA + autogenous welding increased IGC rate. Maximum increment of SA + autogenous welding on IGC rate is 1.0mpy).

ASTM A890-6A

ICT of three ASTM A890-6A heats and one heat of wrought counterpart Zeron 100, were conducted in the as-cast, as-cast + autogenously welded, SA and SA + autogenously welded condition. The IGC rates of ASTM A890-6A materials and wrought Zeron 100 and their autogenously welded condition are approximately the same as that of ASTM A890-5A materials. The results are presented in Table 5-2-3.

Table 5-2-2. Intergranular Corrosion Test and Bend Test Results, ASTM A890-5A

(ASTM A262 Practice B, Ferric Sulfate-Sulfuric Acid, Boiling,120 hrs.)

Material	Code	Condition	Corrosion Rate (mpy)	Bending Results (After ICT)
ASTM A890-5A	Heat 1	As-cast	24.22	Intergranular Separations
			25.46	(Fractured)
ASTM A890-5A	Heat 1	As-cast (A-W)	23.98	Intergranular Separations
			23.91	(Fractured)
ASTM A890-5A	Heat 1	Solution Annealed	8.12	No Separations
			8.33	
ASTM A890-5A	Heat 1	SA (A-W)	7.89	Interdendritic Separations
			7.80	in the WM
ASTM A890-5A	Heat 2	Solution Annealed	6.73	No separations
			6.85	Minor separation
ASTM A890-5A	Heat 2	SA (A-W)	6.25	Separations
			7.29	in the HAZ
ASTM A890-5A	Heat 3	Solution Annealed	6.96	No separations
			6.81	
ASTM A890-5A	Heat 3	SA (A-W)	7.74	Minor separations in WM
			7.33	No separations
ASTM A890-5A	Heat 3 CC*	Solution Annealed	7.59	Minor separations
			7.91	No separations
ASTM A890-5A	Heat 3 CC*	SA (A-W)	8.70	Minor separations
			8.16	in the WM & HAZ
Alloy 2507	Alloy 2507	Wrought	8.17	No Separations
			8.41	
Alloy2507	Alloy2507	Wrought (A-W)	8.74	Minor separations
			9.83	in the HAZ

* CC - centrifugal cast

Table 5-2-3. Intergranular Corrosion Test and Bend Test Results, ASTM A890-6A (ASTM A262 Practice B, Ferric Sulfate-Sulfuric Acid, Boiling,120 hrs.)

Material	Code	Condition	Corrosion Rate (mpy)	Bending Results (After ICT)
ASTM A890-6A	Heat 1	As-cast	33.22	Intergranular separations
			32.50	(Fractured)
ASTM A890-6A	Heat 1	As-cast (A-W)	31.03	Intergranular separations
			30.75	(Fractured)
ASTM A890-6A	Heat 1	Solution Annealed	7.99	No Separation
			7.83	
ASTM A890-6A	Heat 1	SA (A-W)	8.25	No Separation
			7.73	Minor Separation in the WM
ASTM A890-6A	Heat 2	Solution Annealed	7.77	No Separations
			7.83	Minor Separations
ASTM A890-6A	Heat 2	SA (A-W)	7.63	Separations in WM & HAZ
			7.63	
ASTM A890-6A	Heat 3	Solution Annealed	7.21	No separations
			7.12	
ASTM A890-6A	Heat 3	SA (A-W)	7.28	Minor separations
			7.43	in the HAZ
Zeron 100	Zeron100	Wrought	6.81	No Separation
			7.12	
Zeron 100	Zeron100	Wrought (A-W)	7.96	Separation in WM and HAZ
			7.75	

ASTM A890-1B & "CD7MCuN"

Four ASTM A890-1B heats and one heat of wrought Ferralium 255 were ICT tested. Heat 1 was tested in the as-cast, as-cast + autogenously welded, SA and SA + autogenously welded condition. Heats 2, 3 and 4 were tested in the SA and SA + autogenously welded condition.

The two "CD7MCuN" heats were subjected to ICT testing. Heat 1 was tested in the SA statically cast condition. Heat 2 was tested in both the SA static cast and centrifugal cast conditions. Autogenously welded samples in each condition were also ICT tested.

The IGC rates of these materials are presented in Table 5-2-4 and Table 5-2-5 for ASTM A890-1B and "CD7MCuN". These results are similar to the values obtained for ASTM A890-4A materials. In general, the IGC rates of as-cast materials are greater than 25mpy. Intergranular separations occur for the as-cast materials upon bending after ICT. The SA castings and wrought materials exhibit IGC rates in the range of 7.00mpy to 13.00mpy and their bending behavior is similar in terms of no separations or only minor separations observed. An exception is wrought Alloy 2205, revealing an average IGC rate of 16.30mpy without separations observed after bend testing. The effect of autogenous welding on IGC behavior, depends on the material condition. For the as-cast condition, autogenous welding improves IGC performance. For SA castings and wrought materials, autogenous welding generally exacerbates the IGC performance of the materials. In addition, the super duplex grades ASTM A890-5A and 6A have better IGC resistance and bending behavior than the remainder of the materials (ASTM A890-4A, 1B and "CD7MCuN").

Table 5-2-4. Intergranular Corrosion Test and Bend Test Results, ASTM A890-1B

(ASTM A262 Practice B, Ferric Sulfate-Sulfuric Acid, Boiling,120 hrs.)

Material	Code	Condition	Corrosion Rate (mpy)	Bending Results (After ICT)
ASTM A890-1B	Heat 1	As-cast	31.04 30.76	Intergranular Separations (Fractured)
ASTM A890-1B	Heat 1	As-cast (A-W)	28.02 28.81	Separations in the WM & BM
ASTM A890-1B	Heat 1	Solution Annealed	11.39 11.83	Minor Intergranular Separations
ASTM A890-1B	Heat 1	SA (A-W)	12.22 12.22	Minor Interdendritic Separations in the WM
ASTM A890-1B	Heat 2	Solution Annealed	10.43 10.76	Minor intergranular separations
ASTM A890-1B	Heat 2	SA (A-W)	18.71 19.08	Serious separations in the WM & HAZ
ASTM A890-1B	Heat 3	Solution Annealed	9.18 9.02	Minor Intergranular Separations
ASTM A890-1B	Heat 3	SA (A-W)	9.95 11.13	Separations in the WM & HAZ
ASTM A890-1B	Heat 4	Solution Annealed	8.82 9.09	Minor Intergranular Separations
ASTM A890-1B	Heat 4	SA (A-W)	9.28 8.99	Interdendritic Separations in the WM
Ferralium 255	Ferr.255	Wrought	8.49 9.49	No Separations
Ferralium 255	Ferr.255	Wrought (A-W)	10.30 9.77	Separations In the WM & HAZ

Table 5-2-5. Intergranular Corrosion Test and Bend Test Results, CD7MCuN (ASTM A262 Practice B, Ferric Sulfate-Sulfuric Acid, Boiling,120 hrs.)

Material	Code	Condition	Corrosion Rate (mpy)	Bending Results (After ICT)
CD7MCuN	Heat 1	Solution Annealed	9.15 8.83	No separations
CD7MCuN	Heat 1	SA (A-W)	14.78 14.48	Serious interdendritic separations in the WM
CD7MCuN	Heat 2	Solution Annealed	12.40 12.37	Intergranular Separations
CD7MCuN	Heat 2	SA (A-W)	13.67 14.07	Separations in the WM & BM
CD7MCuN-CC	Heat 2 CC*	Solution Annealed	10.01 10.37	No Separations
CD7MCuN-CC	Heat 2 CC*	SA (A-W)	10.73 10.78	Serious separations in the WM & HAZ

* CC - centrifugal cast

2. Effect of Welding on the Properties of DSS

2.1. Effect of Autogenous Welding on Pitting and IGC Behavior

It is evident from the results and discussions on CPT and IGC test results that autogenous welding has a significant effect on the corrosion performance of DSS. It was found that pitting and IGC occur preferentially in the fusion zone of autogenous welds. In general, autogenous welding exacerbates the corrosion behavior of DSS castings and their wrought counterparts. The extent of the influence of autogenous welding on the corrosion performance of DSS depends upon the material and its condition in terms of as-

cast or SA. It is to be recalled, that the entire fusion zone of an autogenous weld is an "unmixed zone", in which depletion of alloy elements through segregation may occur during solidification and subsequent transformation, and thus egregiously result in the degradation of corrosion resistance.

In addition, nitrogen has a significant effect on pitting corrosion behavior of DSS. In general, an increase in nitrogen content in the shielding gas, improves the pitting corrosion resistance. The loss of nitrogen during welding may result in a decrease in corrosion resistance. The study on adding 5% nitrogen into the shielding gas, during autogenous welding, reveals that the corrosion resistance (CPT) was improved or partially restored (Table 5-1-4). However, the extent of CPT improvement, through adding nitrogen into the shielding gas, is not as significant as anticipated. It is to be noted that the dramatic decrease in CPT upon autogenous welding is consistent with what was reported in the literature. Thus, welding DSS without a filler metal is not a recommended practice.

A similar effect of autogenous welding on IGC resistance was also determined for SA cast materials and the wrought counterparts. The bending results of ICG test samples show that IGC preferentially occurred in the fusion zone and/or HAZ. However, for the castings in the as-cast condition, autogenous welding slightly improves the IGC behavior in terms of a decrease in the IGC rate. It is believed that this positive effect of autogenous welding on IGC of as-cast materials is attributed to a refined grain structure in the fusion zone.

2.2. Preliminary Study of Pitting Corrosion Resistance of SMAW of DSS

It should be recognized that welding processes using a filler metal result in a weldment with several different metallurgical zones; a composite zone, an unmixed zone, a heat-affected zone (HAZ) and the un-affected base metal in the fabrication. The metallurgical characteristics of each zone can be significantly different from that of the original base material in terms of microstructure, phase balance and alloying element distribution. Thus, the corrosion performance of welded components can be expected to be different from unwelded base material.

SMAW test coupons were pitting tested to determine the relative corrosion resistance between the composite zone, the unmixed zone, the heat-affected zone (HAZ) and the SA casting base metal. A total of five heats, one from each alloy system (ASTM A890-4A, 5A, 6A, 1B and "CD7MCuN") were selected. The corrosion coupons were extracted from the remnant section of weldability test blocks. Note that the weldability test block was fabricated using a SMAW procedure with recommended or over-matching filler metals. The welding parameters and filler metals are summarized in Table 5-3.

A 1/8" thick transverse cross section was extracted from each of the weldability test blocks as illustrated in Figure 4-7. Due to the limited availability of materials, the 1/8" cross section was further sectioned into four corrosion coupons that all contain a composite zone, unmixed zone, heat-affected zone (HAZ) and un-affected base metal. Coupon extracted are labeled 1, 2, 3, and 4 as shown in Figure 5-1. The initial pitting corrosion test for each material started at the CPT of the corresponding SA base metal with 0.05μm polished surface. It is recalled that the SA base metal CPT was determined on a 600 grit surface finish. The pitting corrosion test was interrupted, at a time interval

Table 5-3. Base Metals, Filler Metals and Welding Parameters

Base Metal	Filler Metal	Electrode Diameter (inches)	Welding Current (A)	Welding Voltage (V)
ASTM 890-4A	Alloy 2209	1/8	93	26
ASTM 890-5A	Alloy 2507	1/8	94	25
ASTM 890-6A	Zeron 100	5/32	152	26
ASTM 890-1B	Ferralium 255	1/8	113	26
"CN7MCuN"	Ferralium 255	1/8	113	26

Note: Welding operations were conducted using DC electrode positive polarity.

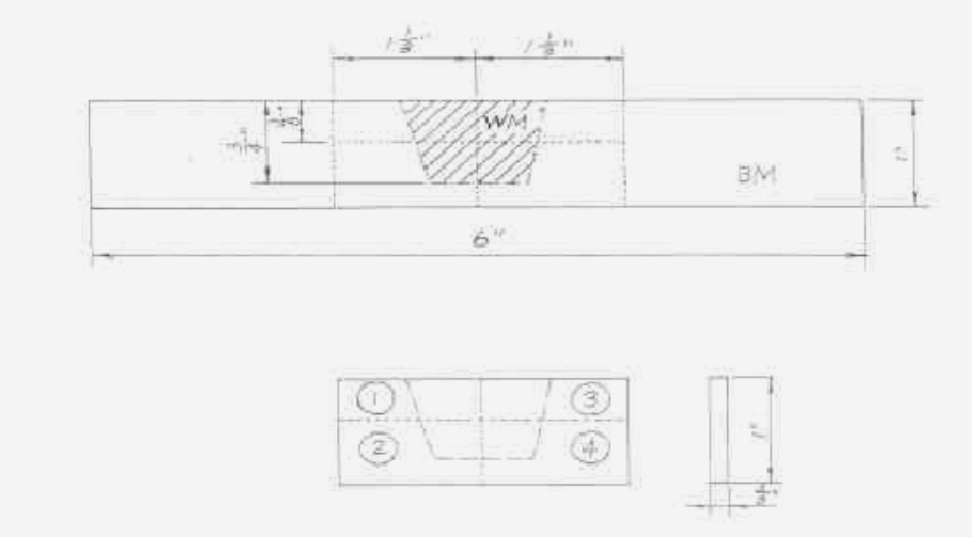

Figure 5-1. Cutting Plan for Corrosion Test Samples for Preliminary Study of Pitting Performance of Composite Welds

of 2^n minutes (n = 1, 2, 3, 4…) to define the preferential pit initiation location; in the composite zone, unmixed zone, heat-affected zone (HAZ) and/or in the un-affected base metal. If no pits were observed at 100X, at a specific time interval, corrosion testing continued until the accumulation of testing time equaled 2 hours. If no pitting was found after 2 hours, the test temperature was increased 5 C° and the test procedure repeated. If pits were observed, the corrosion test was terminated to document the preferential pitting initiation location. For determination of where the pits preferentially initiated, each corrosion coupon was ground and polished to 0.05mm finish, and then lightly electrolyticly etched, using 10% oxalic acid, to reveal each zone present in the coupon before the corrosion testing. In addition, all the welding discontinuities (location and size) present in each sample were carefully documented, and any pits initiating from the welding discontinuities were disregarded. The corrosion test solution was 6% FeCl3 + 1% HCl. Note that no CPT or corrosion rate was determined in this study. The preliminary results of the corrosion performance of the DSS casting SMA welds are summarized and discussed as follows:

ASTM A890-4A

Pitting initiated in the HAZ at 60°C (Figure 5-2)

ASTM A890-5A

Pitting initiated in the FZ and FL/HAZ at 65°C (Figure 5-3, 5-4)

ASTM A890-6A

Pitting initiated in the FZ at 65°C (Figure 5-5)

ASTM A890-1B

Pitting occurred in the FL/HAZ and BM after 126 minutes in testing solution at 35°C

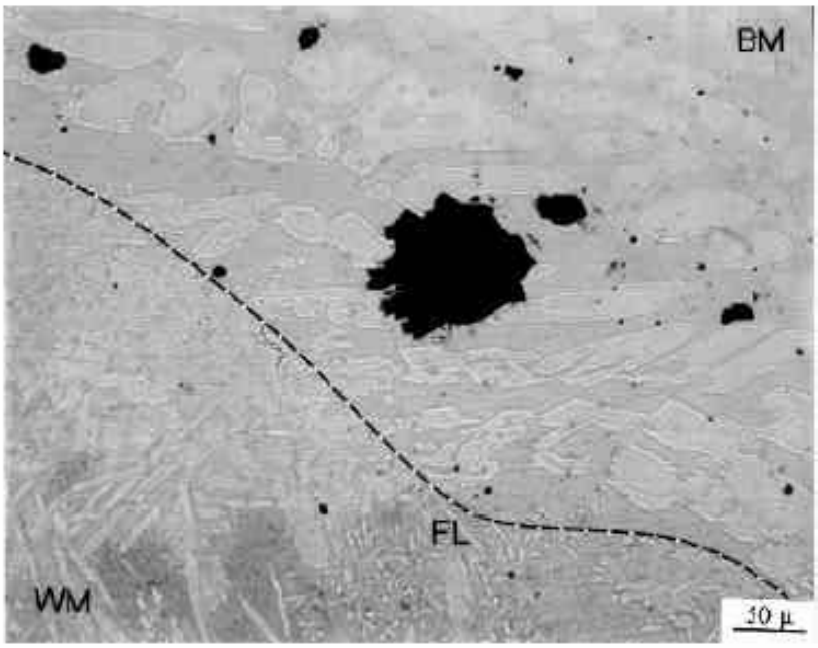

Figure 5-2. ASTM A890-4A, Sample 1, 60C, 6 min, Pits in the HAZ, 200X

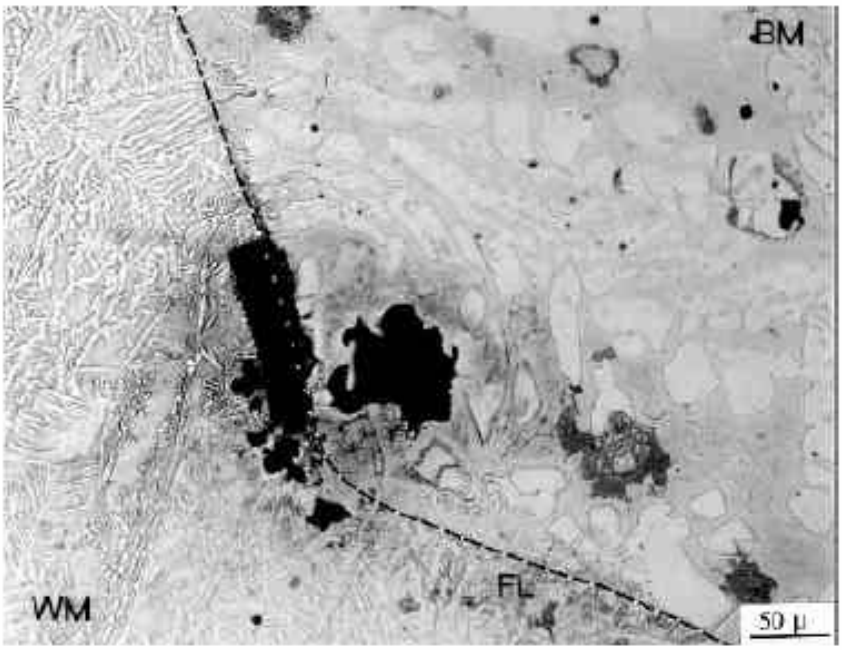

Figure 5-3. ASTM A890-5A, Sample 1, 65^{o}C, 6 min, Pits on FL, 200X

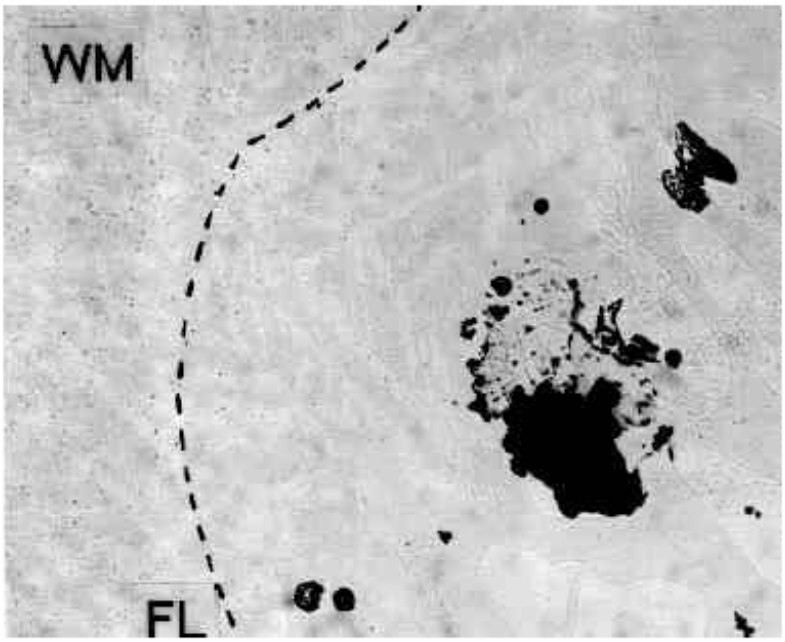

Figure 5-4. ASTM A890-5A, Sample 3, 65°C, 2 min, Pits on HAZ, 200X

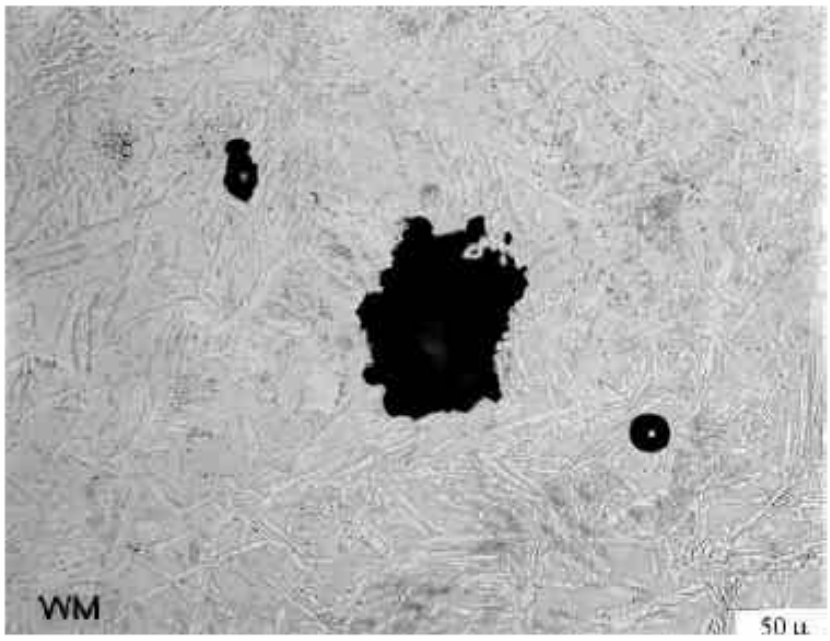

Figure 5-5. ASTM A890-6A, Sample 1, 65°C, 6 min, Pits on WM, 200X

Preliminary conclusions, based on the results of corrosion testing conducted on the SMA welded samples, can be drawn as follows:

1). SMA welding process has a significant effect on the corrosion performance of DSS castings. Pits preferentially initiated in the composite zone, unmixed zone or the heat-affected zone, depending on material.

2). Surface condition (roughness) of a corrosion test sample will influence the base metal CPT. In general, the finer the surface finish, the higher the CPT.

These preliminary results of the trial pitting corrosion test on DSS castings clearly define the necessity for an additional detailed study on the corrosion performance of the DSS composite welds.

3. Effect of heat treatment on the Corrosion Behavior of Cast Duplex Stainless Steels

Solution heat treatments are of vital importance to the corrosion resistance of DSS due to the metallurgical complexities of highly alloyed system. A heat treatment study was conducted on ASTM A890-4A and 6A materials. The purpose of this experiment is to study the corrosion resistance as a function of solution annealing temperature and holding time. Heat 1 of ASTM A890-4A and Heat 3 of 6A were selected for the study. ASTM A890 contains the heat treatment requirements for the two alloy systems. For ASTM A890-4A, castings shall be heated to 2050 °F (1120°C) minimum for sufficient time to heat the casting uniformly to temperature and water quench, or the casting may be furnace cooled to 1850°F (1010°C) minimum hold for 15 minutes and then water quenched. A rapid cool by other means may be employed in lieu of a water quench.

The heat treatment requirements for ASTM A890-6A mandate is that, castings shall be heated to 2010°F (1100°C) minimum, held for sufficient time to heat casting uniformly to temperature, quenched in water or cooled rapidly by other means.

A carefully planed heat treatment schedule, based on the specification and metallurgy of the alloys, was applied to as-cast 4A and 6A materials. This heat treatment schedule is presented in Table 5-4.

Table 5-4. Duplex Stainless Steel Casting Heat Treatment Study Schedule

HT No.	HT Temperature (°F, °C)	Treatment Time	Arrest Method	Quench Method
1	2000°F (1090°C)	4 Hours	N/A	Water Quench
2	2000°F (1090°C)	4 Hours	N/A	Air Cool
3	2050°F (1120°C)	4 Hours	N/A	Water Quench
4	2050°F (1120°C)	4 Hours	N/A	Air Cool
5	2050°F (1120°C)	4 Hours	See Note 1	Water Quench
6	2050°F (1120°C)	4 Hours	See Note 1	Air Cool
7	2050°F (1120°C)	4 Hours	See Note 2	Water Quench
8	2050°F (1120°C)	4 Hours	See Note 2	Air Cool
9	2100°F (1150°C)	4 Hours	N/A	Water Quench
10	2100°F (1150°C)	4 Hours	N/A	Air Cool

Note 1: Thermal Arrest (Per ASTM A890-4A) requires that the castings be cooled to 1850°F (1010°C) minimum for a duration of 15 minutes (minimum) prior to quenching. Total arrest time will be 1 hour.

Note 2: Thermal Arrest will be conducted at 1950°F (1065°C) for a duration of 1 hour prior to quenching.

In the schedule, three heat treatment temperatures were selected (2000°F, 2050°F & 2100°F) followed by different cooling methods (air cool and water quench). Two thermal arrest procedures were applied with the 2050°F heat treatment temperature. One thermal arrest method required castings be cooled to 1850°F (1010°C) minimum for a duration of 15 minutes prior to quenching. The other was conducted at 1950°F (1065°C) for a duration of one hour prior to the final quench. Totally, there were ten different heat treatment conditions for each alloy, making a total of twenty tested lots.

CPT testing, ICG testing results of all the heat treated 4A and 6A materials are as follow.

3.1. CPT

The CPT test results of the heat treatment study samples are presented in Tables 5-5-1 and 5-5-2 for ASTM A890-4A and 6A.

All the ASTM A890-4A water quenched materials in this study reveal the same CPT as foundry SA materials (40°C), except when an 1850°F (1010°C) thermal arrest is applied (35°C). All the air cooled materials exhibit a CPT of 35°C, with the exception of the 1950°F (1065°C) thermal arrest with a CPT of 40°C.

For ASTM A890-6A (Heat 3), the CPT of the foundry SA material is 55°C. 6A does not require a thermal hold in accordance with ASTM A890. The same thermal holds as for 4A were evaluated to determine if thermal holds were detrimental. All the water quenched heat treated materials (CPT 45-55°C) exhibit higher CPT's than the air cooled (CPT 5-50°C) for the same heat treatment temperature and thermal arrest

Table 5-5-1. CPT & IGC Test Results of Heat Treatment Study Materials, ASTM A890-4A, Heat 1

(ASTM G48, 6% $FeCl_3$, 24 hrs.)

	Heat Treatment Temperature (°F, °C)	Treatment Time	Arrest Method	Quench Method	CPT (°C)	Intergranular Corrosion Rate (mpy)*
1	2000°F (1090°C)	4 Hours	N/A	Water Quench	40	12.35
						11.61
2	2000°F (1090°C)	4 Hours	N/A	Air Cool	35	10.15
						9.15
3	2050°F (1120°C)	4 Hours	N/A	Water Quench	40	11.87
						12.11
4	2050°F (1120°C)	4 Hours	N/A	Air Cool	35	9.58
						10.14
5	2050°F (1120°C)	4 Hours	See Table11 Note 1	Water Quench	35	10.50
						10.78
6	2050°F (1120°C)	4 Hours	See Table11 Note 1	Air Cool	35	11.26
						11.36
7	2050°F (1120°C)	4 Hours	See Table11 Note 2	Water Quench	40	11.27
						10.62
8	2050°F (1120°C)	4 Hours	See Table11 Note 2	Air Cool	40	11.29
						10.81
9	2100°F (1150°C)	4 Hours	N/A	Water Quench	40	12.85
						11.95
10	2100°F (1150°C)	4 Hours	N/A	Air Cool	35	11.62
						11.81

Table 5-5-2. CPT & IGC Test Results of Heat Treatment Study Materials, ASTM A890-6A, Heat 3

(ASTM G48, 6% $FeCl_3$, 24 hrs.)

	Heat Treatment Temperature (°F, °C)	Treatment Time	Arrest Method	Quench Method	CPT (°C)	Intergranular Corrosion Rate (mpy)*
1	2000°F (1090°C)	4 Hours	N/A	Water Quench	45	7.27
						6.85
2	2000°F (1090°C)	4 Hours	N/A	Air Cool	40	6.72
						6.58
3	2050°F (1120°C)	4 Hours	N/A	Water Quench	55	7.65
						8.02
4	2050°F (1120°C)	4 Hours	N/A	Air Cool	50	7.30
						6.93
5	2050°F (1120°C)	4 Hours	See Table11 Note 1	Water Quench	45	7.25
						7.52
6	2050°F (1120°C)	4 Hours	See Table11 Note 1	Air Cool	5	8.50
						8.43
7	2050°F (1120°C)	4 Hours	See Table11 Note 2	Water Quench	55	6.88
						7.25
8	2050°F (1120°C)	4 Hours	See Table11 Note 2	Air Cool	50	8.33
						8.13
9	2100°F (1150°C)	4 Hours	N/A	Water Quench	55	7.82
						7.87
10	2100°F (1150°C)	4 Hours	N/A	Air Cool	45	8.68
						8.82

method. In general, the air cooled coupons had CPT's of 5-10C° lower than the water quenched materials. An exception for the CPT response is found for the 1850°F (1010°C) thermal arrested and followed by air cool, with which shows a CPT of 5°C. The heat treatment produced a secondary phase (s) as etched with 40% NaOH per ASTM A923 Method A. Thus, thermal holds at 1850°F followed by air cooling should not be applied for 6A materials. In general, the thermal arrests applied in this study revealed no significant influence on the CPT. The heat treated materials have similar CPT's, regardless of heat treatment temperature and cooling method.

3.2. IGC

The ICT was conducted on the ASTM A890-4A & 6A heat treated materials. The results are presented in Table 5-5-1 for ASTM A890-4A and Table 5-5-2 for 6A. It is evident that the water quenched materials (10.50-12.85mpy) show a slightly lower IGC rate than the air cooled materials (9.15-11.81mpy), for the same heat treatment temperature and thermal arrest method. The difference between water quenched and air cooled materials is approximately 0.5 to 2.0 mpy. The study indicates that the IGC rates will not be influenced significantly by different heat treatment conditions.

4. Toughness of Cast DSS vs. Wrought

Ten heats were selected for Charpy impact testing. Two from ASTM A890-4A (Heats 1 & 2), one from each of ASTM A890-5A (Heat 1), ASTM A890-6A (Heat 1) and ASTM A890-1B (Heat 3), and one from "CD7MCuN" (Heat 2) in the SA static and centrifugal cast condition, as well as wrought Alloy 2205, Alloy 2507, Zeron 100,

Ferralium 255. The “CD7MCuN” heat was tested with both the static and centrifugal casting. Totally, eleven lots were tested.

The Charpy tests were conducted according to ASTM A370 and ASTM E23 in the temperature range of –80 °C to 20°C. Duplicate samples were tested at each test temperature. The energy absorbed, lateral expansion and percent shear of the tested Charpy bars, were recorded for each sample. The Charpy results are presented in Figure 5-6, as a function of test temperature.

The Charpy results (Figure 5-6) show that the toughness of the majority of the heats, over the test temperature interval, falls in the same range. However, ASTM A890-4A Heat 1 and wrought Zeron 100 exhibit outstanding toughness, compared to the other tested materials. Wrought Ferralium 255 possesses the worst toughness at low test temperatures (-40 to -10°C). In addition, the two heats of ASTM A890-4A revealed significant differences in their toughness, as indicated in Figure 5-6.

The toughness was found to be similar for the SA “CD7MCuN” castings in the static and centrifugal cast conditions. This indicates that the two casting methods may not significantly affect the mechanical properties, however, just one heat was tested in the centrifugal cast condition.

Based on the Charpy impact test results, it can be concluded that most of the cast materials have better toughness than their wrought counterparts in the temperature range of –80°C to 20°C, and a heat-to-heat variation in toughness can exist.

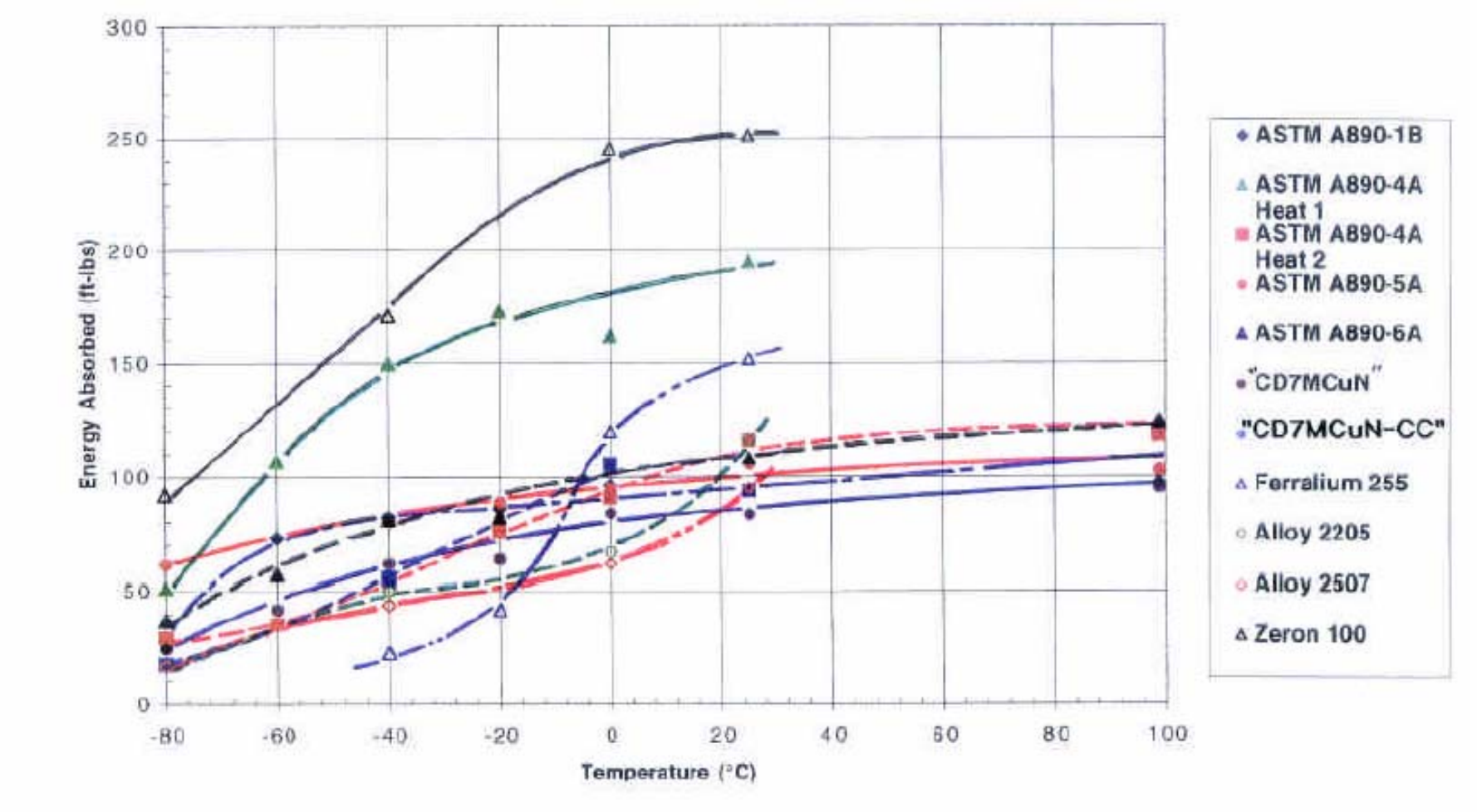

Figure 5-6. Toughness of Solution Annealed Duplex Stainless Steel Castings and Companion Wrought Alloys

5. Weldability Bend Test

Weldability evaluations were conducted on solution annealed ASTM A890-4A, 5A, 6A, 1B and "CD7MCuN" according to ASTM A494 and ASTM A488. Five cast heats (one from each duplex stainless steel alloy system), in the SA condition, were tested. The "bath tub" test blocks, defined in ASTM A494, were used as shown in Figure 4-6. Two 3/8" transverse cross sections (bend test samples) were extracted from each test block at the locations defined in ASTM A494 as shown in Figure 4-6. The surfaces of the bend test region, (i.e., the cross section of the weld region), were carefully examined. Observable weld discontinuities were documented for evaluation after bending. All heats passed the weldability bend test. The results indicate that all the DSS castings have a good weldability. Table 5-6 summarizes the weldability test results, incorporating the filler metal applied for each cast material. Figure 5-7 shows an example of the ASTM A890-5A weldability bend sample with weld discontinuities marked on cross section prior to and after bending.

Table 5-6. Weldability Bend Test Materials and Results

Material	Heat No.	Filler Metal	Pass/Fail
ASTM A890-4A	Heat 4	Alloy 2209	Pass
ASTM A890-5A	Heat 3	Alloy 2507	Pass
ASTM A890-6A	Heat 1	Zeron 100	Pass
ASTM A890-1B	Heat 1	Ferralium 255	Pass
"CD7MCuN"	Heat 2	Ferralium 255	Pass

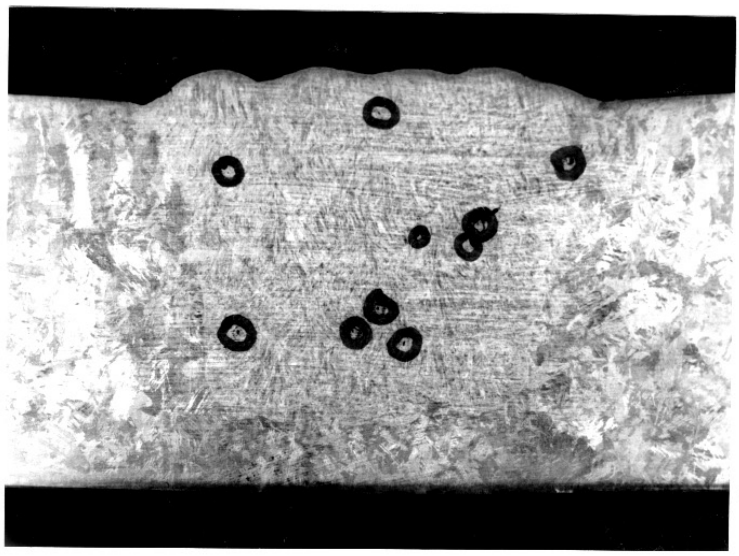

(a)

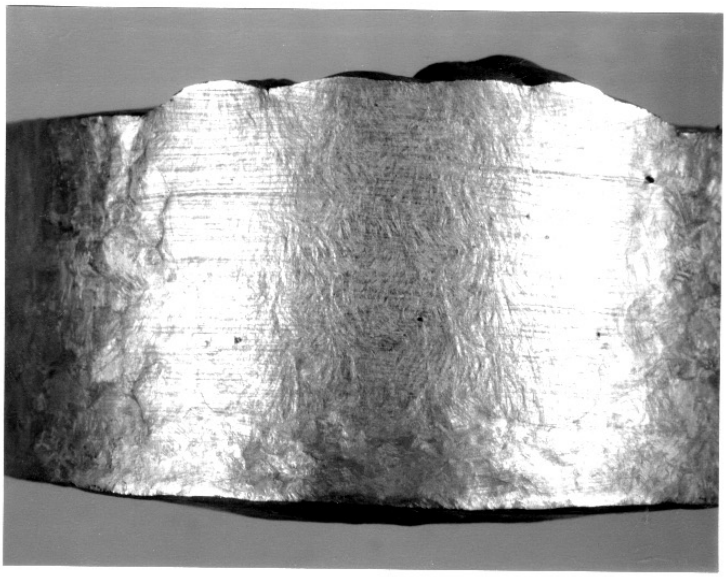

Figure 5-7. ASTM A890-5A Weldability Bend Test Sample (a) with Discontinues Marked on Cross Section Prior to Bending, (b) After Bending

6. ASTM A923 Methods A, B and C Results

Method A: Sodium Hydroxide Etch Test for Classification of Etched Structures of Duplex Stainless Steels

In this study sixteen samples, from as-received ASTM A890-4A, 5A, 6A and 1B in the as-cast, and foundry SA condition together with their wrought counterparts, were polished and NaOH etched according to ASTM A923 method A, as described in Test Method section. The typical microstructure of NaOH etched structure are presented in Figures 5-8-1. Compared to the Etch Structure Classification provided in ASTM A923 method A (see Figures 4-25-1 through 4-25-4), all the as-cast materials show an "Affected Structure", while all of the SA castings show "Unaffected Structures", which implies that all the foundry solution annealed casting are acceptable according this specification.

Beside, ASTM A890-4A samples with different heat treatment conditions were also subjected to the etching test. These samples were heat treated at UTK with the same heat of the as-received 4A castings. Three heat treatment samples were extracted from wedge casting sections and solution annealed at 1950°F (1070°C) followed by water quenching. The samples were then heated to 1550°F (845°C) and held for 10, 20 and 30 minutes respectively. Sample numbers are given as the list below together with their heat treatment schedule for the ease of identification:

Sample #1: 1950°F (1070°C) +WQ, 1550°F (845°C) for 10 minutes +WQ

Sample #2: 1950°F (1070°C) +WQ, 1550°F (845°C) for 20 minutes +WQ

Sample #3: 1950°F (1070°C) +WQ, 1550°F (845°C) for 30 minutes +WQ

The NaOH etched microstructure of these samples are presented in Figures 5-8-2 through 5-8-4.

In contrast with foundry SA sample in Figure 5-8-1, where smooth ferrite/austenite boundaries are observed, the other trial samples all show distinctive secondary phase microconstituents at the austenite/ferrite boundaries, but at different levels due to various holding times at 1550°F (845°C).

In Figure 5-8-2 (10 minutes at 1550°F), most interphase (F/A) boundaries are clear and unprecipitated. However, waviness can be observed for some boundaries, which indicates that precipitation has started. According to ASTM A923, the structure may be classified as "Possible Affected Structure."

As holding time increased, secondary phase(s) began to readily visible along interphase boundaries (Figures 5-8-3) as darker etching secondary particles. Comparing 20 minutes 30 minutes holding, there is no significant morphology change except the growth of the secondary particles. According to ASTM A923, the structures are classified to be "Affected Structure."

Figure 5-8-4 shows the interphase (F/A) boundaries of the 30 minutes hold sample at 1000X. The dark etched secondary phase(s) particles grew at the phase boundaries and into the ferrite matrix.

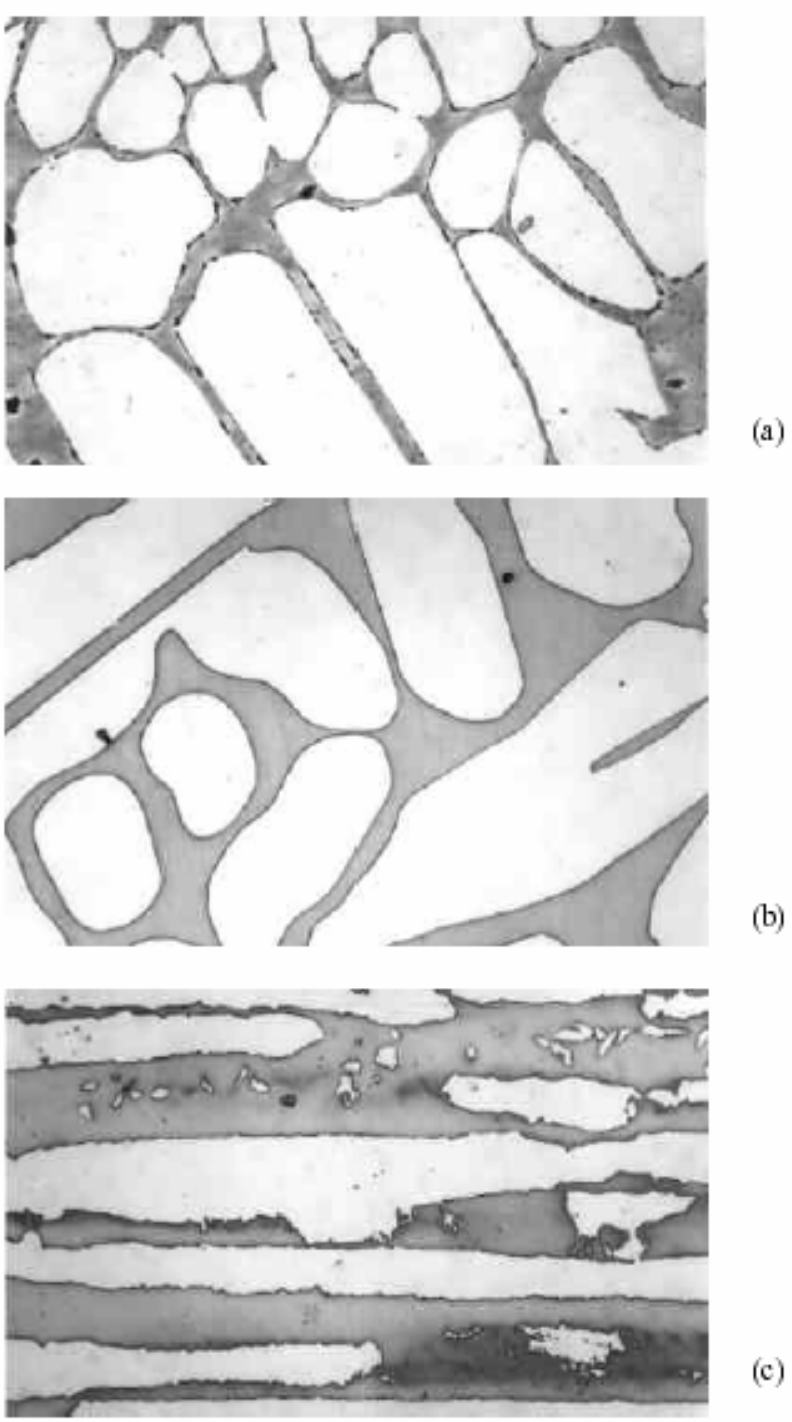

Figure 5-8-1. Sodium Hydroxide Etched Structure of ASTM A890-4A (a) As-cast, (b) SA Casting, (c) Wrought Alloy 2205, 400X

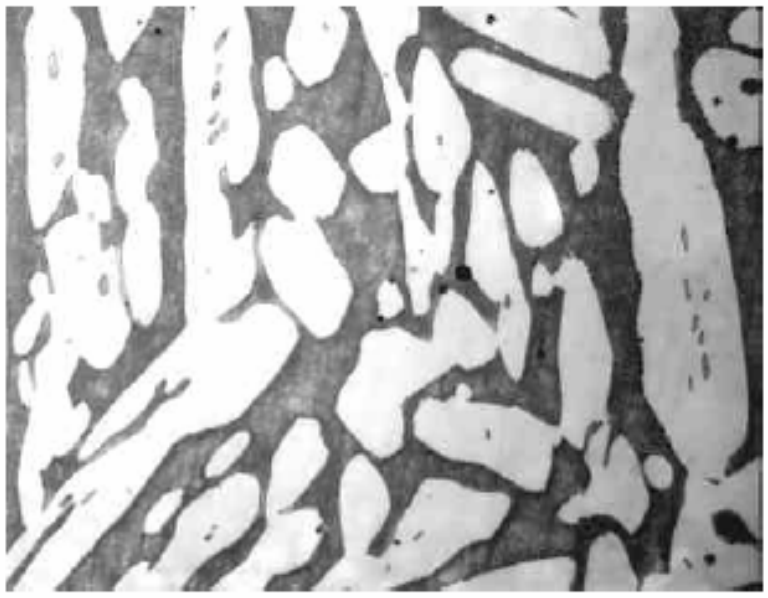

Figure 5-8-2. Sodium Hydroxide Etched "Possible Affected Structure" (Sample #1, 1950^{o}F + WQ, 1550^{o}F for 10 minutes + WQ), 400X

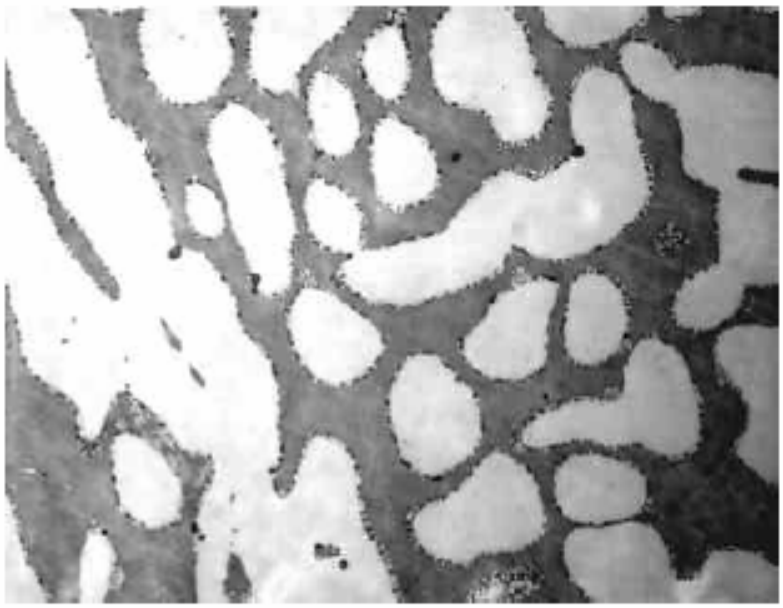

Figure 5-8-3. Sodium Hydroxide Etched "Affected Structure" (Sample #3, 1950^{o}F + WQ, 1550^{o}F for 30 minutes + WQ), 400X

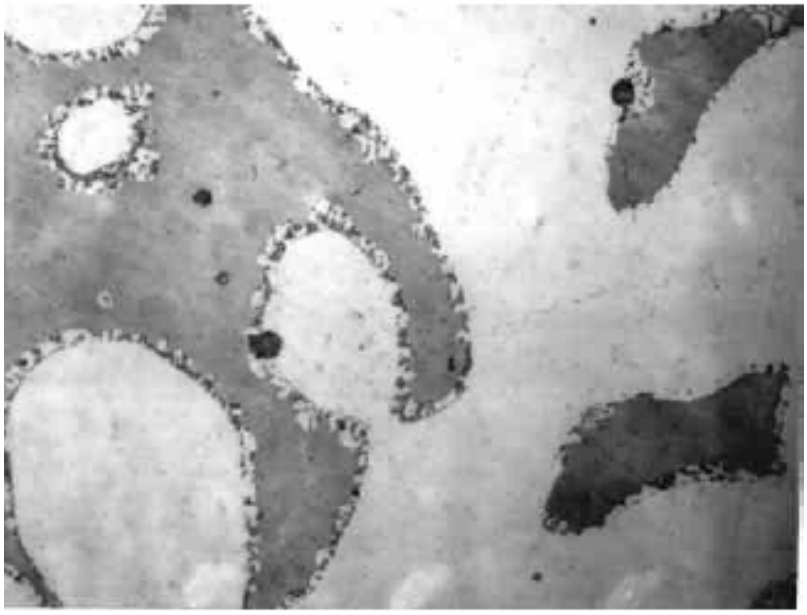

Figure 5-8-4. Sodium Hydroxide Etched Structure of Sample #3 (1950^{o}F + WQ, 1550^{o}F for 30 minutes + WQ), 400X

Method B: Charpy Impact Test for Classification of Structures of Duplex Stainless Steels

ASTM A923 Method B, Charpy impact test, was conducted on ASTM A890-4A, 5A, 6A, 1B, "CD7MCuN" and wrought counterparts at –40°F (-40°C) as well as their wrought counterparts. A total of ten heats were tested. The results are presented in Table 5-7. The solution annealed cast materials of ASTM A890-4A, 5A 1B and "CD7MCuN" reveal better impact toughness than their wrought counterparts at the test temperature of –40°F (-40°C). However, the wrought super duplex stainless steel, Zeron 100, shows the highest toughness at this temperature. The wrought Ferralium 255 is the only material that did not pass ASTM A923 Method B criteria.

Table 5-7. ASTM A923 Method B Results

Code	Impact Energy @ -40°F* (ft-lbs)	Method B P/F**
ASTM A890-4A, Heat 1	55	P
ASTM A89-4A, Heat 2	150	P
Alloy 2205	50	P
ASTM A 890-5A, Heat 1	80	P
Alloy 2507	44	P
ASTM A 890-6A, Heat 1	81	P
Zeron 100	172	P
ASTM A890-1B, Heat 3	82	P
"CD7MCuN", Heat 2	62	P
"CD7MCuN"-CC, Heat 2	56	P
Ferralium. 255	23	F

* Charpy Impact test conducted according to ASTM A370 and E23 utilizing V-notched Charpy test samples

** Acceptance criterion of method B of base metal is 40 ft-lbs (54J) at – 40°F/°C)

Method C: Ferric Chloride Corrosion Test for Classification of Structures of Duplex Stainless Steels

ASTM A923 Method C is a 24-hour pitting corrosion test, in a 6% FeCl3 solution. The sample and solution preparation of this test method follows the same procedure as ASTM G48 Method A. The test temperature of 25°C is defined for wrought base metal and 22°C for welds. The tested samples were evaluated using the weight loss rate criteria specified. A weight loss corrosion rate less than 10mdd (mg/dm2/day) indicates that the material is acceptable by ASTM A923 Method C. It was found that all SA castings met the weight loss criteria. The SA + autogenously welded samples from ASTM A890-1B, 4A and "CD7MCuN" did not meet the criteria. The corrosion results according to ASTM A923 Method C are summarized in Tables 5-8-1 through 5-8-5.

Table 5-8-1 Duplex Stainless Steel ASTM A923 Method C Ferric Test Results, ASTM A890-4A (6% $FeCl_3$, Base Metal@25°C & Weld Metal@22°C, 24 hrs.)

Material	Heat #	Condition	Corrosion Rate (mdd**)	P/F***	CPT (°C)
ASTM A890-4A	Heat 1	Solution annealed	0.73	P	40
ASTM A890-4A	Heat 1	SA Autogenous welded	65.93	F	30
ASTM A890-4A	Heat 2	Solution annealed	2.19	P	35
ASTM A890-4A	Heat 2	SA Autogenous welded	65.93	F	<0
ASTM A890-4A	Heat 3	Solution annealed	0.00	F	50
ASTM A890-4A	Heat 3	SA Autogenous welded	415.20	F	<0
ASTM A890-4A	Heat 4	Solution annealed	0.00	P	45
ASTM A890-4A	Heat 4	SA Autogenous welded	15.10	F	20
ASTM A890-4A	Heat 4 CC*	Solution annealed	2.12	P	50
ASTM A890-4A	Heat 4 CC*	SA Autogenous welded	33.34	F	15
Alloy 2205	-	Wrought	0.00	P	40
Alloy 2205	-	Wrought Autogenous welded	7.92	P	25

* CC - centrifugal cast

**mdd - $mg/dm^2/day$

*** The acceptance criterion is no corrosion rate shall excess 10mdd.

Table 5-8-2 Duplex Stainless Steel ASTM A923 Method C Test Results,

ASTM A890-5A (6% $FeCl_3$, Base Metal@25°C & Weld Metal@22°C,24 hrs.)

Material	Heat #	Condition	Corrosion Rate (mdd**)	P/F***	CPT (°C)
ASTM A890-5A	Heat 1	Solution annealed	2.64	P	65
ASTM A890-5A	Heat 1	SA Autogenous welded	3.05	P	45
ASTM A890-5A	Heat 2	Solution annealed	0.00	P	50
ASTM A890-5A	Heat 2	SA Autogenous welded	4.41	P	40
ASTM A890-5A	Heat 3	Solution annealed	0.00	P	65
ASTM A890-5A	Heat 3	SA Autogenous welded	0.00	P	45
ASTM A890-5A	Heat 3 CC*	Solution annealed	0.00	P	50
ASTM A890-5A	Heat 3 CC*	SA Autogenous welded	3.78	P	30
Alloy 2507	-	Wrought	0.00	P	80
Alloy 2507	-	Wrought Autogenous welded	0.00	P	45

* CC - centrifugal cast

**mdd - $mg/dm^2/day$

*** The acceptance criterion is no corrosion rate shall excess 10mdd.

Table 5-8-3. Duplex Stainless Steel ASTM A923 Method C Test Results,

ASTM A890-6A (6% $FeCl_3$, Base Metal@25°C & Weld Metal@22°C,24 hrs.)

Material	Heat #	Condition	Corrosion Rate (mdd**)	P/F***	CPT (°C)
ASTM A890-6A	Heat 1	Solution annealed	0.00	P	65
ASTM A890-6A	Heat 1	SA Autogenous welded	4.47	P	55
ASTM A890-6A	Heat 2	Solution annealed	0.00	P	70
ASTM A890-6A	Heat 2	SA Autogenous welded	0.00	P	45
ASTM A890-6A	Heat 3	Solution annealed	0.67	P	55
ASTM A890-6A	Heat 3	SA Autogenous welded	2.70	P	40
Zeron 100	-	Wrought	0.00	P	65
Zeron 100	-	Wrought Autogenous welded	0.00	P	30

** mdd - $mg/dm^2/day$

*** The acceptance criterion is no corrosion rate shall excess 10mdd.

Table 5-8-4 Duplex Stainless Steel ASTM A923 Method C Test Results,

ASTM A890-1B (6% $FeCl_3$, Base Metal@25°C & Weld Metal@22°C,24 hrs.)

Material	Heat #	Condition	Corrosion Rate (mdd**)	P/F***	CPT (°C)
ASTM A890-1B	Heat 1	Solution annealed	0.00	P	35
ASTM A890-1B	Heat 1	SA Autogenous welded	16.79	F	25
ASTM A890-1B	Heat 2	Solution annealed	0.00	P	40
ASTM A890-1B	Heat 2	SA Autogenous welded	198.02	F	15
ASTM A890-1B	Heat 3	Solution annealed	3.45	P	30
ASTM A890-1B	Heat 3	SA Autogenous welded	133.92	F	15
ASTM A890-1B	Heat 4	Solution annealed	2.87	P	35
ASTM A890-1B	Heat 4	SA Autogenous welded	184.31	F	10
Ferralium 255	-	Wrought	1.96	P	45
Ferralium 255	-	Wrought Autogenous welded	66.39	F	25

** mdd - $mg/dm^2/day$

*** The acceptance criterion is no corrosion rate shall excess 10mdd.

Table 5-8-5 Duplex Stainless Steel ASTM A923 Method C Test Results,

"CD7MCuN" (6% $FeCl_3$, Base Metal@25°C & Weld Metal@22°C,24 hrs.)

Material	Heat #	Condition	Corrosion Rate (mdd**)	P/F**	CPT (°C)
"CD7MCuN"	Heat 1	Solution Annealed	0.00	P	45
"CD7MCuN"	Heat 1	SA Autogenous Welded	427.03	F	5
"CD7MCuN"	Heat 2	Solution Annealed	0.00	P	40
"CD7MCuN"	Heat 2	SA Autogenous Welded	142.64	F	15
"CD7MCuN"-CC	Heat 2 CC*	Solution Annealed	0.00	P	50
"CD7MCuN"-CC	Heat 2 CC*	SA Autogenous Welded	116.40	F	15

* CC - centrifugal cast

** mdd - $mg/dm^2/day$

*** The acceptance criterion is no corrosion rate shall excess 10mdd.

7. Microstructure Characterization

The testings gave a significant database on characterizing the corrosion and mechanical properties of the DSS castings. In general, the performance of a material is controlled by its microstructure. In order to provide a better understanding of corrosion behavior and mechanical properties of DSS castings, microstructural characterizations were conducted using optical light metallography (OLM), color staining etching, SEM and EDS analysis.

The materials selected for microstructural evaluations include:

1). As-cast, SA static cast, SA centrifugal castings and wrought materials.

2). Pitting corrosion tested samples with and without autogenous welds.

3). Intergranular corrosion tested samples.

4). Solution annealing heat treatment study samples.

In general, duplex stainless steel microstructures consist of approximately equal proportions of austenite and ferrite, with ferrite comprising the matrix. During casting, DSS solidify as essentially 100% ferrite. At elevated temperatures (1300-2370°C), austenite nucleates and grows first at ferrite grain boundaries and later along preferential crystallographic directions within the ferrite grains. Diffusion/segregation of alloy elements must occur as the transformation of ferrite to austenite proceeds. Normally, austenite stabilizing elements (such as C, Ni, N, and Cu) concentrate in the austenite and ferrite stabilizing elements (such as Cr, Mo and W) segregate to the ferrite. The extent of the transformation depends not only on the balance between austenite stabilizing and ferrite stabilizing elements, but also on the time available for diffusion and on the diffusion rate of specific elements. Normally, both cast and wrought DSS exhibit a

ferrite matrix with austenite of varying morphologies, but the cast microstructure is somewhat coarser and displays a different morphology (island-like) of austenite than that observed in the wrought plate (rolling texture directionality). Typical structure are shown in Figure 3-1.

ASTM A890-4A

ASTM A890-4A is an alloy containing approximately 22wt%Cr, 5wt%Ni, 3.0wt% Mo and 0.17wt%N. Three heats (Heat 1, Heat 2 and Heat 3) of ASTM A8904A, from different foundries, were selected for this study in the as-cast, SA and SA + autogenously welded condition. Pitting and IGC tested samples were also examined. For comparison, the wrought counterpart alloy 2205 was included in the microstructure study.

Figures 5-9 through 5-11 show the microstructure of Oxalic etched ASTM A890-4A, Heats 1 & 2, in the as-cast and SA condition together with wrought counterpart

Alloy 2205. The microstructure of ASTM A890-4A Heat 1 in the as-cast and SA conditions is shown in Figure 5-9. In the as-cast condition, austenite islands in a ferrite matrix are evident, and fine precipitates are observed mainly along the ferrite/austenite boundaries as shown in Figure 5-9a. In addition, some randomly distributed inclusions are found in the matrix. Figure 5-9b reveals the microstructure of Heat 1 in the SA condition. It is evident that the particles along the ferrite/austenite boundaries, observed

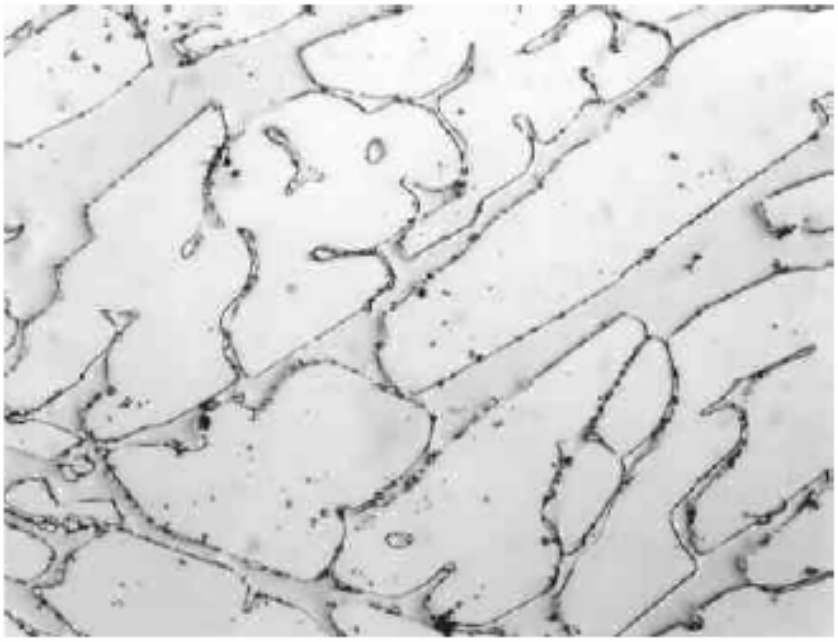

(a) As-cast

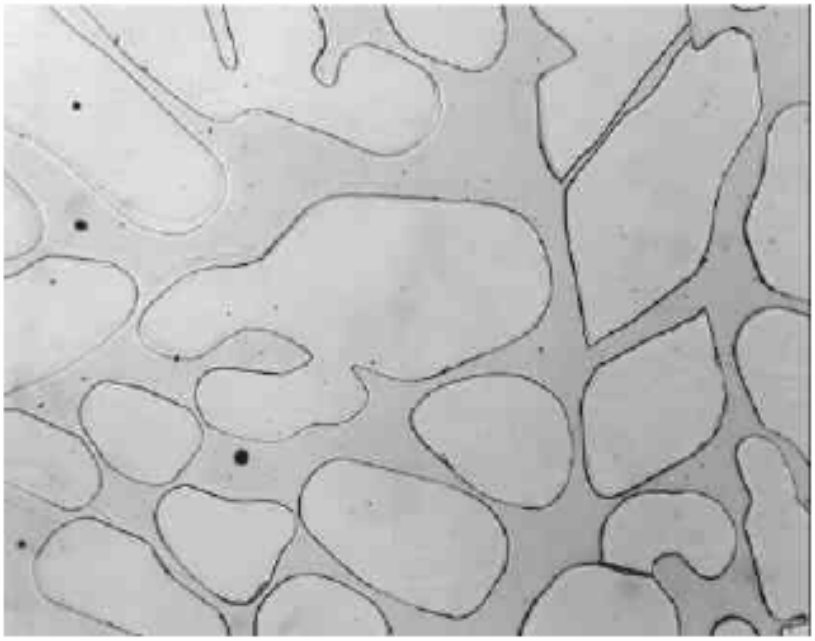

(b) SA

Figure 5-9. Microstructure of ASTM A890-4A, Heat 1, Oxalic, 400X

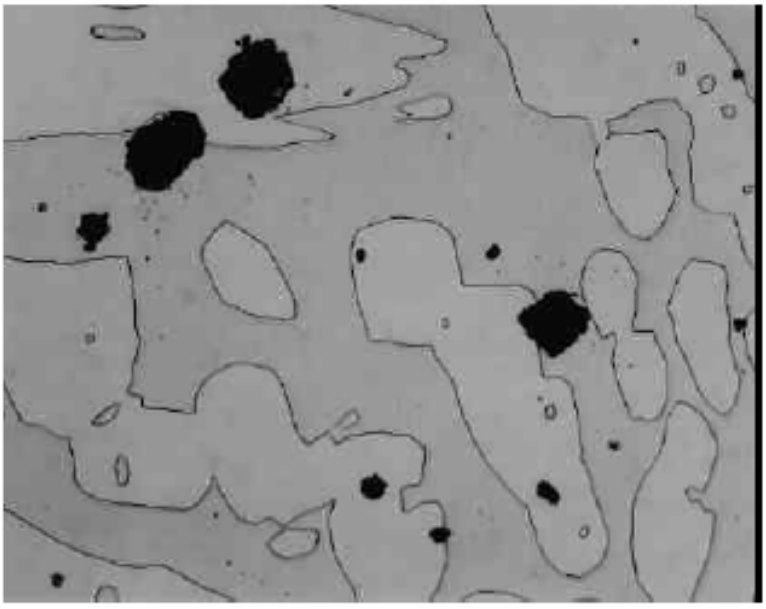

Figure 5-10. Microstructure of ASTM A890-4A, Heat 2, SA, Oxalic, 400X

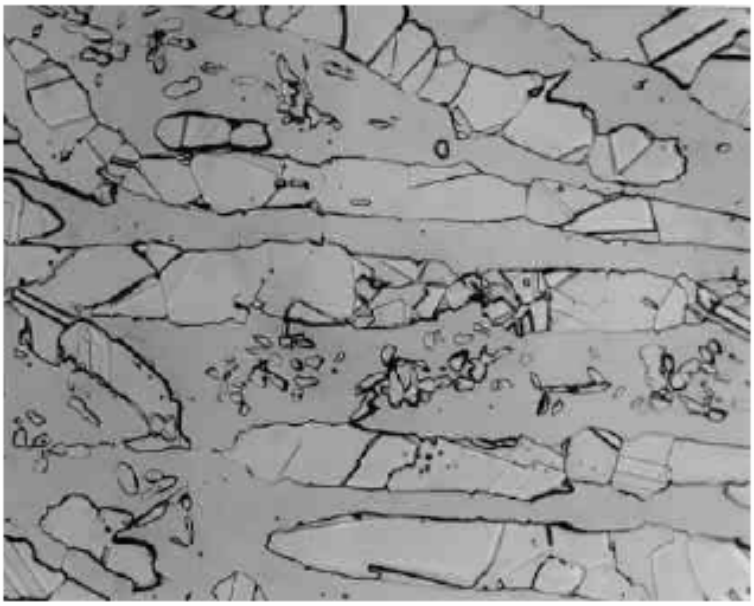

Figure 5-11. Microstructure of Wrought Alloy 2205, Glycerigia, 400X

in the as-cast condition, are dissolved upon solution annealing. Austenite islands with smooth boundaries (no precipitates) are obvious in the ferrite matrix. Inclusions in the matrix remain unchanged after solution annealing. Figure 5-10 shows the microstructure of ASTM A890-4A Heat 2 in the SA condition. It is clear that Heat 2 reveals a microstructure identical to Heat 1 in the SA condition, in terms of austenite islands in a ferrite matrix. However, larger inclusions were observed in the Heat 2 matrix as compared to Heat 1. It is considered that these randomly distributed large inclusions may have an influence the mechanical properties. The microstructure of wrought counterpart Alloy 2205 is presented in Figure 5-11. A rolling texture structure directionality, from hot working, followed by a solution annealing and quenching, is evident in comparison with the cast material.

Figure 5-12 shows the OLM micrograph of ASTM A890-4A Heat 1 after pitting testing in both the as-cast and SA condition. Figure 5-12a shows the microstructural features of pitting on ASTM A890-4A Heat 1 in the as-cast condition. It is evident that pits initiate at the precipitates along the ferrite/austenite boundaries and preferentially grow into ferrite. In the SA condition, pits also initiate at the ferrite/austenite boundaries and preferentially grow into austenite, as presented in Figure 5-12b. The OLM characteristics of pitting in wrought Alloy 2205 base metal are shown in Figure 5-13. The pitting behavior of wrought Alloy 2205, in terms of the initiation and growth, was determined to be identical to the corresponding cast materials in the SA condition.

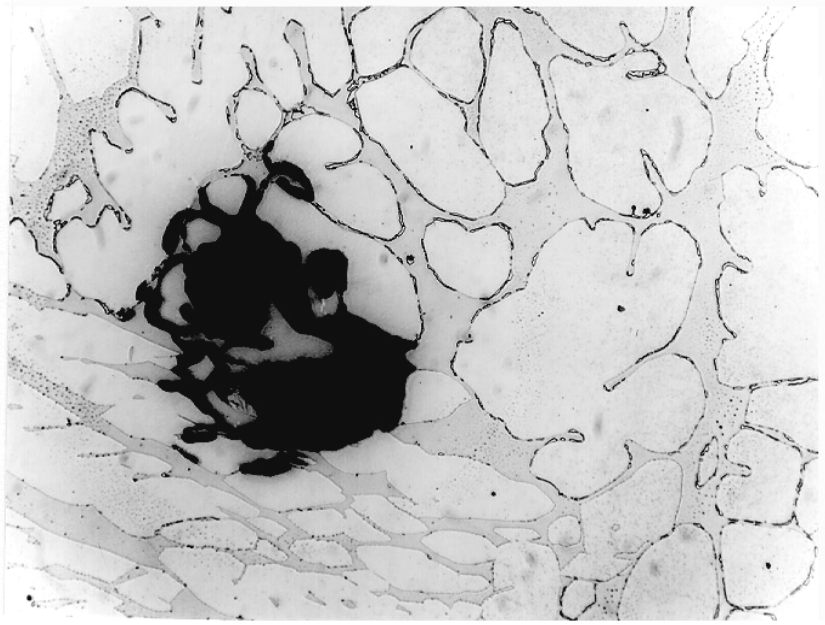

(a) As-cast

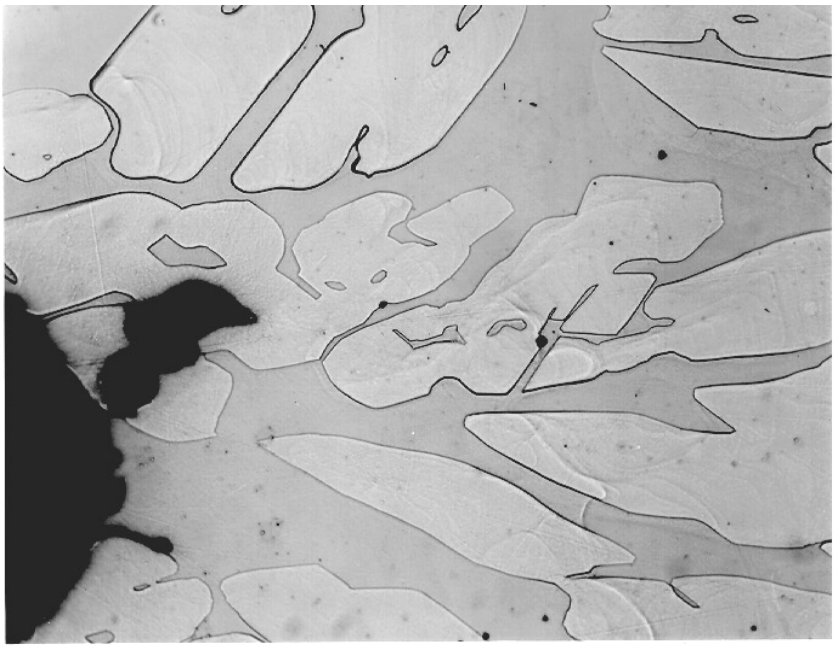

(b) SA

Figure 5-12. Pitting of ASTM A890-4A, Heat 1, Glycerigia, 200X

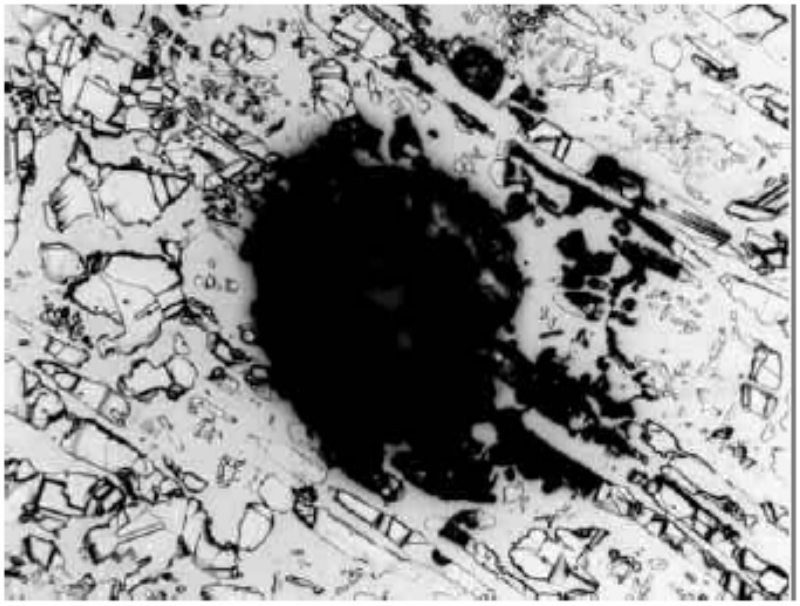

Figure 5-13. Pitting of Wrought Alloy 2205, Glycerigia , 200X

The optical features of the pitting behavior of autogenous welds on ASTM A8904A castings and wrought Alloy 2205 are shown in Figures 5-14 through 5-18. In general, a finer austenite structure in the ferrite matrix is evident in the fusion zone, as compared to the cast base metal. This finer austenite microstructure shows the original solidification pattern in the autogenous weld fusion zone and reflects the rapid cooling upon welding. It should be recalled that all of the autogenous weld samples were tested in the as-welded condition, and no filler was added. Thus, the fusion zone in these autogenous welds is truly an “Unmixed Zone”. It is to be expected that segregation of alloy elements in the fusion zone occurs during solidification. Generally, a greater extent of element segregation occurs in the fusion zone adjacent to the fusion boundary, as compared to the other fusion zone areas. The segregation of Cr and Mo in the

solidification structure can have a significant influence on the corrosion behavior of autogenous welds. In addition, the loss of nitrogen from the fusion zone during welding should be considered in regard to a reduction of corrosion resistance of the autogenous weld fusion zone.

Figure 5-14 shows an OLM micrograph of the pitting tested autogenous welds of as-cast Heat 1. It is evident that pits preferentially initiated in the fusion zone adjacent to fusion line. For the autogenous welds on SA Heat 1, pits were observed both in the fusion zone and at the fusion line, as shown in Figure 5-15.

Figure 5-16 shows the OLM results of pitting in autogenous welds on SA Heat 2. A similar pitting pattern to Heat 1 was observed in the same condition since pitting mainly occurred at the FL, for the autogenous welded SA Heat 3 (Figure 5-17) and pitting tested autogenous welds on wrought Alloy 2205 (Figure 5-18). Pits were found only in the fusion zone. It can be concluded that autogenous welding has a significant influence on the pitting behavior of ASTM A890-4A, regardless of the material condition. The initiation and occurrence of pitting is related to autogenous welds.

The pitting performance of autogenous welds was further evaluated using SEM and EDS. In this study, SEM and EDS analysis was conducted on the optical metallography samples. Figure 5-19 reveals the SEM secondary and back-scattered electron images, of the fusion line area of the autogenous weld, on SA Heat 1 at 300X. The casting base metal, fusion zone and fusion line are clearly identified in this figure. Figure 5-20 shows the typical secondary and back-scattered electron images of the base metal at 1000X. The austenite islands in a ferrite matrix are evident with some dark spherical particles.

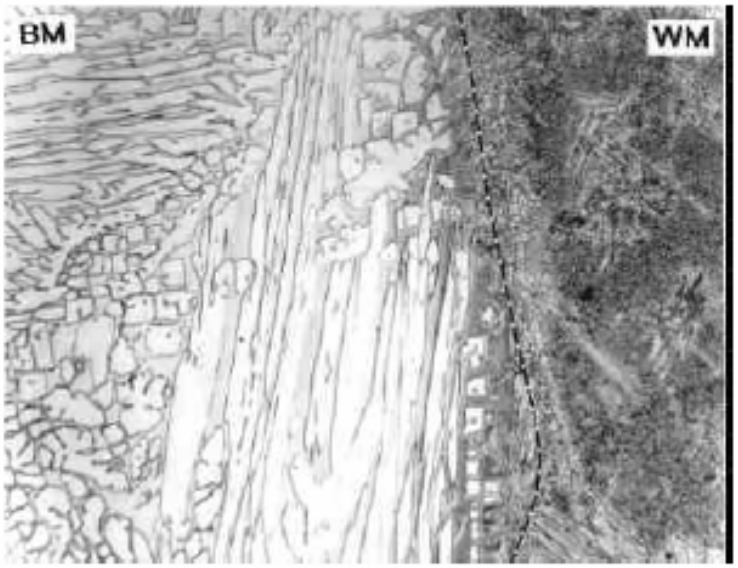

100X

(a)

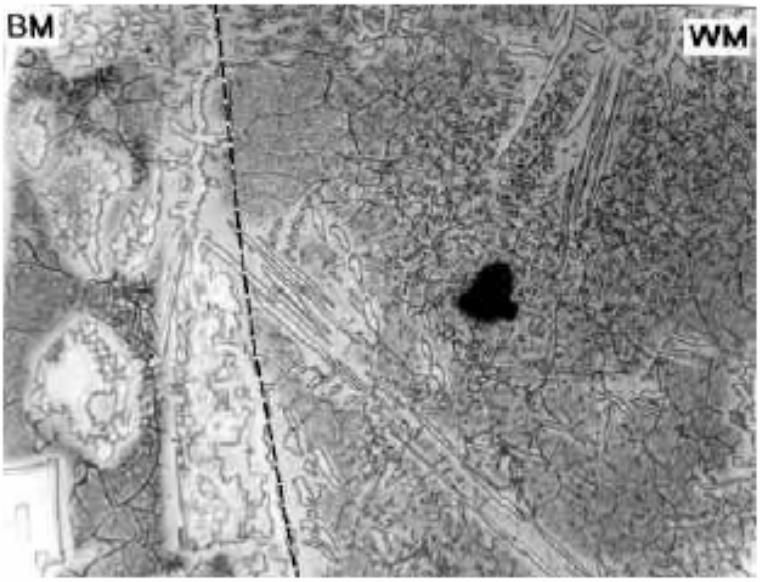

400X

(b)

Figure 5-14. Pitting of Autogenous Weld on As-cast ASTM A890-4A, Heat 1, Oxalic

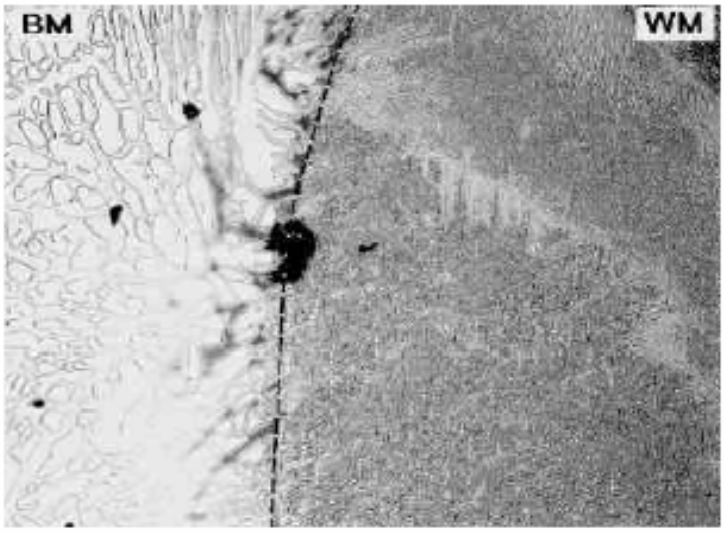

100X

(a)

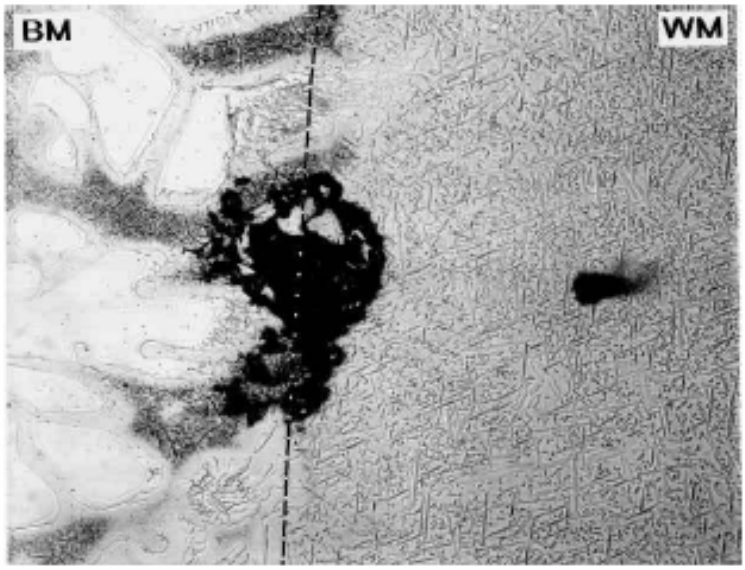

400X

(b)

Figure 5-15. Pitting of Autogenous Weld on SA ASTM A890-4A, Heat 1, Oxalic

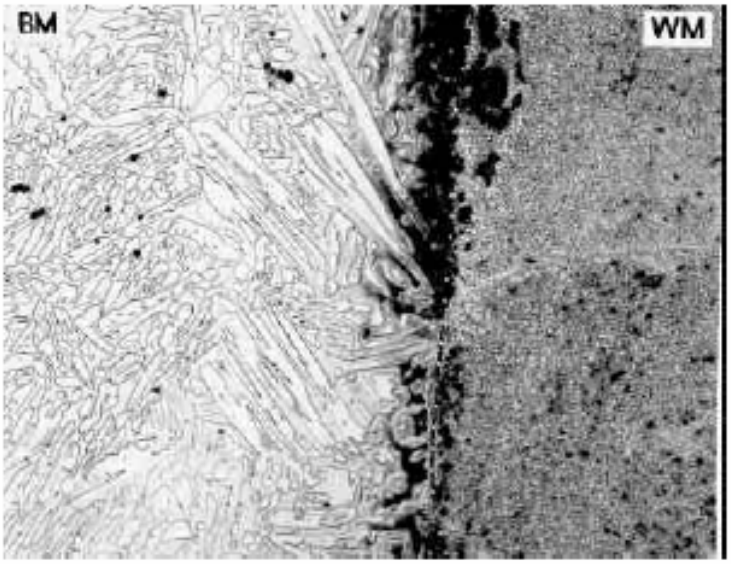

100X

(a)

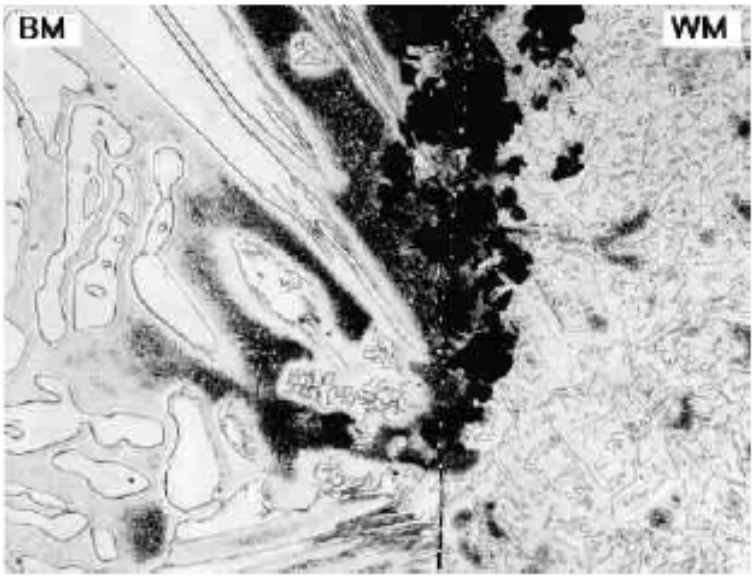

400X

(b)

Figure 5-16. Pitting of Autogenous Weld on SA ASTM A890-4A, Heat 2, Oxalic

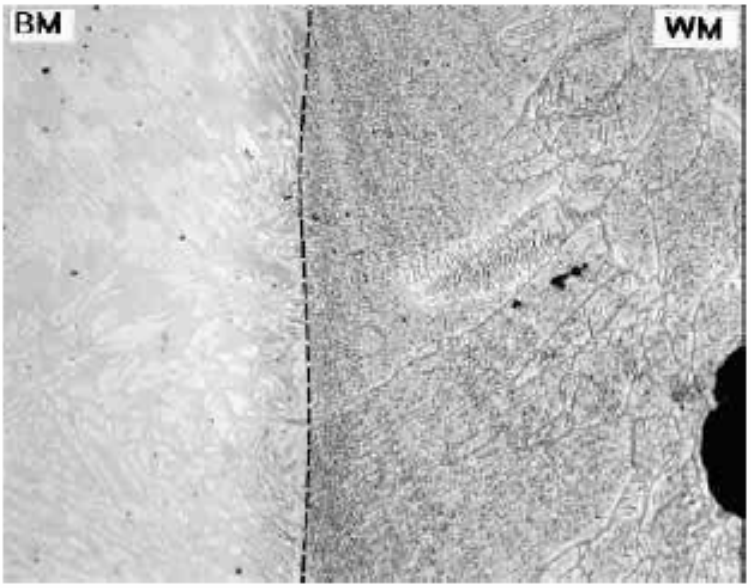

100X

(a)

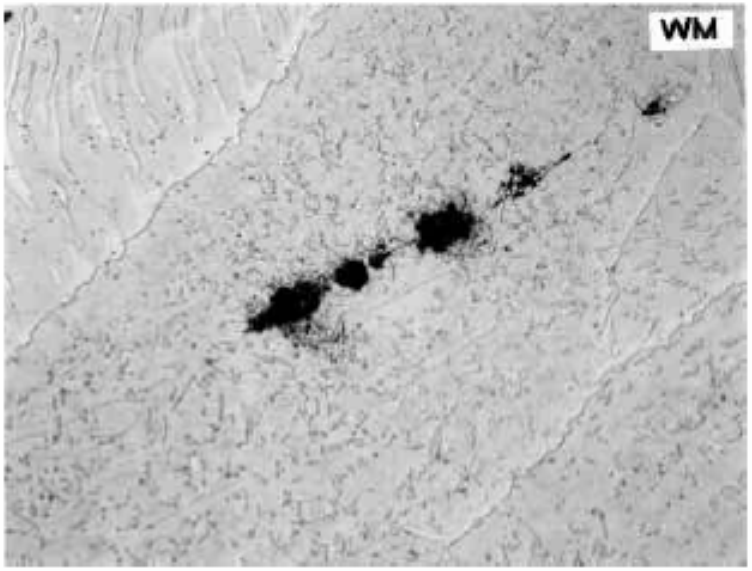

400X

(b)

Figure 5-17. Pitting of Autogenous Weld on SA ASTM A890-4A, Heat 3, Oxalic

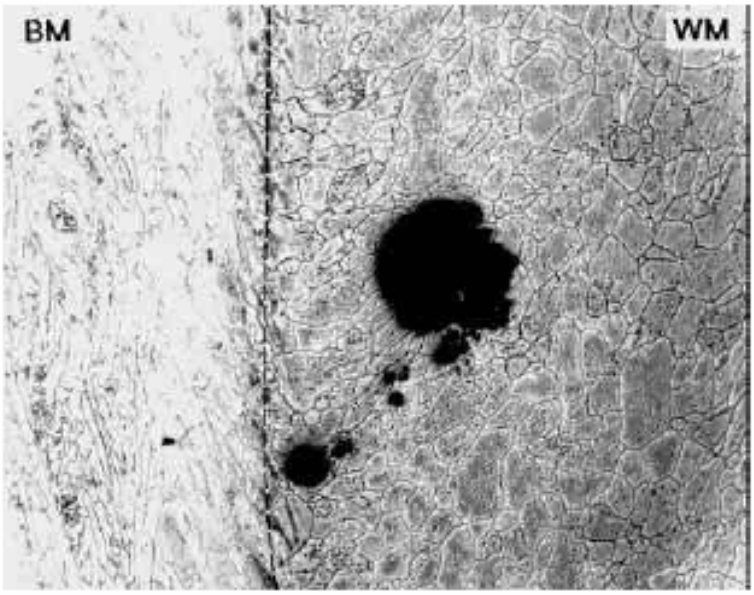

100X

(a)

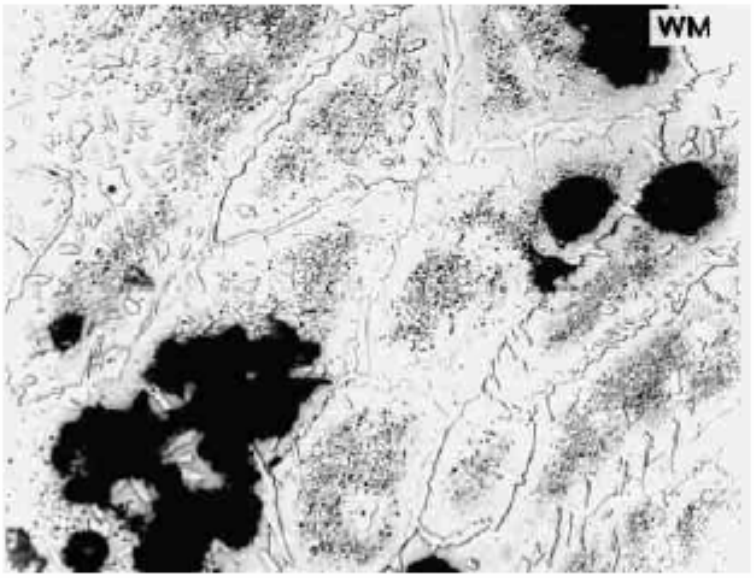

400X

(b)

Figure 5-18. Pitting of Autogenous Weld on Wrought Alloy 2205, Oxalic

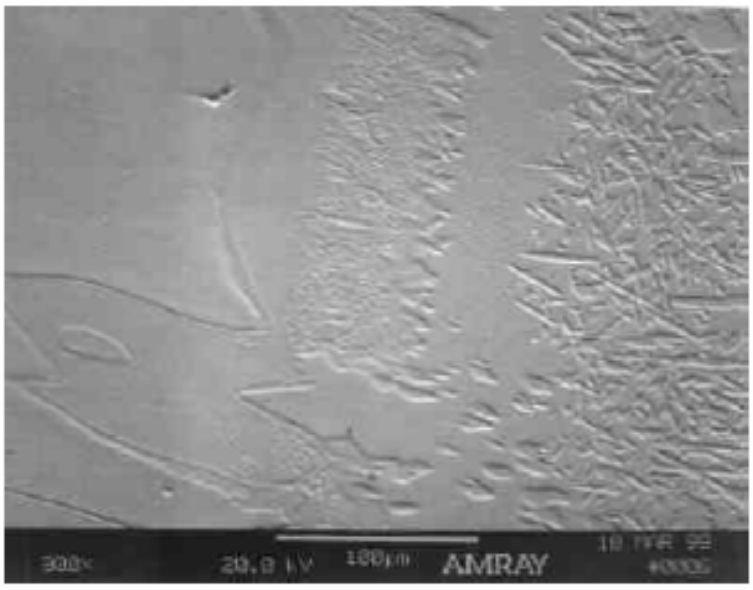

(a)

(b)

Figure 5-19. SEM Secondary (a) and Back-scattered (b) Electron Images of the Fusion Line Area of the Autogenous weld on SA ASTM A890-4A Heat 1, Oxalic, 300X

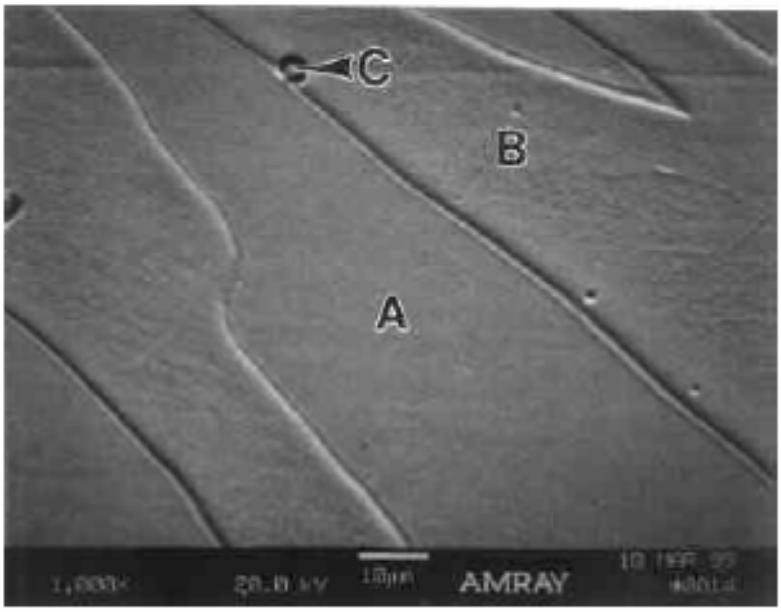

(a)

(b)

Figure 5-20. Typical Secondary (a) and Back-scattered (b) Electron Images of SA ASTM A890-4A Heat 1 Base Casting, Oxalic, 1000X

The EDS analysis of the base metal was conducted at the locations A, B and C, as identified in Figure 5-20a. The EDS spectra are presented in Figure 5-21 for location A and B in Figure 5-20a; and in Figure 5-22 for locations C. It is evident that the austenitic region is slightly richer in Ni than the ferritic region, and the ferritic region is slightly richer in Cr & Mo with some Si, than the austenitic region. The dark particles, shown at Location C in Figure 5-20a, were determined to be rich in Fe, Mn, Cr, Si, Al and O with some Ti and S present. This EDS result indicates that the dark particles in the casting base metal are inclusions. Figure 5-22 shows an EDS spectrum of a dark particle.

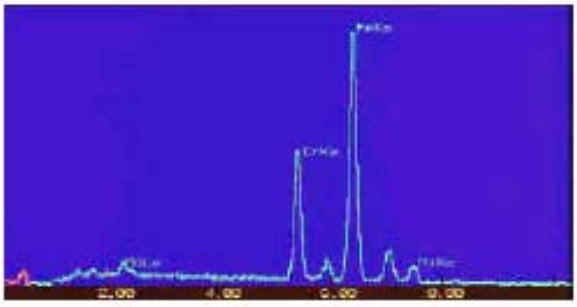

(a)

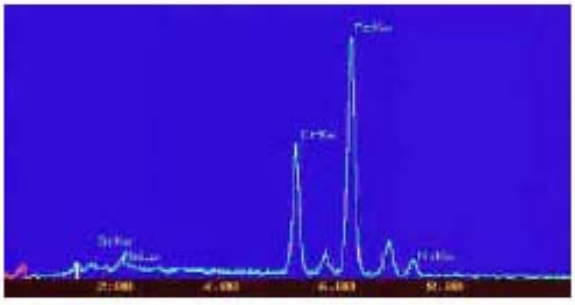

(b)

Figure 5-21. EDS Spectrum of Location A (Austenite) and B (Ferrite) in Figure 5-20a

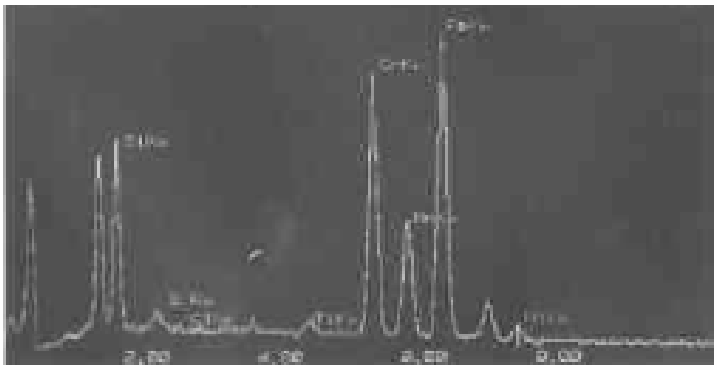

Figure 5-22. EDS Spectrum of Location C (Dark Particle) in Figure 5-20a

The SEM secondary and back-scattered electron images, of the Heat 1 autogenous fusion zone, are presented in Figure 5-23. An acicular shaped austenite structure, in the fusion zone, is evident and is much finer than that in the base casting. EDS analysis was conducted at locations A and B as labeled in Figure 5-23a. The EDS spectra for locations A & B, in the fusion zone, are presented in Figure 5-24 for the austenite (Location A) and Figure 5-25 for the ferrite (Location B), respectively. It is evident that the austenite and ferrite in the autogenous fusion zone have similar compositions.

In addition, EDS line scanning and mapping for Cr, Mo and Ni were conducted across the fusion boundary area on the autogenous weld of Heat 1. Figure 5-26 shows the digital image at the fusion boundary area for the EDS line scan study of Cr, Mo and Ni distributions. The 73.9mm “yellow” colored line in Figure 5-26 indicates the scan location. The Cr, Mo and Ni distributions across the fusion boundary are presented in Figure 5-27. It is evident that a slight Mo depletion was determined at the ferrite/austenite interfaces (Locations 1 and 2), as labeled in Figure 5-26. It is considered that Mo depletion at the ferrite/austenite interfaces is responsible for a reduction in pitting resistance of the fusion zone area, adjacent to the fusion boundary.

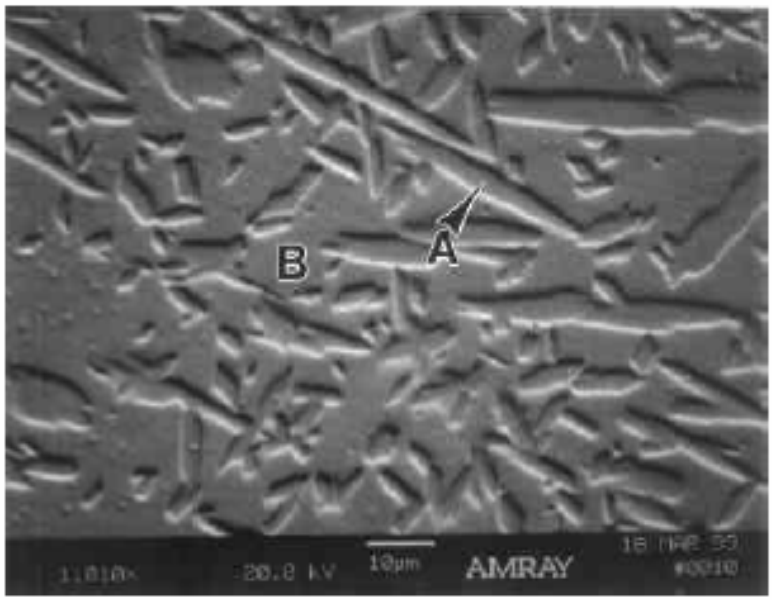

(a)

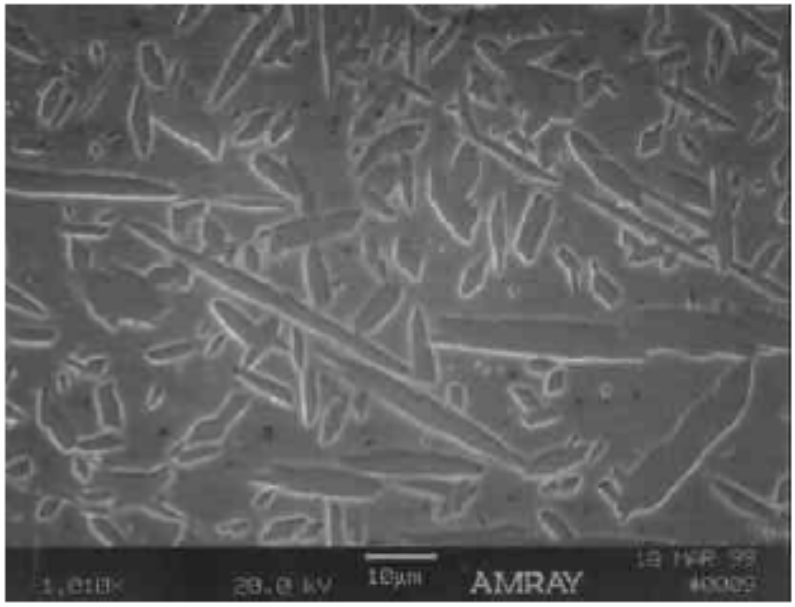

(b)

Figure 5-23. SEM Secondary (a) and Back-scattered (b) Electron images of ASTM A890-4A Heat 1 Autogenous weld Fusion Zone, Oxalic, 1010X

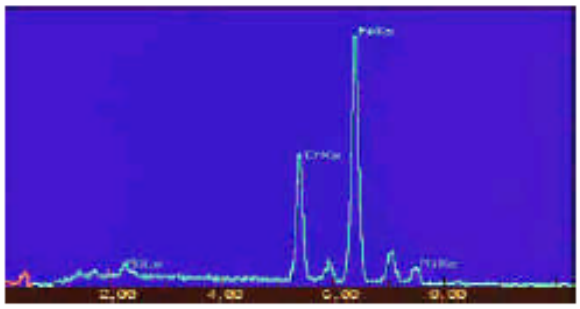

Figure 5-24. EDS Spectrum of A (Austenite) in Figure 5-23a

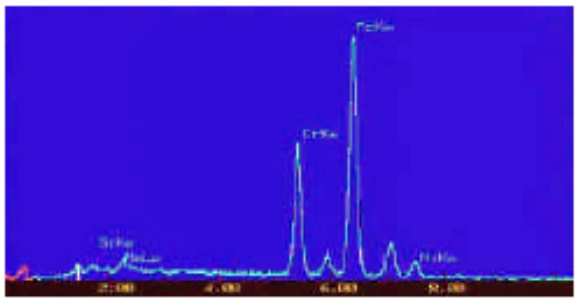

Figure 5-25. EDS Spectrum of B (Ferrite) in Figure 5-23a

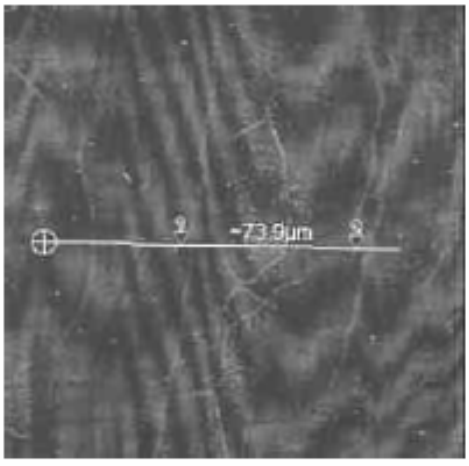

Figure 5-26. Secondary Image of the Fusion Noundry Area for EDS Line Scan

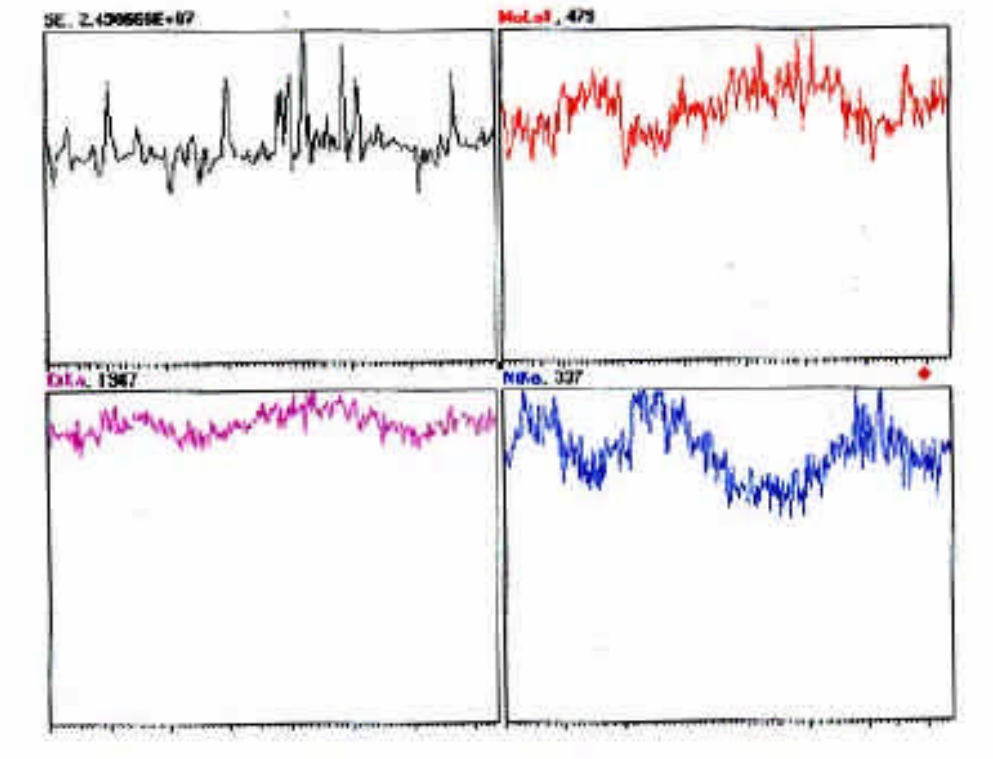

Figure 5-27. Cr, Mo and Ni Distributions Across Fusion Boundary

Two element mappings (Cr, Mo and Ni) were conducted on the same sample across the fusion boundary, as presented in Figures 5-28 and 5-29. It is clear that Cr and Mo are rich in the ferrite region and Ni is rich in the austenite region, for the base casting and the FZ area adjacent to the FL. A smaller extent of Cr, Mo and Ni segregation was detected in the general fusion zone area in comparison with the fusion zone area adjacent to the fusion line. The element mapping results are consistent with the spot EDS results in the austenite and ferrite regions for both the casting base metal and fusion zone.

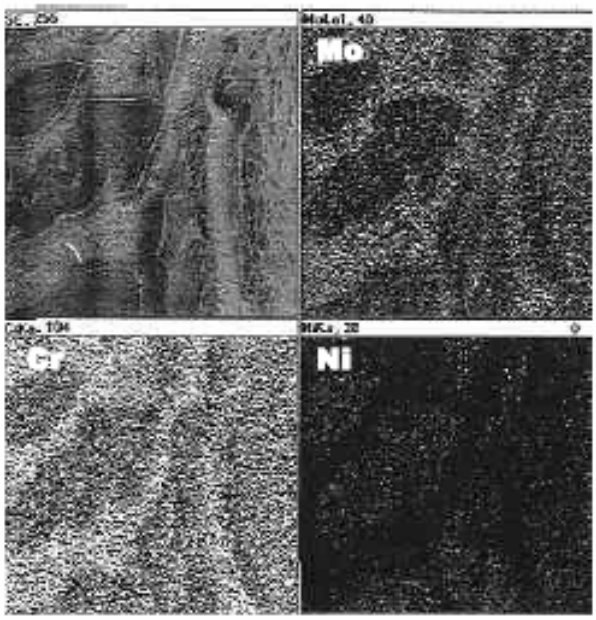

Figure 5-28. Element Mapping (Cr, Mo and Ni) Across Fusion Boundary

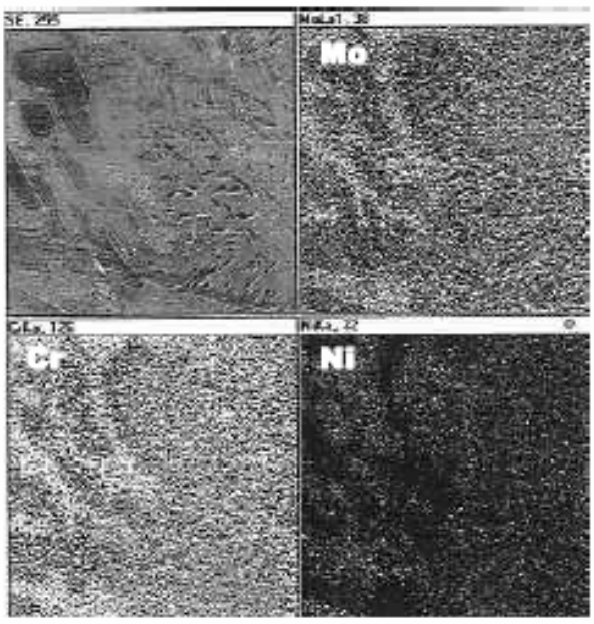

Figure 5-29. Element Mapping (Cr, Mo and Ni) Across Fusion Boundary

In addition, SEM and EDS analysis were also conducted on SA A890-4A Heat 2. Figure 5-30 presents a SEM photomicrograph of the Heat 2 casting base metal. The austenite islands in the ferrite matrix are evident, as well as some light gray particles (marked "A" in Figure 5-30) and some dark gray particles (marked "B" in Figure 5-30). EDS analysis was performed at locations A and B. The spectra of these EDS analysis are presented in Figures 5-31 and 5-32. From Figure 5-31, the light gray particles (Location A in Figure 5-30) are shown to be rich in Ti, Cr and Fe, with some Nb present. It is considered that these light gray particles may be Ti and Cr carbides. Figure 5-32 reveals that the dark gray particles (Location B) are rich in Ti, Cr, Mn and O, with some Al and Nb present. This EDS result indicates that these dark gray particles are inclusions/oxides.

Three intergranular corrosion tested samples were also chosen for study. A8904A Heat 1, in the as-cast and SA condition, and wrought counterpart Alloy 2205. Figure 5-33 reveals the OLM micrographs of the transverse cross section of the intergranular corrosion tested Heat 1, in the as-cast condition (Figure 5-33a) and SA condition (Figure 5-33b), and Alloy 2205 (Figure 5-33c). Note that the transverse cross section is through an intergranularly attacked region and represents the typical extent of attack for each sample. It is evident that IGC is mainly associated with the ferrite/austenite interface, regardless of the material condition (as-cast or solution annealed or wrought). However, as-cast Heat 1 reveals the greatest extent of intergranular attack (60mpy), and SA Heat 1 (12mpy) and wrought Alloy 2205 (16mpy) show basically an identical level of corrosion. It is believed that precipitates, along the ferrite/austenite interface, are responsible for the low IGC resistance of as-cast Heat 1.

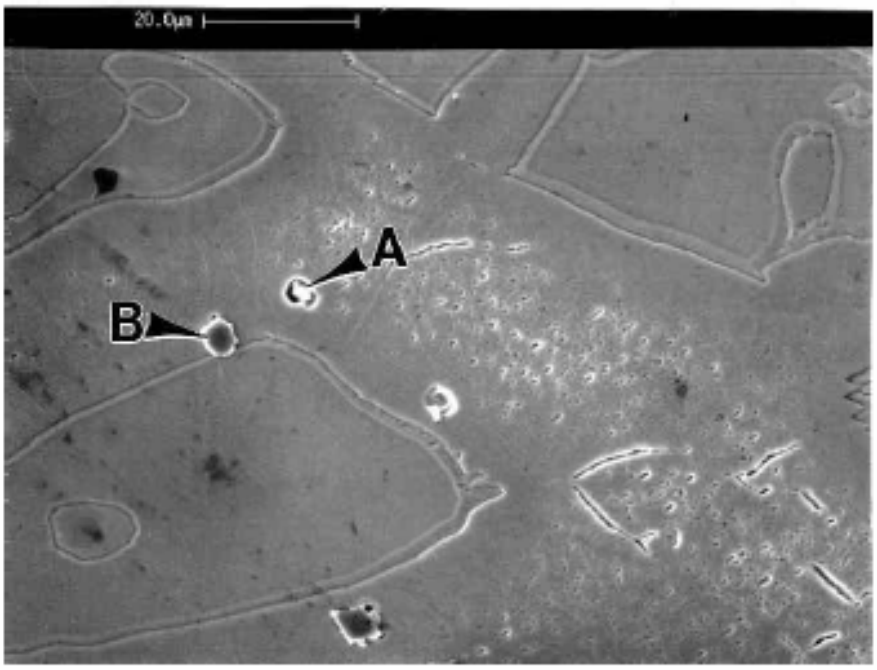

Figure 5-30. SEM Photomicrograph of the Heat 2 Base Metal, Oxalic, 1000X

In addition, fine precipitates (un-identified) were observed in the ferritic regions of SA Heat 1, as shown in Figure 5-33b. It should be recalled that no precipitates were found in SA Heat 1 samples, as presented in Figures 5-9. This result indicates that microstructural variations from location to location are possible, even in the same casting.

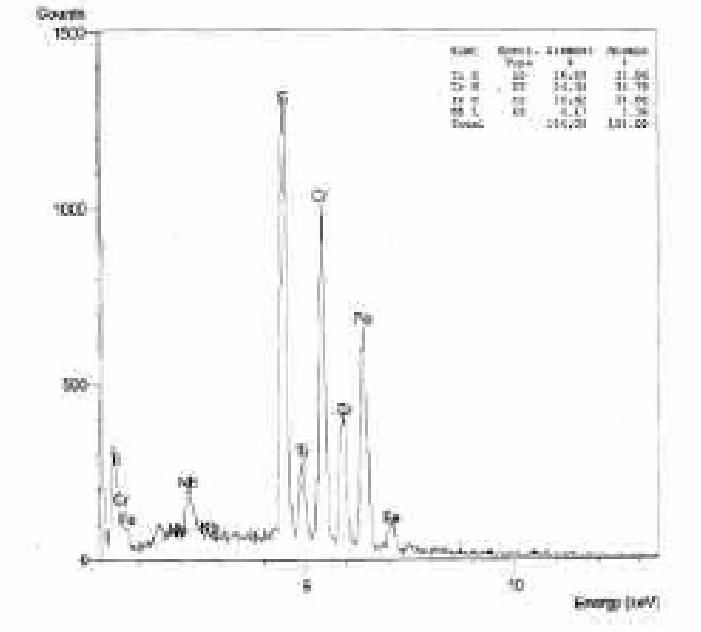

Figure 5-31. EDS Spectrum at Location A in Figure 5-30

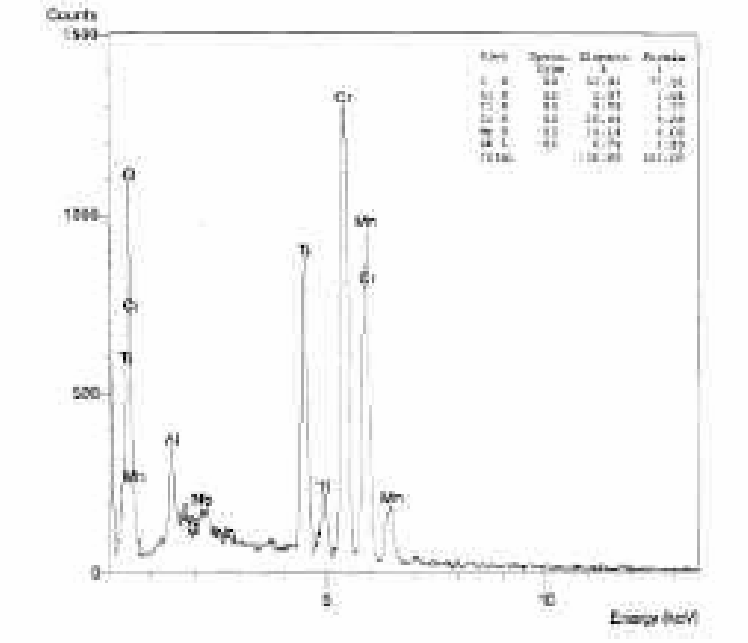

Figure 5-32. EDS Spectrum at Location B in Figure 5-30

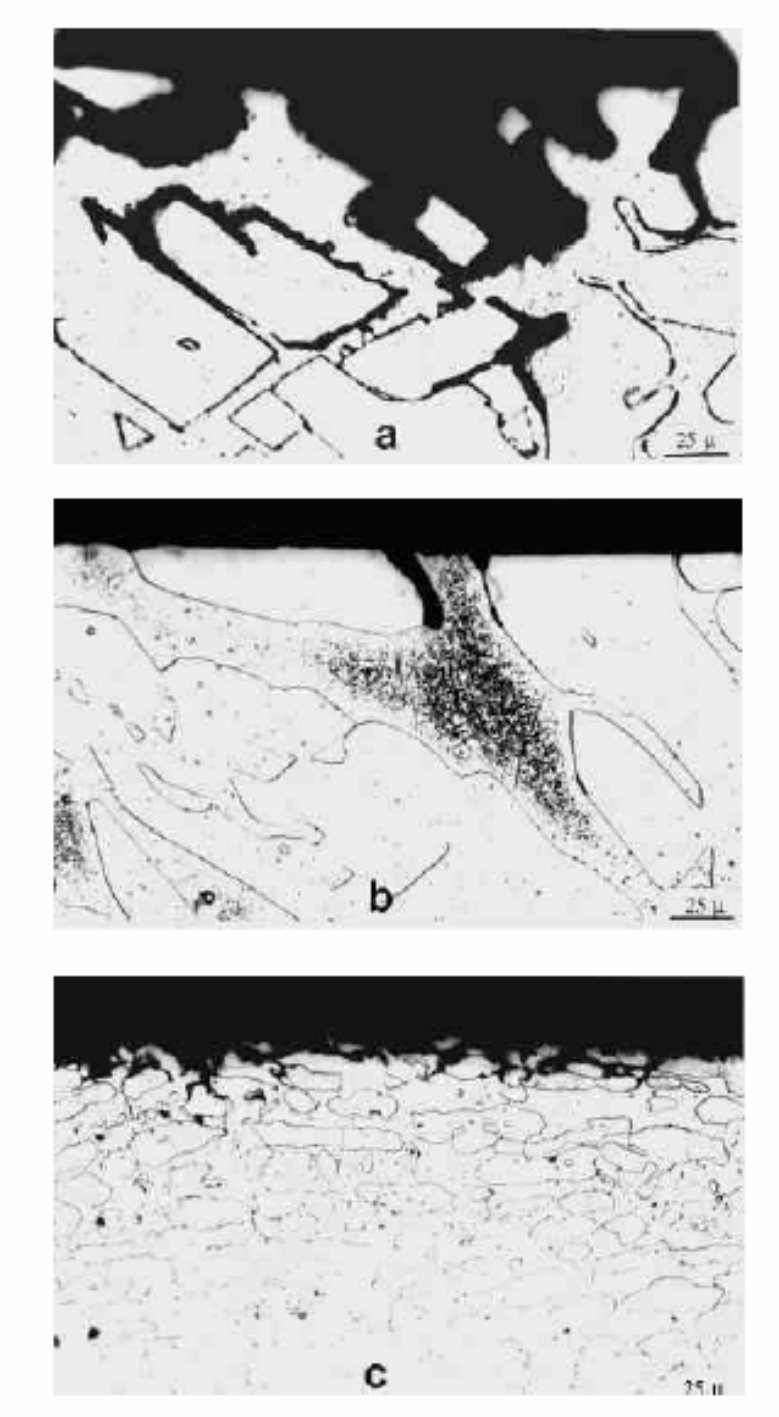

Figure 5-33. Microstructure of Cross Section of Intergranular Corrosion Tested ASTM A890-4A Heat 1, (a) As-cast, (b) SA Casting, (c) Alloy 2205, Oxalic, 400X

ASTM A890-5A

ASTM A890-5A is an alloy containing about 25wt% Cr, 7wt% Ni, 3.5wt% Mo and 0.27wt% N. One heat (Heat 1) of ASTM A890-5A was selected for study in the as-cast and SA condition, in addition to the wrought counterpart Alloy 2507.

Figure 5-34 shows the microstructure of ASTM A890-5A casting base metal in the as-cast and SA condition. Figure 5-34a shows the microstructure of Heat 1 in as-cast condition. A significant amount of irregularly shaped precipitates were observed in the ferrite matrix. It is to be noted that a detailed study of these irregularly shaped precipitates was conducted on ASTM A890-6A. The irregularly shaped precipitates were determined to be Cr and Mo carbides based on the EDS results. Figure 5-34b reveals the microstructure of Heat 1 in the SA condition. The irregularly shaped precipitates present in the as-cast condition were completely dissolved upon solution annealing. A rolling texture structure directionality, obtained by hot working and followed by solution annealing, was observed in the wrought counterpart Alloy 2507, as shown in Figure 5-35.

Figure 5-36 shows the pitting behavior of ASTM A890-5A Heat 1 base casting in both the as-cast and SA conditions. As shown in Figure 5-36a (in the as-cast condition), pits preferentially initiate in the ferrite region and are mainly associated with the irregularly shaped precipitates. However, in the SA condition, as shown in Figure 5-36b, pits initiated at the ferrite/austenite interfaces and preferentially grew into the austenite region, this behavior is similar to ASTM A890-4A in the SA condition.

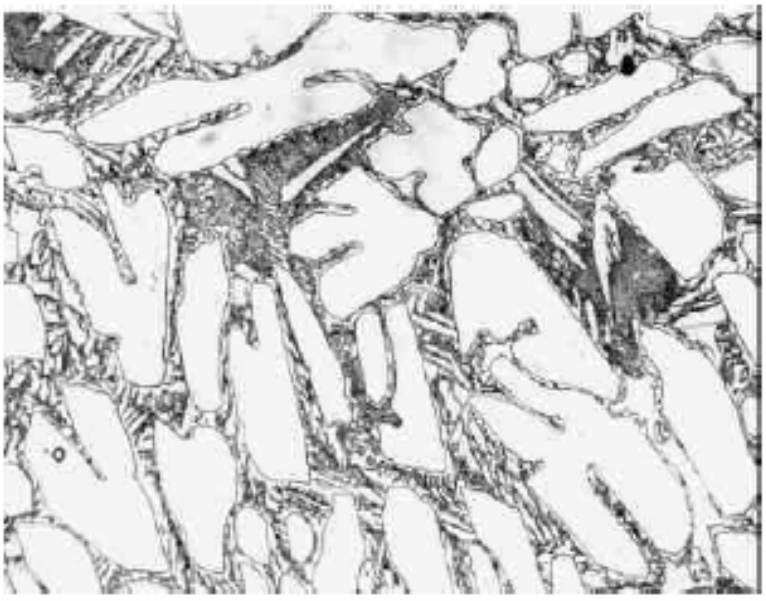

(a) As-cast

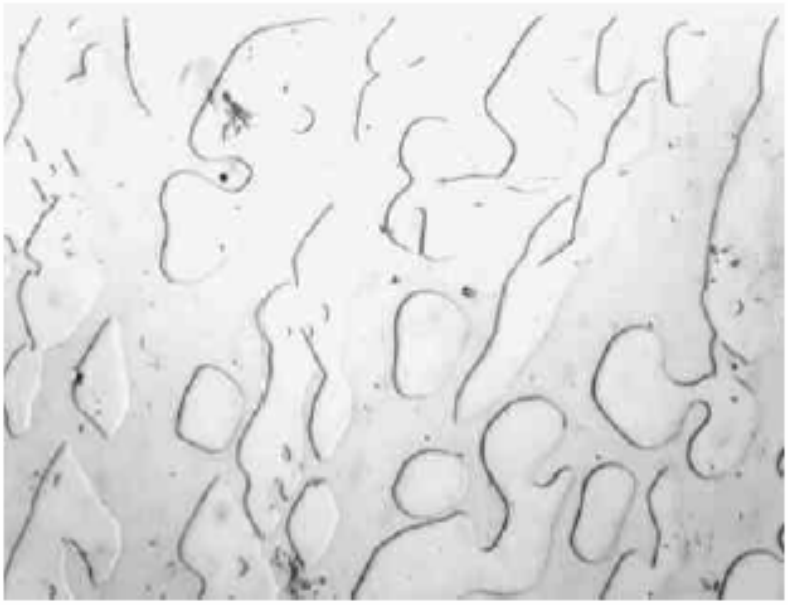

(b) SA

Figure 5-34. Microstructure of ASTM A890-5A, Heat 1, Glyceragia, 400X

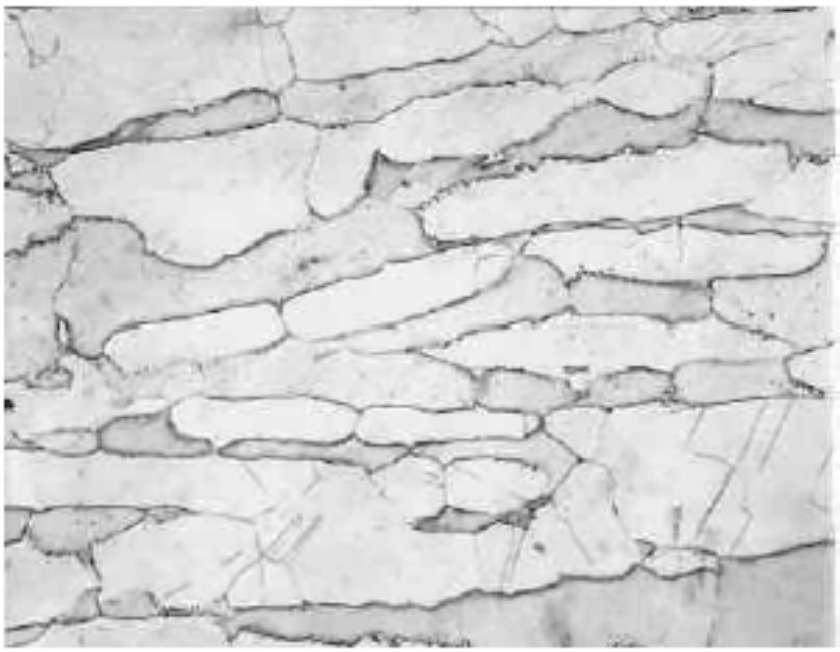

Figure 5-35. Microstructure of Wrought Alloy 2507, Oxalic, 400X

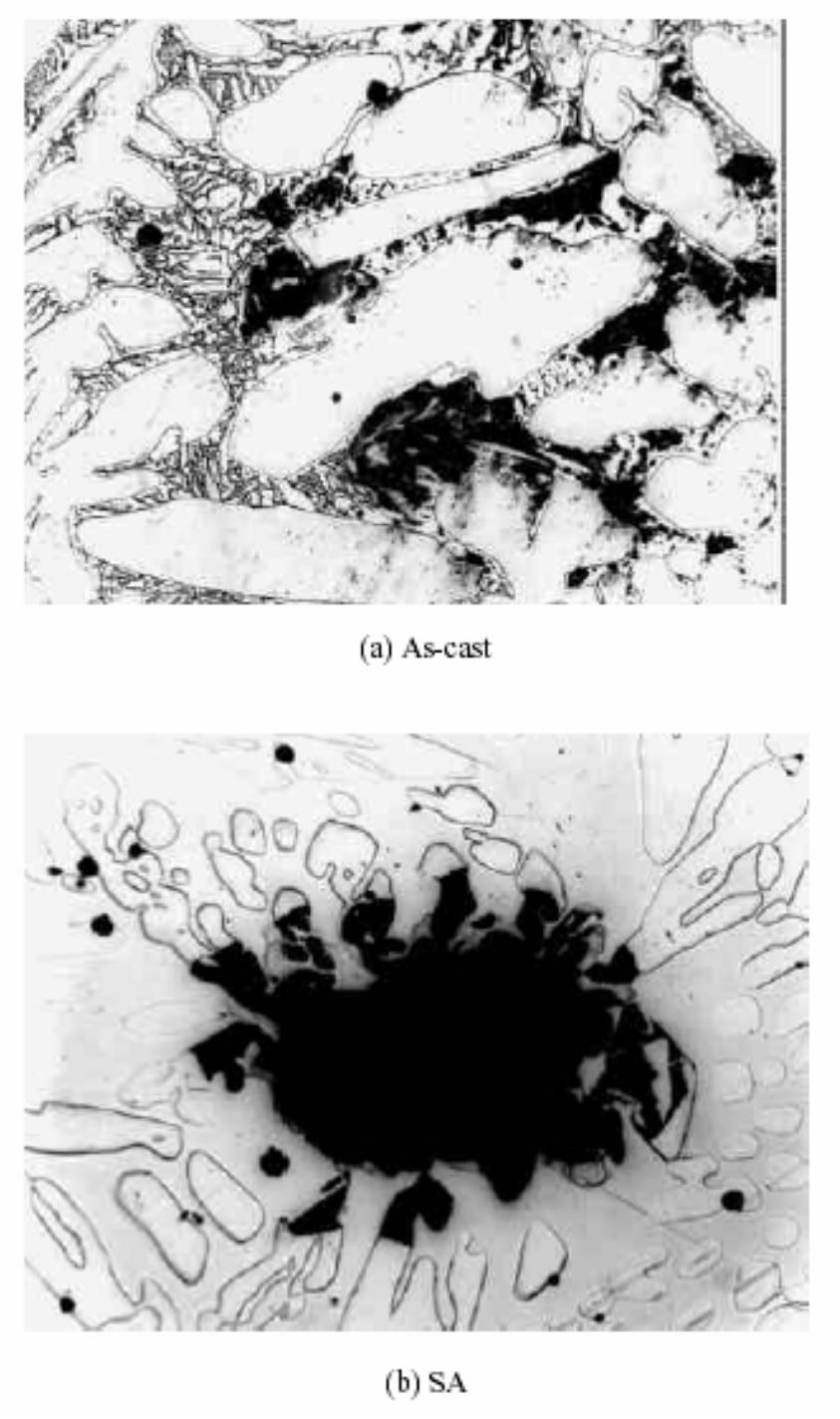

(a) As-cast

(b) SA

Figure 5-36. Pitting of ASTM A890-5A, Heat 1, Glyceragia, 400X

ASTM A890-6A

ASTM A890-6A is a DSS of 25wt% Cr, 7wt% Ni, 3.5wt% Mo and 0.27wt% N. Two heats (Heats 2 & 3) of ASTM A890-6A heats were selected for the microstructural evaluation in the as-cast and SA condition, as well as one heat of ASTM A890-6A (Heat 1), for the ICT. It is to be noted that a Heat 3 sample from the heat treatment study was also selected due to its low CPT value (5°C). This material had been SA at 2050°F (1120°C) followed by a 1850°F (1010°C) thermal arrest before air cooling.

Figure 5-37 shows the microstructure of Heat 2 in the SA condition, which reveals a normal duplex casting microstructure. Figure 5-38 presents the microstructure of Heat 3 in the as-cast and SA condition. Irregularly shaped precipitates in the ferrite matrix are evident, in the as-cast condition (Figure 5-38a). Figure 5-38b reveals that the irregular shaped precipitates in the ferrite matrix were dissolved during the solution annealing treatment, which indicates a normal response of DSS castings to the solution annealing heat treatment. In addition to austenite islands in a ferrite matrix, some randomly distributed dark gray inclusions are also observed in the matrix.

Figure 5-39 shows the microstructure of a Heat 3 sample from the heat treatment study (5°C CPT). It is evident that the irregular shaped precipitates are present in the ferrite matrix after the solution annealing treatment. It is considered that an improper solution annealing heat treatment was applied to this sample. The corresponding pitting corrosion behavior is presented in Figure 5-40. Pits preferentially initiated in the ferrite region and were associated with the irregularly shaped precipitates. These irregular shaped precipitates are responsible for the low CPT value of the SA Heat 3 sample. Further evaluation of the irregular shaped precipitates in the ferrite region was performed

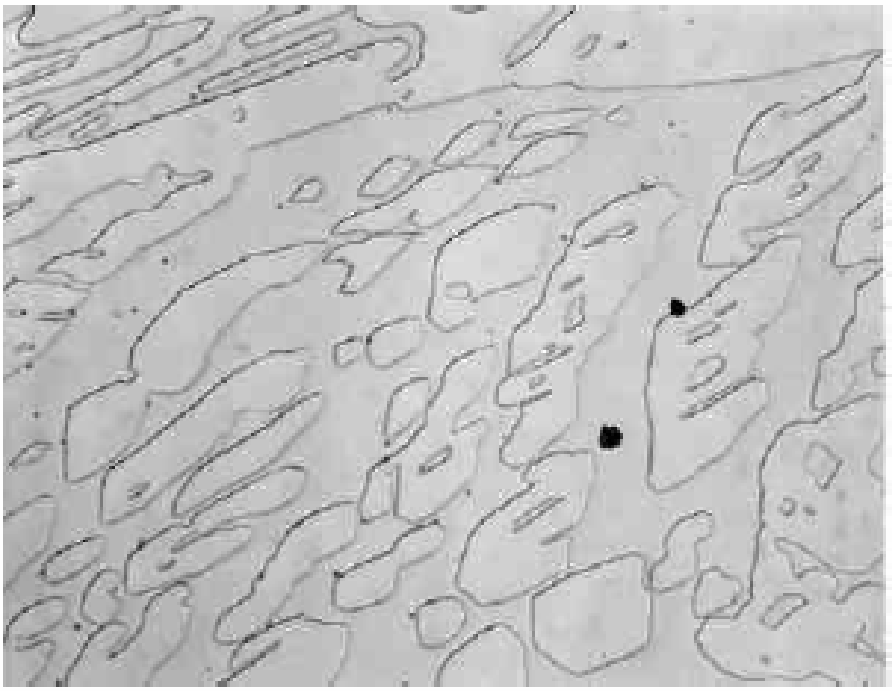

Figure 5-37. Microstructure of SA ASTM A890-6A, Heat2, Oxalic, 400X

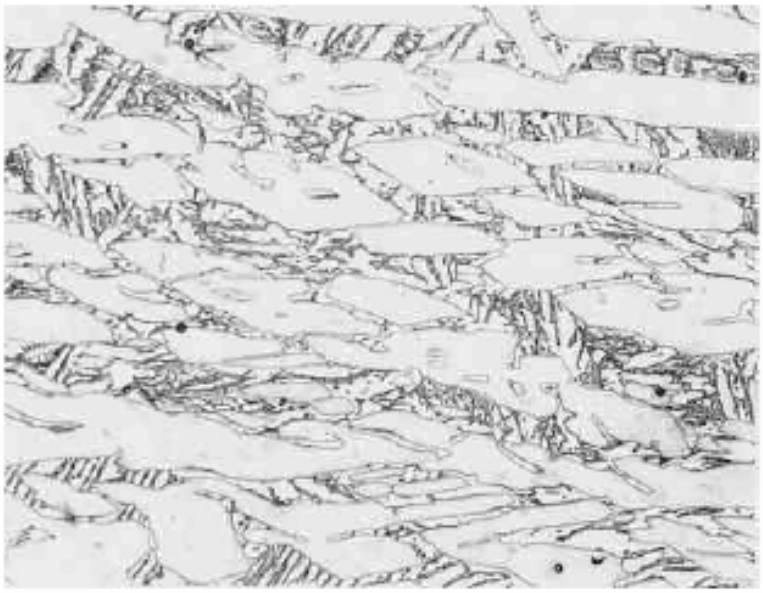

(a) As-cast

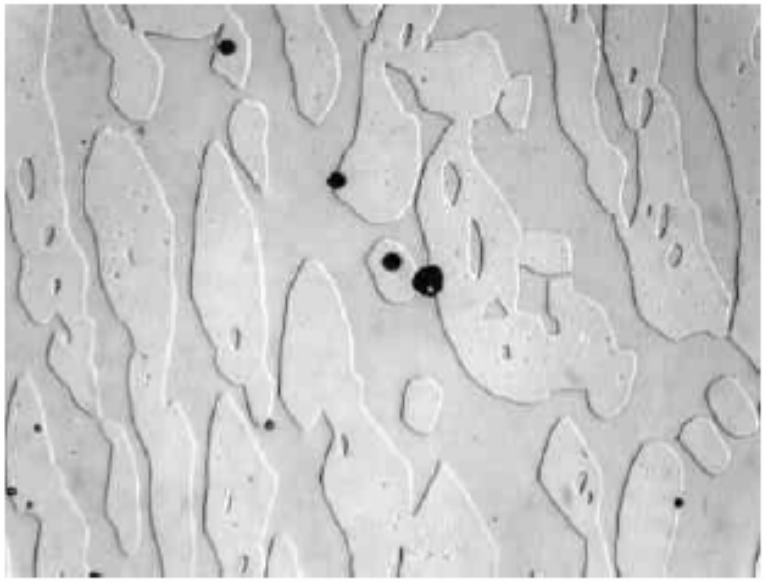

(b) SA

Figure 5-38. Microstructure of ASTM A890-6A, Heat 3, Glyceragia, 400X

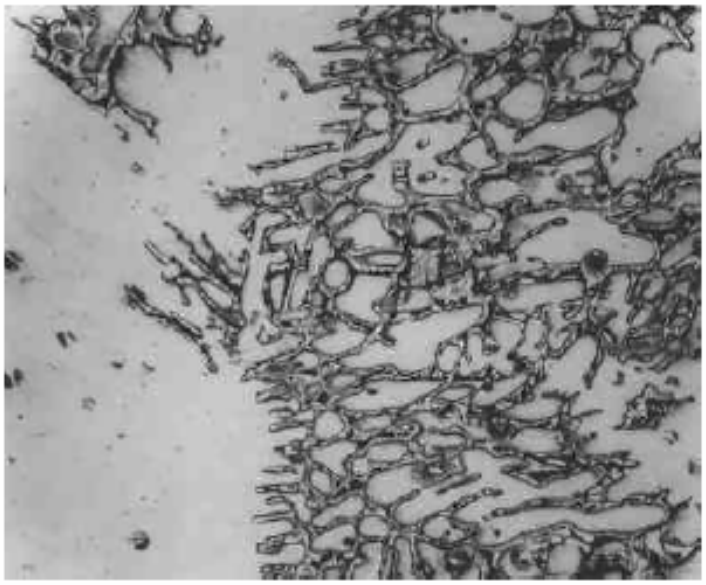

100X

(a)

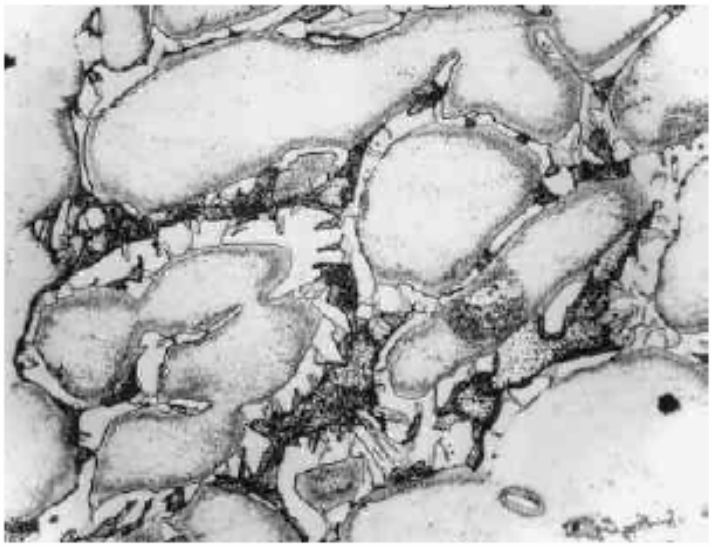

400X

(b)

Figure 5-39. Microstructure of Improperly Heat Treated ASTM A890-6A Heat 3, Glyceragia

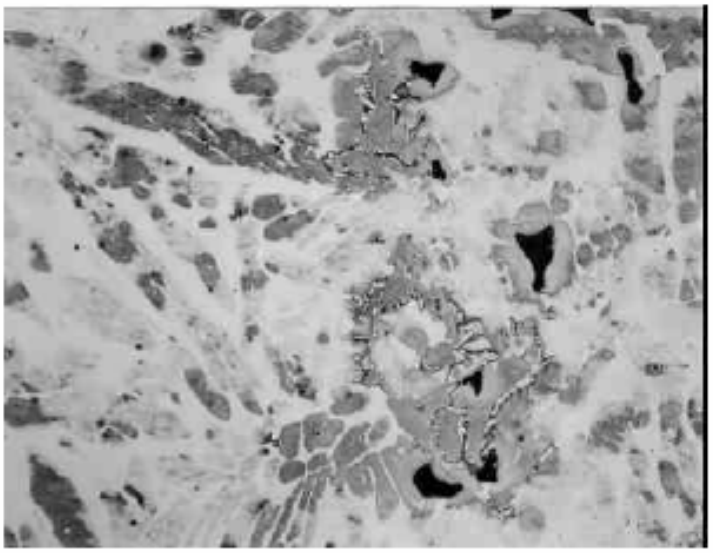

100X

(a)

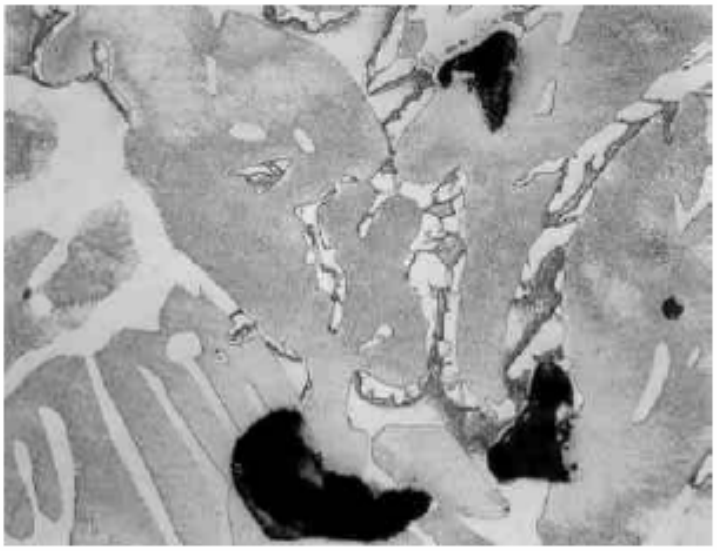

400X

(b)

Figure 5-40. Pitting of Improperly Heat Treated ASTM A890-6A, Heat 3, Oxalic

using SEM and EDS. Figure 5-41 shows a SEM photomicrograph of the irregular shaped precipitates in the ferrite region, in addition to the austenite islands and some gray particles. Noted that the gray particles in Figure 5-41 were optically revealed as the dark gray particles shown in Figures 5-39 and 5-40. The EDS analysis was conducted at locations A, B, C & D (marked in Figure 5-41), and spectra are presented in Figures 5-42 to 5-45. Figure 5-42 reveals a normal EDS spectrum for the austenite region (Location A). The gray particle (Location B) is considered to be an inclusion based on the spectrum (rich in Cr, Mn, Al, Si & O, Figure 5-43). Figures 5-44 and 5-45 show the EDS results of the irregular shaped precipitates in the ferrite region (Locations C & D). They are rich in Cr, Fe and Mo. Based on the EDS spectra, these precipitates are considered to be s-phase. Also it is believed that the presence of s-phase is responsible for the preferential pit initiation in this area and caused the dramatic decrease in CPT for this HT on 6A material. In addition, element mapping (Figure 5-46) for Cr, Mo and Ni was performed in the same area s presented in Figure 5-41. Mo depletion in the ferrite region was determined, as well as the segregation of Cr into the ferrite and Ni into the austenite.

Microstructural characterization was also carried out on the wrought counterpart Zeron 100. Its base metal microstructure reveals a typical wrought DSS structure as shown in Figure 5-47. Three ICT samples were chosen for study; A890-6A Heat 1 in the as-cast, SA conditions and wrought counterpart Zeron 100. Figure 5-48 shows the OLM micrographs of transverse cross sections of intergranular corrosion tested Heat 1, in the as-cast (Figure 5-48a) and SA condition (Figure 5-48b) and Zeron 100 (Figure 5-48c).

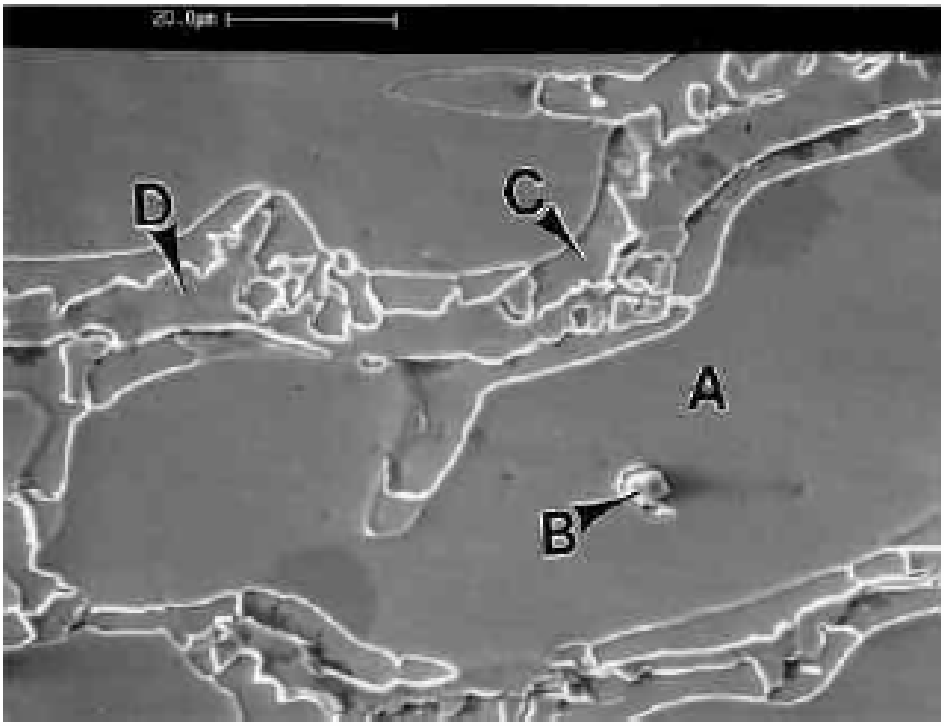

Figure 5-41. SEM Photomicrograph of Irregular Shaped Precipitates in the Ferrite Region, Austenite Islands and Gray Particles of Improperly Heat Treated ASTM A8906A Heat 3, Oxalic, 1000X

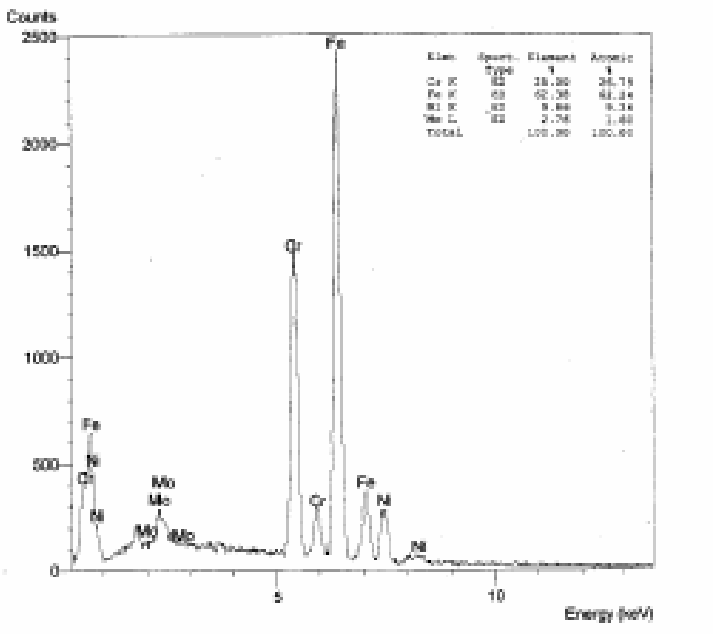

Figure 5-42. EDS Spectrum at Location A in Figure 5-41

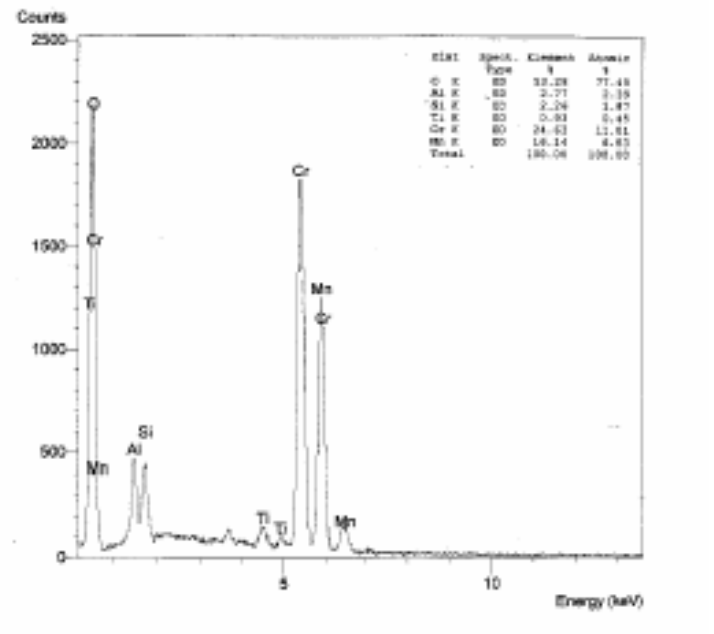

Figure 5-43. EDS Spectrum at Location B in Figure 5-41

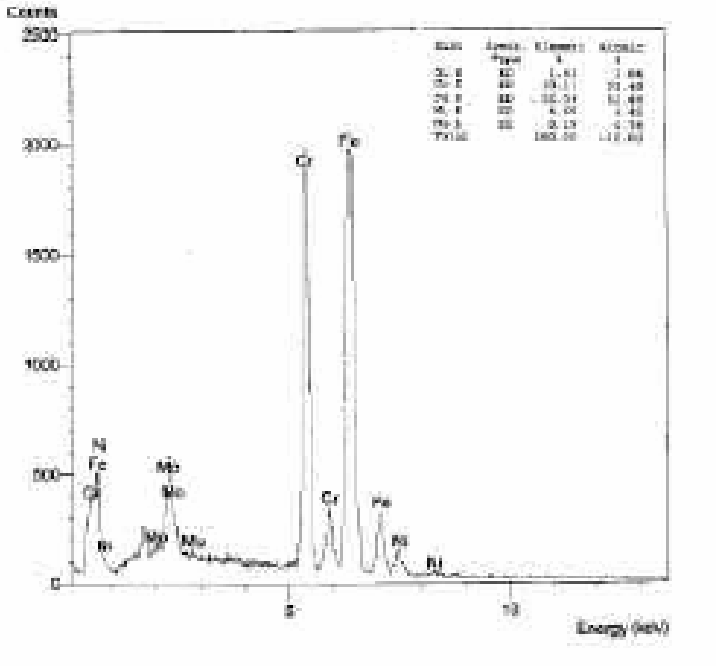

Figure 5-44. EDS Spectrum at Location C in Figure 5-41

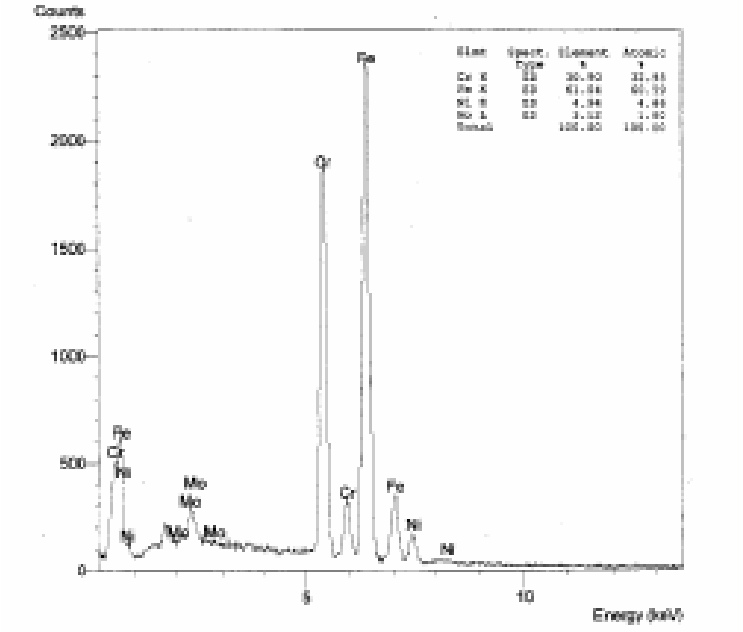

Figure 5-45. EDS Spectrum at Location D in Figure 5-41

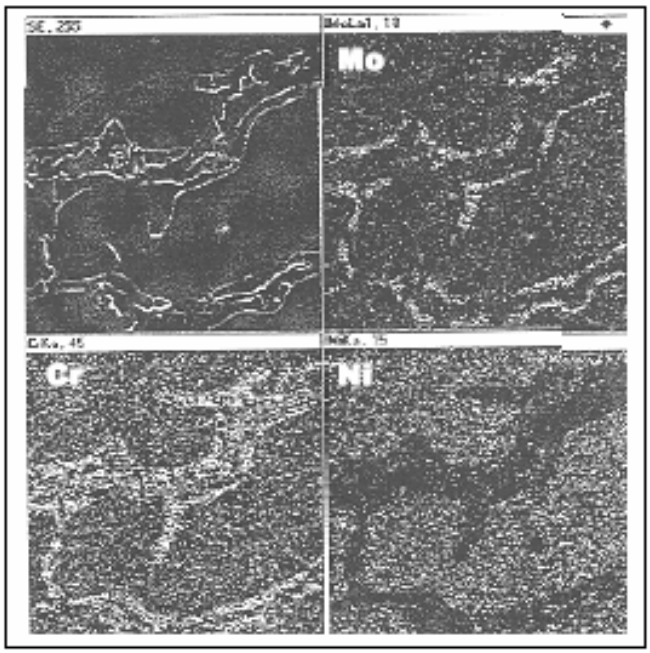

Figure 5-46. Element Mapping (Cr, Mo and Ni) in the Area Presented in Figure 5-41

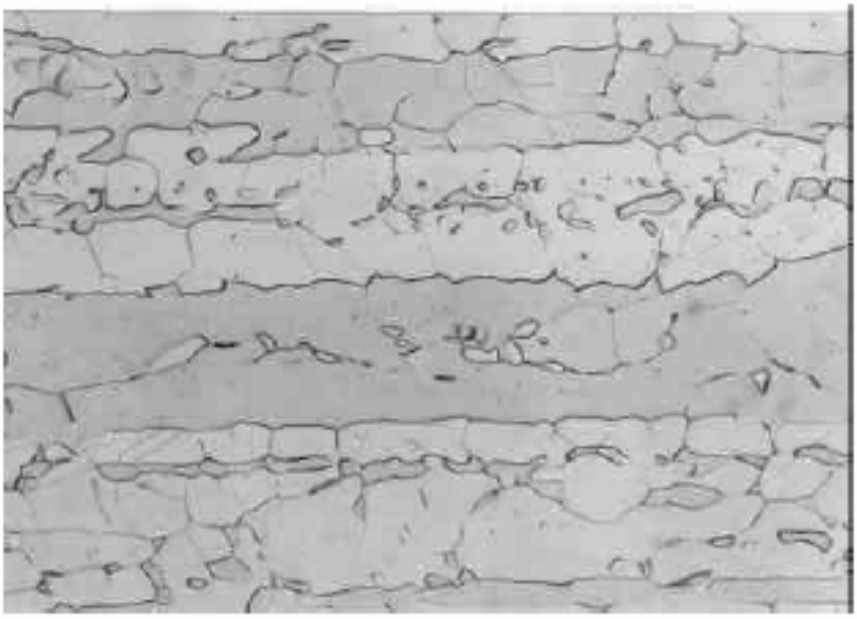

Figure 5-47. Microstructure of Wrought Zeron 100, Glycerigia, 400X

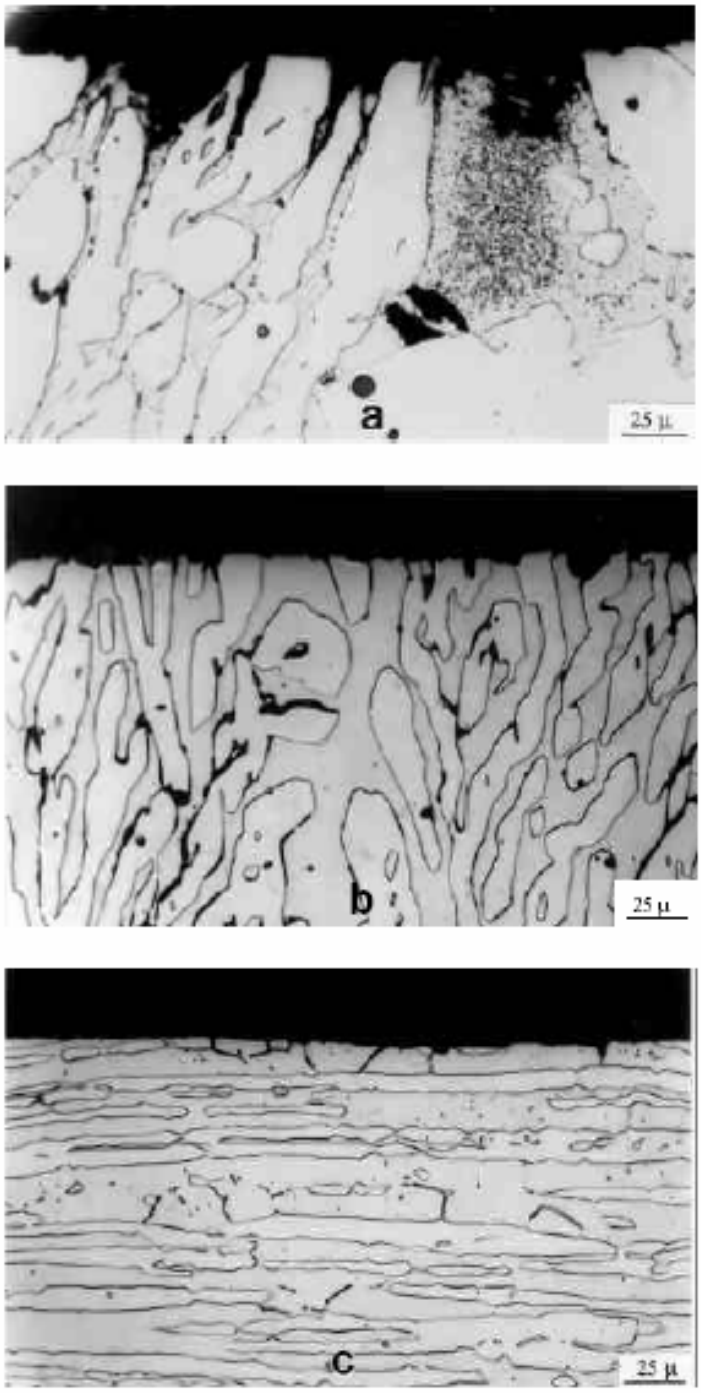

Figure 5-48. Microstructure of Cross Section of Intergranular Corrosion Tested ASTM A890-6A (a) As-cast, (b) SA Casting, (c) Zeron 100, Oxalic, 400X

It is to be noted that the transverse cross section is through intergranularly attacked regions and represents the typical extent of attack. It is evident that the IGC is mainly associated with the ferrite/austenite interface, regardless of the material condition (as-cast or SA or wrought). However, as-cast Heat 1 reveals the greatest extent of the intergranular attack (33mpy), while SA Heat 1 (8mpy) and wrought Zeron 100 (6mpy) show basically identical level of corrosion. It is believed that the precipitates along the ferrite/austenite interface are responsible for the low IGC resistance of as-cast Heat 1. It is to be noted that intergranular attack is only revealed on the sample convex surface. The dark etching appearance along the ferrite/austenite interface inside material showing on the transverse cross section, are not intergranular attack as shown in Figure 5-48b.

ASTM A890-1B & "CD7MCuN"

ASTM A890-1B and its variant "CD7MCuN", belong to the 25 Cr grade varieties with varying contents of Mo and N. They also contain Cu or W as alloying elements. One heat (Heat 1) of ASTM A890-1B, in addition to wrought Ferralium 255, and one heat (Heat 2) of "CD7MCuN" were selected for study. Heat 1 of ASTM A890-1B was evaluated in the as-cast and SA condition. Heat 2 of "CD7MCuN" was characterized in the SA static cast and SA centrifugal cast condition.

Figure 5-49 presents the microstructure of ASTM A890-1B Heat 1 in the as-cast and SA condition. Fine precipitates are observed along the ferrite/austenite interface and in the ferrite region in the as-cast condition as shown in Figure 5-49a.

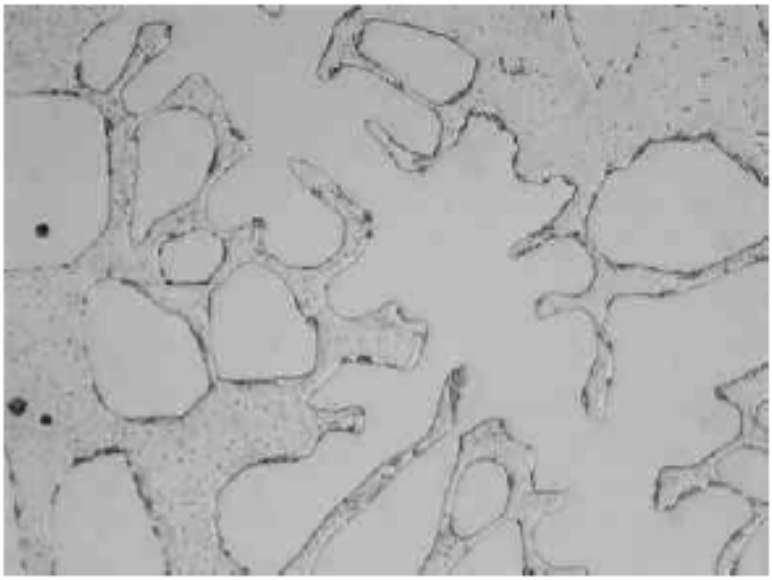

(a) Static Cast

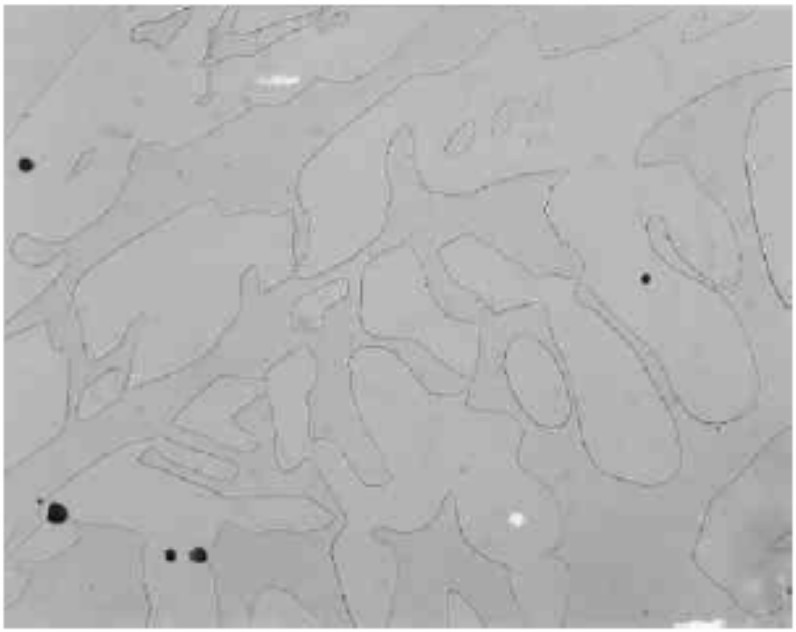

(b) Centrifugal Cast

Figure 5-49. Microstructure of ASTM A890-1B, Heat 1, Glycerigia, 400X

It is predicted that these fine precipitates are Cr or Mo carbides based on the morphology and locations. No SEM or EDS analysis were conducted on this sample. In addition, some dark gray inclusions were also found in the matrix. The fine precipitates were completely dissolved upon solution annealing treatment as presented in Figure 5-49b. The dark gray inclusions were un-changed after solution annealing treatment.

Figure 5-50 illustrates the microstructure of "CD7MCuN" Heat 2 in the SA static cast (Figure 5-50a) and centrifugal cast (Figure 5-50b) condition. A normal DSS cast microstructure, in the SA condition, was revealed for both static cast and centrifugal cast samples. The centrifugal cast material shows a finer austenite structure than the static casting. This finer austenite structure in the centrifugal casting may have a positive influence on the mechanical properties, when compared to static casting. Figure 5-51 shows the microstructure of wrought alloy Ferralium 255. The structure is similar to all other wrought alloys.

It has been established that nitrogen has a significantly positive influence on pitting resistance of duplex castings. Thus, the loss of nitrogen from the fusion zone during welding may cause a decrease in pitting resistance in the fusion zone. A trial experiment, performed by adding 5% nitrogen into Ar shielding gas, was conducted on Ferralium 255 autogenous welds. The CPT of the Ferralium 255 autogenous weld, with 5% nitrogen+95% Ar, was determined to be 30°C compared to 25°C for Ferralium 255 autogenous welds with 100% Ar. The OLM micrographs of the pitting behavior for both Ferralium 255 autogenous welds with and without addition of 5% nitrogen are presented in Figure 5-52. It is evident that pits preferentially initiated in the fusion zone and at the fusion line of the autogenous weld with 100% Ar (without 5% nitrogen), as shown in

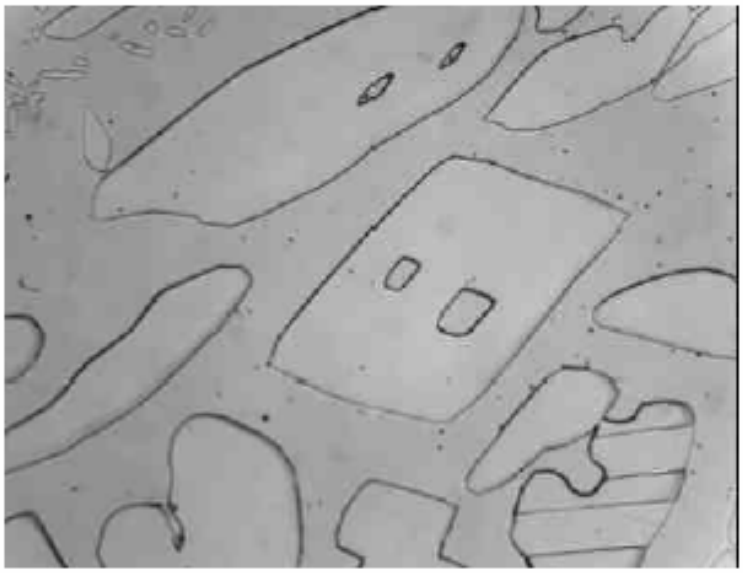

(a) Static Cast

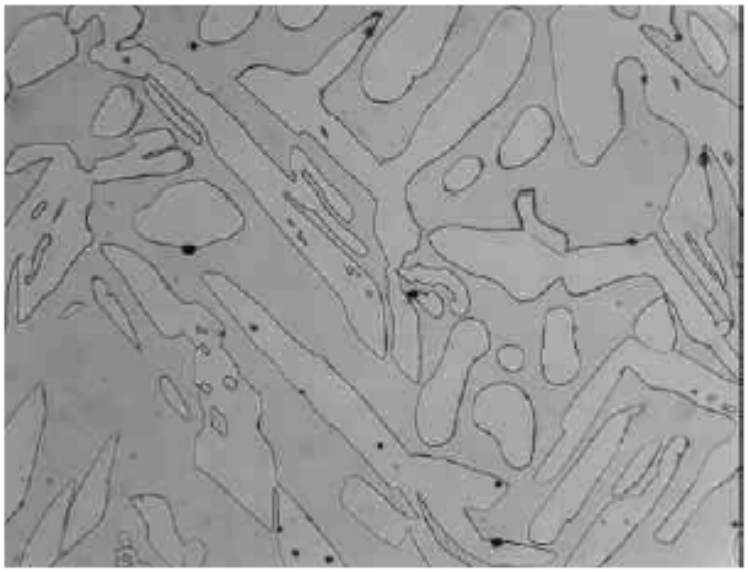

(b) Centrifugal Cast

Figure 5-50. Microstructure of CD7MCuN, Heat 2, Glycerigia, 400X

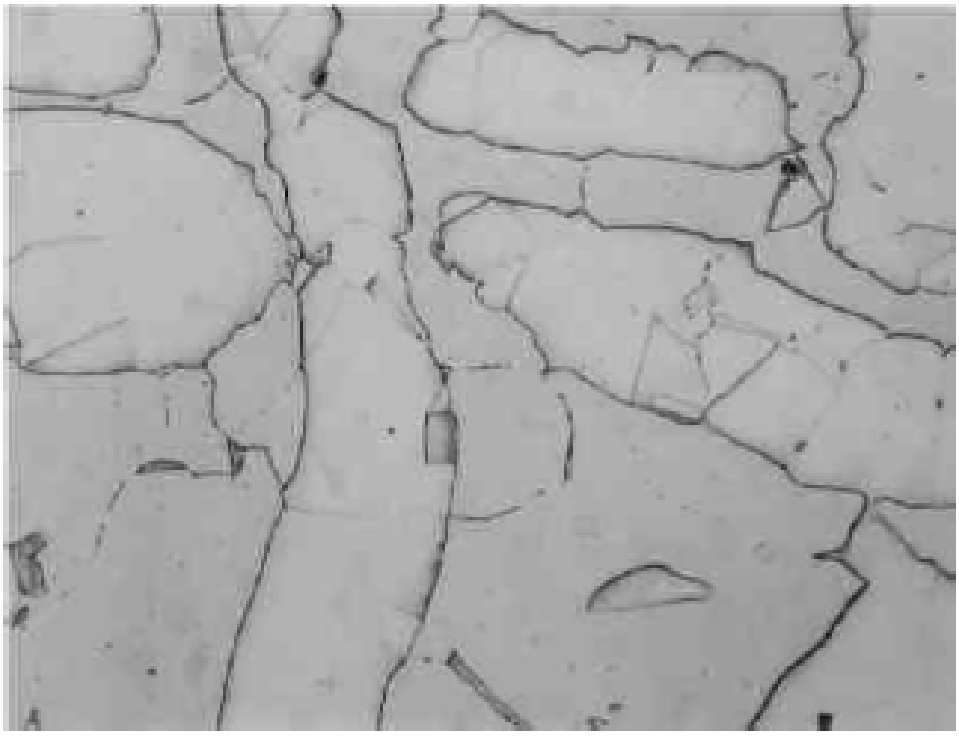

Figure 5-51. Microstructure of Wrought Ferralium 255, Glycerigia, 400X

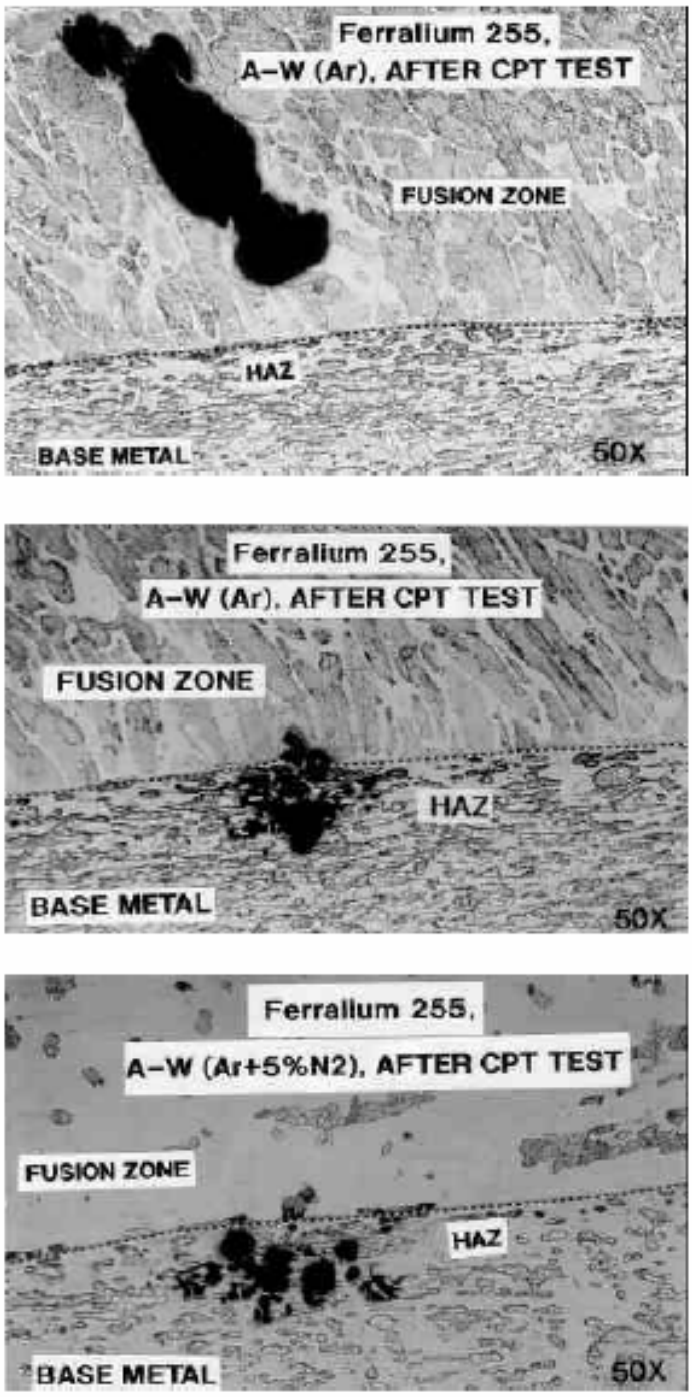

Figure 5-52. Pitting of Autogenous Welds on Wrought Ferralium 255, Glycerigia

Figure 5-52a and b. Upon adding 5% nitrogen into shielding gas, no pits were found in the fusion zone, as presented in Figure 5-52c. All of the pits preferentially initiated in the HAZ of Ferralium 255 autogenous welds (with 5% nitrogen). The improvement in the CPT is not significant because of the primarily HAZ pit initiation and the fact that the nitrogen addition only affects the fusion zone. It should be recognized that there are multiple potential pit initiation locations in the autogenous welds (fusion zone, fusion line and HAZ). Pits will preferentially initiate at where the pitting resistance is the lowest. Thus, an understanding of the effect of welding on the corrosion behavior of duplex stainless steel castings is a necessary and extremely important subject for both foundry and industry.

In order to identify whether there is precipitation of sigma phase in Ferralium weld HAZ, a color staining etching technique, utilizing 10% NaCN, was applied to all the samples evaluated above. No sigma phase was revealed by this color etching technique in any of the samples.

VI. Conclusions

Over a thousand individual tests, including corrosion, impact toughness, weldability and microstructure evaluation, were conducted in this program. A fairly useful database for the corrosion performance of the duplex stainless steel castings has been established. Heat-to-heat and duplex stainless steel alloy system-to-system comparisons were made based on the obtained results. Some conclusions were drawn as follows:

- Both the pitting and intergranular corrosion resistance of cast duplex stainless steels are equal to or better than their wrought counterparts. Thus, cast and wrought products can be produced to the same performance standards.
- The corrosion test methods for wrought stainless materials are suitable for evaluation of duplex stainless steel castings:
    - ASTM G48 Method A – Pitting corrosion test
    - ASTM A923 Method C – Pitting corrosion for microstructure assessment
    - ASTM A262 Practice B – Intergranular corrosion

      It is recommended that a 2t bend evaluation be added to ASTM A262 Practice B to supplement the corrosion rate characterization.
- The solution annealing procedures in ASTM A890 are appropriate for placing cast duplex stainless steel in the proper condition for service.
- Despite the application of thermal arrests, corrosion performance was not degraded when a rapid quench method (water) was applied.
- An appropriate screening test characterizing service performance of duplex stainless steel castings is ASTM A923 Method A, which is currently utilized for wrought

materials. Cast duplex alloys can be added to this specification upon the inclusion of appropriate photomicrographs.

- Welding reduced the pitting and intergranular corrosion resistance for both the wrought and cast duplex alloys of similar composition. The effect of welding should be considered when selecting an alloy type for specific corrosion service. Thus, the same fabrication considerations apply to the entire cast/wrought system.
- The data obtained in this study suggests that ASTM A923 can be expanded in coverage to include the cast duplex materials of ASTM A890. Thus, one specification will cover both wrought and cast materials making selection independent of product form.
- Charpy impact test results show that castings generally have better toughness than their wrought counterparts in the temperature range of –80°C to +20°C. Thus, specification requirements are simplified for an entire system fabrication (both wrought and cast).
- Weldability bend tests (ASTM A494) were performed on castings with the appropriate (matching) filler metals. All tested heats passed. Therefore, welding is not a significant factor when considering duplex stainless steel applications.

References

1. Gunn, R., ed. *Duplex Stainless Steels - Microstructure, Properties and Applications.* 1997, Abington Publishing: Cambridge England.
2. Charles, J. *Super Duplex Stainless Steel: Structure and Properties. in 2nd. Duplex Stainless Steels*. 1991.
3. Taylor, R. *Duplex Stainless Steel Production. in SFSA T&O conference*. 1994.
4. Davison, R.M.R., J. D., *Practical Guide to Using Duplex Stainless Steels*. Materials Performance, 1990. **29(1):** p. 57-62.
5. Vannevik, H., Nilsson, J.-O., Frodigh, J. and Kangas, P., *Effect of Elemental Partitioning on Pitting Resistance of High Nitrogen Duplex Stainless Steels*. ISIJ International, 1996. **36(7):** p. 807-812.
6. Fruytier, D.J.A. *Industrial Experiences with Duplex Stainless Steel Related to Their Specific Properties. in 2nd. Duplex Stainless Steels*. 1991.
7. Thual-Duret, C.a.M., J.L. *Duplex Stainless Steel Wirelines for Use in H2S Containing Aqueous Chloride Environments. in 2nd. Duplex Stainless Steels*. 1991.
8. Gooch, T.G., *Corrosion Behavior of Welded Stainless Steel*. Welding Journal, 1996. **75(5):** p. 135s-154s.
9. Machado, I.F.a.P., A.F., *Precipitation Behavior of 25% Cr - 5.5 Ni Austenitic Stainless Steel Containing 0.87% Nitrogen*. Steel Research, 1996. **67(7):** p. 285290.
10. Lai, J.K.L., Wong, K.W. and Li, D.J., Materials Science and Engineering A, Nov. 1995, *Effect of Solution Treatment on the Transformation Behavior of Cold*

Rolled Duplex Stainless Steels. Materials Science and Engineering A, 1995. **203(1-2):** p. 356-364.

11. Nilsson, J.O.a.W., A., *Influence of Isothermal Phase Transformation on Toughness and Pitting Corrosion of Super Duplex Stainless Steel SAF 2507*. Materials Science and Technology, 1993. **Vol. 9**: p. 545-554.
12. Atamert, S.a.K., J.E. ,", *Sigma-Phase Formation and Its Prevention in Duplex Stainless Steels.* Journal of Materials Science Letters, 1993. **12(14):** p. 1144-1147.
13. Redjaimia, A., Metauer, G. and Gantois, M. *Decomposition of Delta Ferrite in a Fe-22Cr-5Ni-3Mo-0.03C Duplex Stainless Steel. A Morphological and Structural Stud. in Duplex Stainless Steels '91.* 1991.
14. Wang, X.G., Dumortier, D. and Riquier, Y. *Structural Evolution of Zeron 100 Duplex Stainless Steel between 550 and 1100 °C. in Duplex Stainless Steels '91*. 1991.
15. Josefsson, B., Nilsson, J.-O. and Wilson, A. *Phase Transformation in Duplex Steels and the relation Between continuous cooling and Isothermal Heat Treatment. in Duplex Stainless Steels 91*. 1991.
16. Thorvaldsson, T., Nilsson, J.-O., and Liu, P., *Microstructural Characterization of Stainless Steel - Industrial Applications*. Micron and Microscopic Acta, 1991. **22(1/2):** p. 185-186.
17. Karlsson, L., Ryen, L. and Pak, S., *Precipitation of Intermetallic Phases in 22% Cr Duplex Stainless Weld Metals*. Welding Journal, 1995. **74(1):** p. 28s-40s.
18. Nilsson, J.-O., *Overview: Super Duplex Stainless Steels*. Materials Science and Technology, 1992. **8(8):** p. 686-700.

19. Charles, J. *Structure and Mechanical Properties of Duplex Stainless Steels. in Duplex Stainless Steels 94*. 1994.

20. Karlsson, L.a.P., S., *Influence of Intermetallic Phases on the Corrosion Properties of Duplex Stainless Steel Weld Metals*. Welding International, 1995. **9(7):** p. 554-562.

21. Nilsson, J.-O., Wilson, A., Huhtala, T., Karlsson, L., and Jonsson, P., *Structural Stability of Super Duplex Stainless Weld Metals and Its Dependence on Tungsten and Copper.* Metallurgical and Materials Transactions A. Vol. 27A(8). 1996. 2196-2208.

22. Varol, I., Lippold, J.C. and Baeslack III, W.A., *Welding of Duplex Stainless Steels*. Key Engineering Materials, 1992. **69&70**: p. 217-252.

23. Nilsson, J.-O.a.L., P., *Aging at 400-600 °C of Submerged Arc Welds of 22Cr3Mo-8Ni duplex stainless steel and Its effect on Toughness and Microstructure*. Materials Science and Technology, 1991. **7(9):** p. 853-862.

24. Adhe, K.N., Kain, V., Madangopal, K. and Gadiyar, H.S., *Influence of Sigma-phase formation on the Localized Corrosion Behavior of a Duplex Stainless Steel.* Journal of Materials Engineering and Performance, 1996. **5(4):** p. 500-506.

25. Nilsson, J.-O., Karlsson, L. and Anderson, J.-O., *Secondary Austenite Formation and Its Relation to Pitting Corrosion in Duplex Stainless Steel Weld Metal*. Materials Science and Technology, 1995. **11(3):** p. 276-283.

26. Charles, J., *Composition and Properties of Duplex Stainless Steels*. Welding in the World, 1995. **Vol. 36**: p. 43-55.

27. Kuroda, T.a.M., F., *Role of Secondary Austenite on Corrosion and Stress Corrosion Cracking of Sensitized Duplex Stainless Steel Weldments, in Transactions of JWRI.* 1994. p. 205-211.

28. Ravindranath, K.a.M., S.N., *Influence of Aging on Intergranular Corrosion of a 25%Cr-5% Ni Duplex Stainless Steel*. Corrosion, 1994. **50(4):** p. 318-328.

29. Hoffmeister, H.a.L., G., *Effects of Chemical Composition of Duplex Stainless Steels on Microstructure and Pitting Corrosion after Solution Heat Treatment and Various Weld Simulation Cooling Cycles*. Welding in the World, 1994. **33(2):** p. 18-23.

30. Kokawa, H., Tsory, E. and North, T.H., *Nitride Precipitation in Duplex Stainless Steel Weld Metal.* ISIJ International, 1995. **35(10):** p. 1277-1283.

31. Karlsson, L.a.P., S., *Welding Duplex and Super Duplex Stainless Steels*. Anti-Corrosion Methods and Materials, 1995. **42(6):** p. 30-35.

32. Atamert, S.a.K., J.E., *Super Duplex Stainless Steels Part I: Heat Affected Zone Microstructures*. Materials Science and Technology, 1992. **8(10):** p. 896-911.

33. Soylu, B.a.H., R.W.K., *Microstructural Refinement of Duplex Stainless Steels*. Materials Science and Technology, 1991. **7(2):** p. 137-145.

34. Sriram, R.a.T., D., *Pitting Corrosion of Duplex Stainless Steels*. Corrosion, 1989. **45(10):** p. 804-810.

35. Cheng, T.P., Tsai, W.T. and Lee, J.T., *Electrochemical and Corrosion Behavior of Duplex Stainless Steels in Hank's Solution.* Journal of Materials Science, 1990. **25(2A):** p. 936-943.

36. SCRATA *Materials Fact Sheets on Duplex Cr-Ni Steels, Section D, Apr.*. 1991.

37. Ogawa, T., Koseki, T. and Inoue, H. *Weld Phase Chemistries of Duplex Stainless Steels. in Weldability of Materials*. 1990.

38. Ogawa, T.a.K., T., *Effect of Composition Profiles on Metallurgy and Corrosion Behavior on Duplex Stainless Steel Weld Metals*. Welding Journal, 1998**. 68(5)**: p. 181s-191s.

39. Miura, M., Koso, M., Kudo, T. and Tsuge, H., *The Effects of Nickel and Nitrogen on the Microstructure and Corrosion Resistance of Duplex Stainless Steel Weldments.* Welding International, 1990. **4(3):** p. 200-206.

40. Anson, D.R., Pomfret, R.J., Hendry, A. and Beattie, G.T. *Castable High-Nitrogen Duplex Stainless Steels. in The Institute of British Foundrymen 91st Annual Conference.* 1994. Castcon.

41. Hertzman, S., Nilsson, M. and Jargelius-Pettersson, R. *Influence of W and Cu on Microstructure, Mechanical Properties and Corrosion Resistance in Super Duplex Weld Metals.* in Duplex Stainless Steels '94. 1994.

42. Ogawa, K., Okamoto, H., Ueda, M., Igarashi, M., Mori, T. and Kobayashi, *Effects of Tungsten on Pitting Corrosion Resistance and Impact Toughness in the HAZ of Duplex Stainless Steel - Study of Weldability of High-Tungsten Duplex Stainless Steel (1st Report)*. Welding International, 1996. **10(6):** p. 466-472.

43. Kotecki, D.J.a.S., T.A., *WRC-1992 Constitution Diagram for Stainless Steel Weld Metals: A Modification of the WRC-1988 Diagram*. Welding Journal, 1992. **71(5):** p. 171s-178s.

44. Charles, J. *Why and Where Duplex Stainless Steels. in 5th World Duplex Stainless Steels.* 1997.

45. Charles, J. *How to Improve Duplex Stainless Steel Properties with Copper Addition. in 6th World Duplex Stainless Steels*. 2000. Venezia, Italy.

46. P. V. Scheers, J.K., R. Paton. *Characterization of A 20Cr-Ni Duplex Stainless Steel with Additions of Manganese and Nitrogen. in 6th World Duplex Stainless Steel.* 2000. Venezia, Italy.

47. C.del Campo, R.S., J. Botella. *Non-standard Low-Ni High-Mn-N Duplex Stainless Steel Microstructure Balance Through Thermal History. in 6th World Duplex Stainless Steel.* 2000. Venezia, Italy.

48. S. K. Ahn, K.T.K., Y. H. Lee and Y. D. Lee. *Development of a New Type of Duplex Stainless Steel. in 6th World Duplex Stainless Steel*. 2000. Venezia, Italy.

49. Farrar, R.A., *The Importance of Microstructural Transformations for Welding and the Stability of Long Term Service Properties*. Welding in the World, 1995. **vol. 36**: p. 143-151.

50. Radenkovic, G., Cvijovic, Z. and Mihajlovic, D., *Effect of Quenching Temperature on Microstructure and Properties of Cast Duplex Stainless Steel*. Acta Stereol, 1994. **13(2):** p. 439-444.

51. Kotecki, D.J.a.S., T.A., *Heat Treatment of Duplex Stainless Steel Weld Metals*. Welding Journal, 1989. **68(11):** p. 431s-441s.

52. Garfisa-Mesias, L.F., Sykes, J.M. and Tuck, C.D.S., *The Effect of Phase Compositions on the Pitting Corrosion of 25 Cr Duplex Stainless Steel in Chloride Solutions.* Corrosion Science, 1996. **38(8**): p. 319-1330.

53. Nicholls, J.M. *Corrosion Properties of Duplex Stainless Steels: General Corrosion, Pitting and Crevice Corrosion. in Duplex Stainless Steels 94*. 1994.

54. Bernhardsson, S. *The Corrosion Resistance of Duplex Stainless Steels. in Duplex Stainless Steels 91*. 1991.

55. Walker, R.A.a.G., T.G., *Pitting Resistance of Weld Metal for 22Cr-5Ni Ferritic-Austenitic Stainless Steels.* British Corrosion Journal, 1991. *26(1):* p. 51-59.

56. Gooch, T.G. *Corrosion Resistance of Welds in Duplex Stainless Steels. in Duplex Stainless Steel 91*. 1991.

57. Ravindranath, K.a.M., S.N., *The Influence of Aging on the Intergranular Corrosion of 22 Chromium - 5 Nickel Duplex Stainless Steel*. Corrosion Science, 1995. **37(1):** p. 121-132.

58. Merino, P., Nóvoa, X.R., Pena, G., Porto, E. and Espada, L., *Intergranular Corrosion Susceptibility of Austenitic-Ferritic Duplex Stainless Steels: Application of Potentiokinetic Reactivation Tests.* Materials Science and Technology, 1993. **9(2):** p. 168-171.

59. Otero, E., Merino, C., Fosca, C and Fernandez, P., ¢94,. *Electrochemical Characterization of Secondary Phases in a Duplex Stainless Steel by EPR Test. in Duplex Stainless Steels 94*. 1994.

60. Atamert, S.a.K., J.E., *Elemental Partitioning and Microstructural Development in Duplex Stainless Steel Weld Metal*. Acta. Metall. Mater., 1991. **39(3):** p. 273-285.

61. Bonnefois, B., Charles, J., Dupoiron, F. and Soulignac, P. *How to Predict Welding Properties of Duplex Stainless Steels. in Duplex Stainless Steel 91*. 1991.

62. Cao, H.L.a.H., S. *The Relationship between Impact Properties and Welding Simulated Microstructures in Three Duplex Stainless Steels. in Duplex Stainless Steel 91*. 1991.

63. Lindbolm, B.E.S.a.H., N. *Austenite Reformation in HAZ of Ferritic Austenitic Stainless Steels. in Duplex Stainless Steel 91*. 1991.

64. Dufrance, J.J. *Heat Affected Zone Simulation of Super Duplex Stainless Steel UNS S 32760 - Zeron 100. in Duplex Stainless Steel 91*. 1991.

65. Draugelates, U., Schram, A., Boppert, C. and Liu, J. *Investigation on the Effect of the Peak Temperature and Cooling Time on the Heat Affected Zone in Duplex Cast Steel. in Duplex Stainless Steel 91*. 1991.

66. Draugelates, U., Schram, A. and Boppert, C. *Effect of the Thermal Welding Process Conditions on the Structure and Properties in the Heat Affected Zone of Duplex Cast Steel, in Duplex Stainless Steel 91*. 1991.

67. Roberti, R., Nicodemi, W., La Vecchia, G.M. and Basha, Sh. *Fracture Toughness of Simulated Duplex Stainless Steel Heat Affected Zones. in Duplex Stainless Steel 91*. 1991.

68. Boppert, C.a.D., U. *Mechanical Properties and Corrosion Resistance of Welded Superduplex Cast Alloys. in Duplex Stainless Steel 94*. 1994.

69. Lippold, J.C., Lin, W., Brandi, S., Varol, I. and Baeslack III, W.A. *Heat-Affected Zone Microstructure and Properties in Commercial Duplex Stainless Steels. in Duplex Stainless Steel 94*. 1994.

70. Kivineva, E.I.a.H., N.E., "," Duplex Stainless Steel ¢94, Vol. 1, 1994, Paper 7. *The Properties of Gleeble Simulated Heat Affected Zone of SAF 2205 and SAF 2507 Duplex Stainless Steels. in Duplex Stainless Steel 94*. 1994.

71. Hoffmeister, H.a.L., G. *Quantitative Effects of Nitrogen Contents and Cooling Cycles on d-g transformation, Chromium Nitride Precipitation and Pitting*

Corrosion after Weld Simulation of Duplex Stainless Steels. in Duplex Stainless Steel 94. 1994.

72. Jana, S., *Effect of Heat Input on the HAZ Properties of Two Duplex Stainless Steels.* Journal of Materials Processing Technology, 1992. **33**: p. 247-261.

73. Lindblom, B.E.S., Lundqvist, B. and Hannerz, N.E. *Grain Growth in HAZ of Duplex Stainless Steels. in Duplex Stainless Steel 91*. 1991.

74. Ferreira, P.J.a.H., S. *d-Ferrite grain Growth in Simulated High Temperature HAZ of Three Duplex Stainless Steels. in Duplex Stainless Steel 91*. 1991.

75. Lippold, J.C., Varol, I. and Baeslack III, W.A. *Microstructural Evolution in Duplex Stainless Steel Weldments. in Duplex Stainless Steel 91*. 1991.

76. Atamert, S., Reed, R.C. and King, J.E.. *Modeling of Multipass Duplex Stainless Steel Weld Deposit Microstructures. in Duplex Stainless Steel 91*. 1991.

77. Walker, R.A.a.N., D.N. *Effect of Welding Conditions on Corrosion Resistance of Duplex Stainless Steels. in Weldability of Materials*. 1990.

78. Lundqvist, B.a.N., P., *Weldability Aspects and Weld Joint Properties of Duplex Stainless Steels.* Welding Journal, 1988, July. **67(7):** p. 45-51.

79. Liljas, M. *The Welding Metallurgy of Duplex Stainless Steels. in Duplex Stainless Steel 94*. 1994.

80. Nelson, D.E., Baselack III, W.A. and Lippold, J.C., *An Investigation of Weld Hot Cracking in Duplex Stainless Steels*. Welding Journal, 1987. **66(8)**: p. 241s-250s.

81. Suutala, N., Takalo, T. and Moisio, T., *Ferritic-Austenitic Solidification Mode in Austenitic Stainless Steel Welds, in Metallurgical Transaction*. 1980. p. 717-725.

82. Lippold, J.C., Baeslack III, W.A. and Varol, I., "" l, 71(1), 1992, pp. 1s-14s., *Heat-Affected Zone Liquation Cracking in Austenitic and Duplex Stainless Steels.* Welding Journal, 1992**. 71(1):** p. 1s-14s.

83. Shinozaki, K., Ke, L. and North, T.H., *Hydrogen Cracking in Duplex Stainless Steel Weld Metal.* Welding Journal, 1992. **71(11):** p. 387s-396s.

84. Ogawa, K.a.M., M., *Hydrogen Cracking in Duplex Stainless Steel Weldments.* Welding International, 1991. **5(9):** p. 691-696.

85. Kotecki, D.J.a.S., T.A. *Phase Transformations and Weldability of Duplex Stainless Steels. in The First United States - Japan Symposium on Advances in Welding Metallurgy.* 1990, June.

86. Hoffmeister, H., Volden, L. and Grong,. *Hydrogen Induced Weld Cracking of Duplex Stainless Steels as Affected by Shielding Gas Composition with TIG Welding. in Duplex Stainless Steels 94*. 1994.

87. van der Mee, V., Meelker, H. and van Nassau, L. *How to Avoid Hydrogen Cracking in (Super) Duplex Stainless Steel Weldments. in Duplex Stainless Steels 94.* 1994.

88. Fang, P.J., Kirkwood, D., Power, L.J. and Baxter, C.F.G., *The Resistance of Super Duplex Stainless Steel to Hydrogen Cracking. in Duplex Stainless Steels 94.* 1994.

89. Lundin, C.D.e.a., *Measurement of Diffusible Hydrogen and Hydrogen Effects on the Weldability of 2205/2209 Duplex Stainless Steel*.

90. Karlsson, L., *Intermetallic Phase Precipitation in Duplex Stainless Steels and Weld Metals: Metallurgy, Influence on Properties, Welding and Testing Aspects*. WRC Bulletin, 1999(#438).

91. Woollin, P. *Effect of Intermetallic Phases on Environmental Cracking Resistance of Superduplex Weld Metal in Sour Media. in 6th World Duplex Stainless Steel.* 2000.

92. Holmberg, B. *Filler Material Selection for Optimum Duplex Weldment Properties in Steel UNS 31803. in Duplex Stainless Steels 94*. 1994.

93. Atamert, S., Stekly, J.J.K., and Pease, C. *Development of Flux-Cored Super Duplex Stainless Steel Consumables. in Duplex Stainless Steels 94*. 1994.

94. Pak, S.a.R., S. *Experiences of Welding Duplex Stainless Steels with the FCAW Process. in Duplex Stainless Steels 94*. 1994.

95. Ödegärd, L.a.F., S.-A. *Choice of Right Filler Metal for Joining Sandvik SAF 2507 to a Superaustenitic Stainless 6Mo-Steel. in Duplex Stainless Steels 91*. 1991.

96. Van Nassau, L., Meelker, H. and Hilkes, J., *Welding Duplex and Super-duplex Stainless steels*. Welding in the World, 1993(31(5)): p. 322-343.

97. Sandvik, *Your Guide to Easy Welding of Duplex Stainless Steel.*

98. Metrode, *Metrode Welding Consumables* - Technical Handbook.

99. Bonnefois, B., Soulignac, P. and Charles, J. *Some Aspects of Nitrogen Introduction in the Duplex Weld Pool. in Duplex Stainless Steels 91*.

100. Urmston, S.A., Creffield, G.K., Cole, M.A., and Huang, W. *Effect of Nitrogen Containing Shielding Gases on Weldability and Corrosion Performance of Duplex Stainless Steels. in Duplex Stainless Steels 94.* 1994.

101. Gunn, R.N.a.A., P.C.J. *Development of Special Ar-He-N2 Gases for TIG Welding of Duplex and Superduplex Stainless Steels. in Duplex Stainless Steels 94*. 1994.

102. Rabensteiner, G.a.T., J. *The Specific Effect of Nitrogen in the Fabrication of a Super Duplex Stainless Steel Weld. in Duplex Stainless Steels 94*. 1994.

103. Bradshaw, R.a.C., R.A. *The Effect of Nitrogen Additions to Argon Shielding Gases on the Properties of Duplex Stainless Steel GTA Welds. in Duplex Stainless Steels 94*. 1994.

104. Stenbacka, N., Persson, K.-A. and Runnerstam, O., *Shielding Gas Technology When Welding Ordinary and High Alloyed Stainless Steels*. Welding in the World, 1995. **36**: p. 83-90.

105. Bonnet, C., Linden, G. and Rouault, P. *A New Shielding Gas for the Gas Metal Arc Welding of Duplex and Superduplex Stainless Steels*,. in Duplex Stainless Steels 94. 1994.

106. Ricardo A. Fedele, S.D.B.a.S.G.L. *Multipass SMAW of Duplex Stainless Steels. in Duplex American 2000*. 2000.

107. Bekkers, K., *Practice in Welding Duplex- and Super-duplex Stainless Steel Worldwide*. Welding in the World, 1995. **36**: p. 111-123.

108. Noble, D.N.a.G., R.N., *Welding of Duplex Stainless Steel - a Reader's Digest: Part 1*. Stainless Steel Europe.

109. Fager, S.-Å.a.Ö., L., *Influence of Different Welding Conditions on Mechanical Properties and Corrosion Resistance of Sandvik SAF 2507*. Corrosion Review, 1993. 11(3-4): p. 83-100.

110. Hilkes, J.a.B., K., *Welding Duplex Stainless Steel.* Welding Journal, 1995. **74(11):** p. 51-54.

111. Holmberg, B., *Welding of Super Duplex Steel Avesta SAF 2507*. Welding Review International, 1992. **11(1)**: p. 22-27.

112. Cles-Ove Perrersson (AB Sandvik Steel, *GMAW, an Excellent Process for the Welding of Duplex Stainless Steels. in Duplex American 2000*. Huston, USA.

113. Kotecki, D.J.a.H., J. *Welding Process for Duplex Stainless Steels. in Duplex Stainless Steels 94*. 1994.

114. Doyen, R.a.N., M. *Welding of Duplex and Super-duplex Stainless Steels. in Duplex Stainless Steels*. 1991.

115. Weir Materials, L., *Guidelines for Welding Zeron 100 Super Duplex Stainless Steel.*

116. Druce, S.G., Gage, G. and Popkiss, E., *Effects of Notch Geometry on the Impact Fracture Behavior of a Cast Duplex Stainless Steel*. The International Journal of Pressure Vessels and Piping, 1988. **33(1):** p. 59-81.

117. Gossett, J.L. *Use of Duplex Stainless Steel Castings in Control Valves. in 2nd International Symposium on the Mechanical Integrity of Process Piping*. 1996.

118. Schaeffler, A., *Constitution Diagram for Stainless Steel Weld Metal*. Metal Progress, 1949. **56(5):** p. 680, 680B.

119. Delong, W.T., Ferrite *in Austenitic Stainless Steel Weld Metal*. Welding Journal, 1974. **53(7):** p. 273s-286s.

120. Kotecki, D.J., Ferrite *Control in Duplex Stainless Steel Weld Metal*. Welding Journal, 1986. **65(10):** p. 352s-361s.

121. Kotecki, D.J., "Extension of the WRC Ferrite Number System, *Extension of the WRC Ferrite Number System.* Welding Journal, 1982. **61(11):** p. 352-361.

122. Kotecki, D.J.a.H., J., *Duplex Alloy Weld Ferrite Content: Measurement and Mechanical Property Effects*. ASM Metal/Materials Technology Series, 1982. **8201-021.**

123. Neumaier, P., *On-site Eddy Current Measurement of Ferrite Content in Austenitic and Duplex Steel Components*. Materials Evaluation, 1990. **48(9):** p. 1065-1072.

124. Kotecki, D.J., *Ferrite Determination in Stainless Steels Welds - Advances Since 1974*. Welding Journal, 1997. **76(1):** p. 24s-37s.

125. Brantsma, L.H. *Ferrite Measurements: An Evaluation of Methods and Experiences. in Duplex Stainless Steel 86*. 1986. Netherlands.

126. Niederau, H. J. *High Quality Castings from Duplex and Super-Duplex Stainless Steels for FGD and Off-shore Applications. in Duplex Stainless Steels 94*. 1994.

127. Neubert, V. *DSS Castings - Metallurgy, Manufacturing, Mechanical properties, Corrosion Resistance and Welding. in Duplex Stainless Steels 94*. 1994.

128. Sikkenga, S. *Duplex Stainless Steels. in Investment Casting Institute: 42nd Annual Technical Meeting.* 1994.

129. Nixon, P.G. *Centrispun Components in Duplex Stainless Steels. in Duplex Stainless Steels* 91. 1991.

130. Birks, S.a.R., *Producing Duplex Stainless Steel Castings.*

131. Johansson, K. *Duplex Stainless Steels; Past, Present and Future. in 6th Duplex Stainless Steels*. 2000.

132. Charles, J. *10 years Later, Obviously duplex Grades in Industrial Applications Look Like a Success Story. in 6th World Duplex 2000 Conference and Expo.* 2000. Venezia, Italy.

133. Falkland, J.O. *The Versatility of Duplex. in Duplex American 2000*. Huston, US.

Specifications

1. ASTM A890-94: “Standard Specification for Castings, Iron-Chromium-Nickel-Molybdenum Corrosion Resistant, Duplex (Austenitic/Ferritic) for General Application”
2. ASTM G48-92: “Standard Test Methods for Pitting and Crevice Corrosion Resistance of Stainless Steels and Related Alloys by Use of Ferric Chloride Solution”
3. ASTM G48-97: “Standard Test Methods for Pitting and Crevice Corrosion Resistance of Stainless Steels and Related Alloys by Use of Ferric Chloride Solution”
4. ASTM A 262-93a: “Standard Practice for Detecting Susceptibility to Intergranular Attack in Austenitic Stainless Steels”
5. ASTM A923-94: “Standard Test Methods for Detecting Detrimental Intermetallic Phase in Wrought Duplex Austenitic/Ferritic Stainless Steels”
6. ASTM A 370: “Standard Methods and Definitions for Mechanical Testing of Steel Products”
7. ASTM E23: “Standard Method for Notched Bar Impact testing of Metallic Materials”
8. ASTM A494-94: “ Standard Specification for Castings, Nickel and Nickel Alloy”
9. ASTM A488: “Standard Practice for Steel Castings, Welding, Qualifications of Procedures and Personnel”
10. ASTM A799/A 799 M -91: “Standard Practice for Stainless Steel Castings, Instrument Calibration, for Estimating Ferrite Content”